Final Report

FHWA/IN/JTRP-2004/21

Limits States Design of Deep Foundations

by

Kevin Foye
Graduate Research Assistant

Grace Abou Jaoude
Graduate Research Assistant

Rodrigo Salgado
Professor

School of Civil Engineering
Purdue University

Joint Transportation Research Program
Project No. C-36-36HH
File No. 6-14-34
SPR-2406

Conducted in Cooperation with the
Indiana Department of Transportation
and the U.S. Department of Transportation
Federal Highway Administration

Purdue University
West Lafayette, Indiana
December 2004

TECHNICAL REPORT STANDARD TITLE PAGE

1. Report No.	2. Government Accession No.	3. Recipient's Catalog No.
FHWA/IN/JTRP-2004/21		

4. Title and Subtitle	5. Report Date
Limit States Design of Deep Foundations	December 2004
	6. Performing Organization Code

7. Author(s)	8. Performing Organization Report No.
Kevin Foye, Grace Abou Jaoude, and Rodrigo Salgado	FHWA/IN/JTRP-2004/21

9. Performing Organization Name and Address	10. Work Unit No.
Joint Transportation Research Program 550 Stadium Mall Drive Purdue University West Lafayette, IN 47907-2051	
	11. Contract or Grant No. SPR-2406

12. Sponsoring Agency Name and Address	13. Type of Report and Period Covered
Indiana Department of Transportation State Office Building 100 North Senate Avenue Indianapolis, IN 46204	Final Report
	14. Sponsoring Agency Code

15. Supplementary Notes

Prepared in cooperation with the Indiana Department of Transportation and Federal Highway Administration.

16. Abstract

Load and Resistance Factor Design (LRFD) shows promise as a viable alternative to the present working stress design (WSD) approach to foundation design. The key improvements of LRFD over the traditional Working Stress Design (WSD) are the ability to provide a more consistent level of reliability and the possibility of accounting for load and resistance uncertainties separately. In order for foundation design to be consistent with current structural design practice, the use of the same loads, load factors and load combinations would be required. In this study, we review the load factors presented in various LRFD Codes from the US, Canada and Europe. A simple first-order second moment (FOSM) reliability analysis is presented to determine appropriate ranges for the values of the load factors. These values are compared with those proposed in the Codes. The comparisons between the analysis and the Codes show that the values of load factors given in the Codes generally fall within ranges consistent with the results of the FOSM analysis.

For LRFD to gain acceptance in geotechnical engineering, a framework for the objective assessment of resistance factors is needed. Such a framework, based on reliability analysis is proposed in this study. Probability Density Functions (PDFs), representing design variable uncertainties, are required for analysis. A systematic approach to the selection of PDFs is presented. Such a procedure is a critical prerequisite to a rational probabilistic analysis in the development of LRFD methods in geotechnical engineering. Additionally, in order for LRFD to fulfill its promise for designs with more consistent reliability, the methods used to execute a design must be consistent with the methods assumed in the development of the LRFD factors. In this study, a methodology for the estimation of soil parameters for use in design equations is proposed that should allow for more statistical consistency in design inputs than is possible in traditional methods.

Resistance factor values are dependent upon the values of load factors used. Thus, a method to adjust the resistance factors to account for code-specified load factors is also presented. Resistance factors for ultimate bearing capacity are computed using reliability analysis for shallow and deep foundations both in sand and in clay, for use with both ASCE-7 (1996) and AASHTO (1998) load factors. The various considered methods obtain their input parameters from the CPT, the SPT, or laboratory testing.

Designers may wish to use design methods that are not considered in this study. As such, the designer needs the capability to select resistance factors that reflect the uncertainty of the design method chosen. A methodology is proposed in this study to accomplish this task, in a way that is consistent with the framework.

17. Key Words	18. Distribution Statement
Load and Resistance Factor Design (LRFD); Geotechnical Engineering; Foundation Design; in-situ testing; Reliability-Based Design (RBD); Probability.	No restrictions. This document is available to the public through the National Technical Information Service, Springfield, VA 22161

19. Security Classif. (of this report)	20. Security Classif. (of this page)	21. No. of Pages	22. Price
Unclassified	Unclassified	234	

Form DOT F 1700.7 (8-69)

ACKNOWLEDGEMENTS

Bryan Scott and Bumjoo Kim, former Purdue Graduate students, were responsible for writing the material on load factors. Bryan Scott also made significant contributions to the assessment of shallow foundation uncertainty and resistance factors. Their work is greatly appreciated as it is a significant contribution to this final report.

TABLE OF CONTENTS

Page

LIST OF TABLES

Table Page

LIST OF FIGURES

CHAPTER 1. INTRODUCTION

1.1 Background

Foundation design consists of selecting and proportioning foundations in such a way that limit states are prevented. Limit states are of two types: Ultimate Limit States (ULS) and Serviceability Limit States (SLS). ULSs are associated with danger, involving such outcomes as structural collapse. SLSs are associated with impaired functionality, and in foundation design are often caused by excessive settlement. Reliability-based design (RBD) is a design philosophy that aims at keeping the probability of reaching limit states lower than some limiting value. In other words, the goal of design is to produce structures that have probabilities of failure less than a prescribed acceptable value. Thus, a direct assessment of risk is possible with RBD. This evaluation is not possible with traditional working stress design. The use of RBD directly in projects is not straightforward and is cumbersome to designers, except in large-budget projects. Load and Resistance Factor Design (LRFD) is a design methodology that is similar to existing practice, but can be developed using RBD concepts. LRFD shares most of the benefits of RBD while being much simpler to apply. LRFD has traditionally been used for ULS checks in structures, but SLS have been brought into the LRFD framework recently (AASHTO 1998).

Load and Resistance Factor Design (LRFD) is a design method in which design loads are increased and design resistances are reduced through multiplication by factors that are greater than one and less than one, respectively. In this method, foundations are proportioned so that the factored loads are not greater than the factored resistances:

$$(RF) \cdot R_n \geq \sum (LF)_i \cdot Q_i \qquad \textbf{(1.1)}$$

where *RF* is the resistance factor, R_n is the nominal (unfactored) resistance, $(LF)_i$ is the load factor for a particular load and load combination, and Q_i is a load of one particular type (i.e. dead, live, etc.). Nominal resistance R_n is analogous to the allowable load computed in traditional Working Stress Design (WSD). Load factors $(LF)_i$ have been developed by a number of code writing organizations (ASCE, ACI, AASHTO). The applicability of these load factors to geotechnical design is considered in Chapter 2. A useful set of resistance factors (*RF*) is required for geotechnical LRFD. In this report, recommended values of resistance factors are proposed for use with both AASHTO and ASCE-7 load factors. Reliability-Based Design tools are used to develop these resistance factors.

Variable uncertainties are necessary inputs to reliability analysis. Most design variables have some uncertainty associated with them that is often expressed using the standard deviation. Standard deviations are only a part of the definition of uncertainty for a variable. Probability Density Functions (PDFs) are used to describe completely this uncertainty in RBD. Some common types of PDFs include normal, lognormal, uniform, and beta distributions. Thus, a reliability analysis requires the determination of the relevant PDFs. A systematic approach to assessing uncertainty is required if RBD methods are to achieve useful results and gain wide acceptance. This approach is especially important to LRFD, since resistance factors must be developed with as much rigor as possible. Tools for a systematic approach to PDF assessment are presented in Chapter 3 and used in subsequent Chapters to determine resistance factors.

As a first step in design, geotechnical engineers interpret tests and other data to assess soil parameters. Soil parameters for use in a design equation must be determined in a reproducible way that is consistent with the resistance factor. This is a crucial issue among several that must be addressed before reliability-based design methods, such as LRFD, reach their full potential in geotechnical design (Becker 1996, Kulhawy and Phoon 2002). The cone penetration test (CPT) is used to illustrate a method to estimate soil parameters in a statistically consistent manner in Chapter 5.

1.2 Study Objectives

The primary objective of this study is to propose a Limit States Design method for shallow and deep foundations that is based on a rational, probability-based investigation of design methods. In particular, Load and Resistance Factor Design is used to facilitate the Limit States Design methodology. Specifically, the objectives of the study are to

- provide guidance on the choice of values for load factors for permanent and temporary loads of different types and under various combinations;

- Develop recommendations on how to determine characteristic soil resistances under various design settings (including type of soil, type of soil investigation, type of analysis, etc.);

- Develop resistance factors compatible with the load factors and the method of determining characteristic resistance.

1.3 Report Organization

- Chapter 2 is a discussion of available code prescribed load factors and the results of an investigation into their applicability to geotechnical design.
- In Chapter 3 we propose a framework for LRFD factor development. We also present probability tools to assess the variable uncertainty and resistance factors.
- In Chapters 4 and 5 we apply the framework from Chapter 3 to shallow foundations. Section 5.2 describes a method to determine characteristic resistance that is compatible with the resistance factors proposed in this report.
- In Chapter 6 we demonstrate shallow foundation design using the characteristic resistance method and the LRFD factors.
- Chapter 7 is an introduction to the deep foundation design methods that we aim to integrate into the LRFD framework.
- In Chapter 8 and 9 we present the resistance factors for deep foundations in sand and clay, respectively. Section 9.2.1 describes a method for designers to select resistance factors for design methods other than those discussed in this report.
- In Chapter 10 we demonstrate deep foundation design using the characteristic resistance method and the LRFD factors.
- In Chapter 11 we summarize the study, highlight its contributions and identify potential future directions for research.

CHAPTER 2. ASSESSMENT OF CURRENT LOAD FACTORS

2.1 Introduction

Over the past 4 decades, a load and resistance factor design (LRFD) method was brought into practice in the United States with the adoption of the American Concrete Institute Building Design Code (ACI) in 1963 (Goble 1999). In structural design practice, LRFD is currently accepted worldwide along with a traditional design method, allowable stress design (ASD), or as it is also known, working stress design (WSD). With the trend toward the increased use of LRFD, new LRFD Codes in the US, Canada and Europe (AASHTO 1994, API 1993, MOT 1992, NRC 1995, and ECS 1994) have included the implementation of LRFD for geotechnical design over the past several years. Additionally, an ACI document in preparation also advocates LRFD design of shallow foundations. The AASHTO (1994, 1998) Code proposes the use of the same loads, load factors and load combinations for foundation design as those used in structural design. The resistance factors in the AASHTO Code were calibrated for the same load factors used in the design of structural members. Since the load and resistance factors for structural design have been calibrated and adjusted through their use in practice over many years, it would be appropriate to use the same loads, load factors and load combinations in foundation design to be consistent with current structural practice. Through the use of the same load factors, not only can a consistent design between superstructures and substructures be attained, but also the design process itself may be significantly simplified (Withiam, et al. 1997).

The successful unification of the structural and geotechnical design processes may be achieved through the use of appropriate resistance factors in foundation LRFD, such

that for the given set of load factors and load combinations, LRFD produces a design consistent with current practice, or even a more economic design for a desired reliability level. Compared with structural design, however, LRFD in foundation design is still new. To facilitate its general use in practice, continuous calibration efforts to determine the appropriate resistance factors, as was done for structural design codes, are desirable. While attempting to develop the resistance factors, a general understanding of the load factors proposed in current LRFD Codes may provide a means to easily compare and evaluate resistance factors proposed recently or in the future. In this chapter, load factors presented in various LRFD Codes from the US, Canada and Europe are reviewed, and the similarities and differences between the values of load factors are assessed. A simple reliability analysis is conducted to determine an appropriate range for the values of load factors. The results of this analysis are then compared with the values presented in the reviewed Codes. We conclude with recommendations on how to best develop LRFD for acceptance in geotechnical practice.

2.2 Load And Resistance Factor Design (LRFD) and Limit States

The basic design inequality for LRFD can be given as:

$$\sum LF_i \cdot S_{ni} \leq RF \cdot R_n \qquad \textbf{(2.2.1)}$$

Where: LF, S_n, RF, and R_n = load factor, nominal load, resistance factor, and nominal resistance, respectively. The resistance is set such that the factored load effects do not exceed the factored resistance for pre-defined possible limit states. Here, the term “limit state” refers to any set of conditions that may produce unsatisfactory performance of the

structural or geotechnical system. The limit states would be associated with the various loads and load combinations considered in the design. In general, limit states are grouped into two categories, ultimate limit states (ULS) and serviceability limit states (SLS). Ultimate limit states are associated with the concepts of danger (or lack of safety), usually involving structural damage that may lead to instability or collapse of the structure. An ULS may involve, for example, the rupture of critical parts of the structure, progressive collapse of a structural member, or instability due to deformations of the structure (MacGregor 1997). For foundations, the classical notion of a bearing capacity failure is clearly an ULS.

Serviceability limit states are defined as conditions that may undermine the function or service requirements (performance) of the structure under expected service or working loads (Becker 1996). Examples of serviceability limit states include cracking of architectural finishings or walls, excessive deformation (differential movement) of the superstructure, rupture of utility lines, or pavement cracking or undulation (which would lead to a “rough ride” on a bridge).

2.3 Load Factors Proposed By LRFD Codes in the US, Canada, And Europe

To review the load factors proposed by various LRFD Codes, a total of eight bridge, building and on- and offshore foundation LRFD Codes from the US, Canada and Europe were collected. These were the following: “AASHTO LRFD Bridge Design Specifications (AASHTO 1998)”, “Building Code Requirements for Structural Concrete (ACI 1999)”, “LRFD Specification for Structural Steel Buildings (AISC 1994)”, “Recommended Practice for Planning, Designing, and Constructing Fixed Offshore

Platforms-LRFD (API 1993)", "Ontario Highway Bridge Design Code (MOT 1992)", "National Building Code of Canada (NRC 1995)", "Code of Practice for Foundation Engineering (DGI 1985)" and "Eurocode 1 (ECS 1994)". The load factors in the above Codes have been determined through calibration processes either before or after the Codes adopted LRFD for implementation in design practice. Code calibration may be done in several ways: using judgment and experience, fitting with traditional design Codes (i.e. ASD), using reliability analysis based on rational probability theory, or using a combination of these approaches (Barker, et al. 1991). The load and resistance factors in the LRFD Codes of the US and Canada have been primarily calibrated using probability theory, which has provided a theoretical basis for LRFD since the late 1960s in the US. In Denmark and other European countries, the load and resistance factors in the Codes have been mainly derived from fitting with previous Codes and adjusted through their use in practice. In Denmark, LSD has been used for geotechnical applications since the 1960s.

There are many differences in the types of limit states considered for design and in the load types and load combinations defined for each limit state when comparing the bridge and offshore Codes to the building Codes. Usually a greater number of limit states and load types apply to the design of special structures such as bridges and offshore foundations. However, certain types of loads appear in most design situations for all types of structures. These are dead loads, live loads, wind loads and earthquake loads. In this study, load factors for these four major load types are considered. Some load types that are not considered include collision loads, snow and ice loads, and earth pressure loads.

Load factors for Ultimate Limit States (ULS)

Table 2.3.1 shows the ranges of values of load factors for ultimate limit states (ULS) in the Codes discussed earlier. In general, for the bridge Codes (AASHTO 1998, MOT 1992) and offshore foundation Code (API 1993), the range of load factor values is rather wide compared with that for building or onshore foundation Codes. For example, the range of values of load factors for dead loads in AASHTO and MOT extends from 1.25 to 1.95 and 1.1 to 1.5, respectively, whereas the range for the building Codes, except ECS (1995), is 1.2 to 1.4. The values of live load factors in the bridge and offshore foundation Codes lie between 1.1 and 1.75. The values of live load factors for the building Codes, except ACI (1999), are in the range of 1.3 to 1.5.

Many different dead load types are considered in AASHTO (1998) and MOT (1992). These include the weight of the structural members, the weight of wearing surfaces such as asphalt, and earth pressure loads. A different value of load factor is applied to each of these load types. For example, in AASHTO (1998), while the value of load factor for structural components is 1.25, the load factor values for the weight of wearing surfaces and the vertical earth pressure applied to flexible buried structures are 1.5 and 1.95, respectively. The relatively high values of the load factors for the wearing surface weight and the earth pressure applied to buried structures reflect high variability in estimating the magnitude of the corresponding loads. On the other hand, the dead loads in the building Codes such as ACI (1999) and NRC (1995) consist mostly of the weight of structural components, partitions and all other materials incorporated into the building to be supported permanently by the structural components. The same load factor

is used for all of these loads as they are all treated simply as dead loads. The rather wide ranges for the dead load factors in the bridge Codes, therefore, are associated with the various types of dead loads accounted for in the design of bridges.

For the live loads in Table 2.3.1, the values for the load factors that are less than 1.0 apply when the load is used together with other transient loads (i.e. live, wind, or earthquake loads) in a load combination. This is based on the assumption that the simultaneous occurrence of the maximum value of each load is not likely, and some loads may counteract other loads when they occur together. To account for this, most Codes, except the bridge Codes (AASHTO, MOT), apply a load combination factor less than 1.0 when more than two different transient loads are used in a load combination. As an example, NRC (1995) proposes a value of 0.7 for the load combination factor when both a live and a wind load are present. In that case, therefore, 70% of each factored load effect for both the live and the wind loads are considered in design. That is:

$$S = (LF)_D S_D + 0.7((LF)_L S_L + (LF)_W S_W) \qquad \textbf{(2.3.1)}$$

The load combination factor usually varies with the number of transient loads that are present. That is, in the case where only one transient load applies, the value of the load combination factor is unity.

In the bridge Codes (AASHTO and MOT), different values of the load factors are defined in different load combinations, instead of multiplying the proposed load factors for each load by the load combination factor. As an example, AASHTO defines one load combination when live load is present, but wind load is not:

$$S = 1.25S_D + 1.75S_L \qquad (\textbf{2.3.2})$$

but defines another load combination when both live load and wind load are present:

$$S = 1.25S_D + 1.35S_L + 0.4S_W \qquad \textbf{(2.3.4)}$$

To make comparisons between the values easier, the values of load factors for a representative load combination will be used. The load combination will be a gravity load combination (i.e., dead load plus live load). Table 2.3.2 shows a comparison of the gravity load combinations for the different Codes. From Table 2.3.2, it can be seen that the variations among the Codes for the values of load factors for dead and live loads fall into a relatively narrow range, 1.0 to 1.4 and 1.3 to 1.75, respectively. Excluding the values in the Danish foundation Code (DGI 1985) from the comparison, the range of values for dead loads becomes even narrower (i.e. 1.2 to 1.4).

For wind and earthquake loads, the values of load factors for the different Codes show comparatively better agreement than for gravity loads. The values of wind load factors vary from 1.2 to 1.5. For earthquake loads, the values of the load factors are 1.0 in most Codes. Earthquake loads are site-dependent loads, which means that there may exist regional variations for design loads. Therefore, most Codes state that nominal earthquake loads should be determined relatively conservatively and a value of 1.0 should be used for the earthquake load factor. This is done in order to avoid a load factor value that varies from site to site.

In summary, the comparisons show that the values of load factors for ULS are generally consistent for all the Codes reviewed. A major difference appears in dead load factors between the building Codes and bridge Codes. Compared with the building Codes, the bridge Codes subdivide dead loads into more specific load types (e.g., vertical earth pressure applied to flexible buried structures), for which different values of load factor are used, resulting in wide ranges of load factor values. However, when

considering a gravity load combination, the values fall within rather narrow ranges for all the Codes.

Load factors for Serviceability Limit States (SLS)

Though ULSs are the focus of the current research, serviceability limit states (SLS) must be considered as well. Table 2.3.3 shows the values of load factors for serviceability limit states in the Codes reviewed. SLSs are treated differently from ULSs. Load factors are applied in both cases, but resistance factors are not used for SLS checks. Instead, the settlements resulting from the factored loads must not exceed the allowable settlements. Load factors of unity are typically prescribed for SLS checks. The bridge Codes, such as AASHTO (1998) and MOT (1991), use load factor values less than 1.0 for wind and live loads. In MOT, values of 0.7 and 0.75 apply to wind and live loads, respectively, while AASHTO uses a value of 0.3 for wind load factor.

The use of values less than 1.0 is derived from the reasoning that the time-dependent loads such as live and wind loads are not likely to remain at their maximum value for significant periods of time and therefore, factored loads for SLS checks will be less than the design loads. Furthermore, live loads considered in bridge designs are traffic loads that may be highly dependent on time compared with live loads in buildings that are mostly occupancy loads. Using a live load factor of 0.75, the MOT Code accounts for the time-dependent characteristic of the traffic loads. However, the use of a load factor value of 1.0 may be more appropriate for SLS checks for foundations on granular soils, as the settlement of granular soils is immediate. This is not a problem for

most codes, as load factors of 1.0 are used for SLS checks in all of the Codes, except the two bridge Codes. Earthquake loads are not considered for SLS in the Codes.

2.4 Simple Reliability Analysis

A simple reliability analysis was conducted to determine the appropriate ranges of the load factor values in ULS for the four different types of loads considered in this study. The method employed was the first-order second-moment (FOSM) method, assuming lognormal distributions for the design variables (i.e. load and resistance). This method was developed largely by Cornell (1969) and Lind (1971).

Loads may not be distributed lognormally; in fact, the exact distribution characteristics of loads are never known. The distribution used to model the loads should be the least biased distribution, using the given information. This given information is typically the mean and the variance (or coefficient of variation) of the loads. In order to determine which distribution is in fact the least biased, the principle of maximum entropy may be employed. This principle states that the least biased distribution is the distribution that maximizes entropy subject to the constraints imposed by the given information (Jaynes 1957). Entropy H for a discrete random variable is given by (Harr 1987):

$$H = -\sum p_i \ln p_i \qquad \textbf{(2.4.1)}$$

where p_i is the probability of event i. For a continuous random variable, entropy is given by (Harr 1987):

$$H = -\int_a^b f(x) \ln f(x) dx \qquad \textbf{(2.4.2)}$$

where *a* and *b* are the lower and upper limits, respectively, of the variable. The negative sign in each of these equations makes entropy positive. If the only data available about a variable are the values of the upper and lower limit, the principle of maximum entropy states that the uniform distribution (the distribution such that all values within the range of possible values are equally likely) is the least biased distribution (Harr 1987).

In geotechnical engineering, information about the mean and variance of a load or resistance is typically available, even though the exact distribution may not be known. The lower and upper limits of the load or resistance may be unknown. In this case the principle of maximum entropy states that the normal distribution is the least biased distribution. However, the magnitudes of load and resistance found in geotechnical problems cannot take negative values. This firmly establishes a lower limit for both loads and resistances. The upper limit of the load or resistance is typically unknown. This is especially true for transient loads (i.e., live loads, wind loads, and earthquake loads), which can assume values that are extremely large, though quite improbable. These transient loads are typically modeled by load specification committees using more precise distributions, namely, the Type I or Type II extreme-value distributions (Ellingwood et al. 1980), but these distributions require more knowledge of the variable than simply the mean, variance, and minimum value. Therefore, these distributions do not represent the least biased distribution for the loads for the information generally available. Accordingly, the lognormal distribution better models transient loads, as it is fully characterized by its first two moments, allowing easier implementation in FOSM analysis. This leads to a distribution that is not only relatively simple to implement, but also gives reasonable results (MacGregor 1976). Moreover, the lognormal distribution better represents the

product of several positive random variables, even if these variables are not themselves lognormally distributed. In load modeling, the nominal load itself may be modeled as the product of several components, each of which may also be modeled as a random variable. For example, wind loads are usually modeled as the product of wind speed and other empirical or experimental parameters that are treated as random variables (ASCE 7-95). Occasionally, an engineer on a project will have detailed load information specific to that project. In this case, specific load factors could be developed or a more complex analysis could be used, if the effort is justified by the economics of the project.

An overall resistance is frequently modeled as the product of nominal resistance and several parameters to account for the different sources of uncertainty. In the design of a bridge structure, the overall resistance of a structural member is commonly modeled as the product of nominal resistance and a material factor, a fabrication factor, and an analysis factor, which are used to account for the uncertainties for the material strengths, component dimensions, and analytical models, respectively (Nowak and Grouni 1994). This can be expressed mathematically as:

$$R = R_n \eta_m \eta_f \eta_a \qquad \textbf{(2.4.3)}$$

where: η_m is a material factor that accounts for the uncertainty of the strength of the material, η_f is a fabrication factor that accounts for the uncertainty of the size of the fabricated member (e.g. the variability of the size of formwork for cast in place concrete), and η_a is an analysis factor that accounts for the uncertainty of the analytical model used to calculate resistance. Soil resistance for foundation design may also be modeled in several cases as the product of nominal resistance and several components that account for the uncertainties of inherent soil variability, measurement (testing), and analytical

methods. Perhaps this is best illustrated by considering the general bearing capacity equation for clays,

$$q_{bL} = (s_c d_c i_c b_c g_c) c N_c \qquad \textbf{(2.4.4)}$$

which uses a series of multiplicative correction factors to model the bearing capacity of a shallow foundation. Measurement uncertainty would be seen in *c*, as cohesion is a soil strength parameter that must be measured using in-situ testing, lab tests, or correlations with other measured parameters. Additional variability due to the inherent uncertainty of the bearing capacity equation itself would result in the analysis uncertainty.

In this context, the lognormal assumption for both loads and resistances appears to be reasonable, as both can be treated as the product of several random variables. The load effects and resistances of a structural or geotechnical system may then be expressed as shown in Figure 2.4.1. Let the load effect *S* and the resistance *R* be random variables; then, failure (the attainment of an ULS) occurs when $\ln R - \ln S < 0$ (represented by the shaded area in Figure 2.4.1). The probability of failure P_f can be written as:

$$P_f = P[(\ln R - \ln S) < 0] \qquad \textbf{(2.4.5)}$$

Assuming that the random variables, ln *R* and ln *S*, are statistically independent, the mean $\overline{U}$ and standard deviation σ_U of $U = \ln R - \ln S$ are given by:

$$\overline{U} = \overline{\ln R} - \overline{\ln S} \qquad \textbf{(2.4.6)}$$

$$\sigma_U = \sqrt{\sigma^2_{\ln R} + \sigma^2_{\ln S}} \qquad \textbf{(2.4.7)}$$

The safety index or reliability index β, which is a relative measure of safety for a given system, can be expressed as a function of the mean and standard deviation of *U* (Figure 2.4.1):

$$\beta = \frac{\overline{\ln R} - \overline{\ln S}}{\sqrt{\sigma^2_{\ln R} + \sigma^2_{\ln S}}} \qquad \textbf{(2.4.8)}$$

For a lognormal distribution:

$$\sigma^2_{\ln S} = \ln(1 + V_S^2), \qquad \sigma^2_{\ln R} = \ln(1 + V_R^2) \qquad \textbf{(2.4.9)}$$

where: V_S and V_R = the coefficients of variation of S and R, respectively, defined as the ratio of the standard deviation to the mean. For small V_S or V_R, (say, less than 0.6), the following expressions are acceptable approximations (MacGregor 1976):

$$V_S^2 \cong \sigma^2_{\ln S}, \qquad V_R^2 \cong \sigma^2_{\ln R} \qquad \textbf{(2.4.10)}$$

According to MacGregor (1976), the error in (2.4.10) is less than 2% for V_R = 0.3, increasing to about 10% for V_R = 0.6. For comparison, the reported values of V_R for various geotechnical properties and resistances lie in a wide range of about 0.05 to 0.85 (Becker 1996). Considering the mean values of the reported values, the range varies from about 0.1 to 0.5. The assumption of (2.4.10) overestimates the uncertainty of the resistance, and is therefore slightly conservative. Based on (2.4.9) and (2.4.10), (2.4.8) can be rewritten as follows:

$$\overline{\ln R} - \overline{\ln S} \geq \beta \sqrt{V_S^2 + V_R^2} \qquad \textbf{(2.4.11)}$$

Lind (1971) has shown that:

$$\sqrt{V_S^2 + V_R^2} \cong \alpha V_S + \alpha V_R \qquad \textbf{(2.4.12)}$$

where: α = separation coefficient having values between 0.707 and 1.0 (depending on the value of the ratio V_R / V_s), and MacGregor (1976) has shown that:

$$\overline{\ln R} - \overline{\ln S} \cong \ln\left(\frac{\overline{R}}{\overline{S}}\right) \qquad \textbf{(2.4.13)}$$

which can be used to approximate (2.4.11). Taking (2.4.12) and (2.4.13) into (2.4.11):

$$\ln(\overline{R}/\overline{S}) \geq \beta\alpha V_S + \beta\alpha V_R \qquad \textbf{(2.4.14)}$$

or

$$\overline{R}/\overline{S} \geq e^{(\beta\alpha V_S + \beta\alpha V_R)} \qquad \textbf{(2.4.15)}$$

Rearranging (2.4.15) gives:

$$\overline{R}(e^{-\beta\alpha V_R}) \geq \overline{S}(e^{\beta\alpha V_S}) \qquad \textbf{(2.4.16)}$$

The mean load effect $\overline{S}$ and resistance $\overline{R}$ can be defined as:

$$\overline{S} = S_n k_S, \qquad \overline{R} = R_n k_R \qquad \textbf{(2.4.17)}$$

where: S_n, R_n, k_S, and k_R are the nominal load, the nominal resistance, and the bias factors (i.e. the ratio of mean to nominal) for load and resistance, respectively. Using (2.4.17), (2.4.16) can be rewritten in a form analogous to the LRFD fundamental equation:

$$R_n k_R (e^{-\beta\alpha V_R}) \geq S_n k_S (e^{\beta\alpha V_S}) \qquad \textbf{(2.4.18)}$$

or

$$RF \cdot R_n \geq LF \cdot S_n \qquad \textbf{(2.4.19)}$$

where: LF and RF = load factor and resistance factor, respectively. From (2.4.18) and (2.4.19), the value of the load factor and the resistance factor can be calculated by:

$$LF = k_S e^{\beta\alpha V_S} \qquad \textbf{(2.4.20)}$$

$$RF = k_R e^{-\beta\alpha V_R} \qquad \textbf{(2.4.21)}$$

With (2.4.20), if appropriate values of the parameters α, β, k_S, and V_S are known, the value of the load factor for each load type can be obtained in a simple manner. In most cases, however, the estimation of these parameters is difficult. This is so not only

because α is a function of both the load effects and the resistance, but also because the values of k_S and V_S are not well known due to limited statistical data.

A similar derivation can be employed for determining load and resistance factors if the underlying distributions are normal. This will be useful for determining the load factor for dead load, as dead loads are typically modeled as having a normal distribution (Ellingwood, et. al. 1980). For normally distributed variables, the probability of failure is given by (Haldar and Mahadevan 2000):

$$P_f = P\left[(R-S) < 0\right] \qquad \textbf{(2.4.22)}$$

The reliability index β is given by:

$$\beta = \frac{\overline{R} - \overline{S}}{\sqrt{\sigma_R^2 + \sigma_S^2}} \qquad \textbf{(2.4.23)}$$

Using the separation coefficient α, (2.4.23) can be written as:

$$\beta = \frac{\overline{R} - \overline{S}}{\alpha\left(\sigma_R + \sigma_S\right)} \qquad \textbf{(2.4.24)}$$

Rearranging (2.4.24) gives:

$$\overline{R} - \alpha\beta\sigma_R = \overline{S} - \alpha\beta\sigma_S \qquad \textbf{(2.4.25)}$$

Noting that $V_R = \sigma_R / \overline{R}$ and $V_S = \sigma_S / \overline{S}$,

$$\overline{R}\left(1 - \alpha\beta\sigma_R\right) = \overline{S}\left(1 - \alpha\beta\sigma_S\right) \qquad \textbf{(2.4.26)}$$

With $\overline{S} = S_n k_S$ and $\overline{R} = R_n k_R$,

$$LF = k_S\left(1 + \alpha\beta V_S\right) \qquad \textbf{(2.4.27)}$$

$$RF = k_R\left(1 - \alpha\beta V_R\right) \qquad \textbf{(2.4.28)}$$

2.5 Selection of Parameters Used in the Analysis

From (2.4.12), the separation coefficient α can be written as:

$$\alpha = \frac{\sqrt{1+(V_R/V_S)^2}}{1+(V_R/V_S)} \qquad \textbf{(2.5.1)}$$

The separation coefficient is a function of the ratio V_R/V_S. In other words, it is a function of the uncertainties in both the loads and the resistances. To derive a load factor based on (2.4.20), therefore, a representative value of V_R/V_S should be chosen. Values of V_R range from about 0.1 to 0.5 as presented previously. The representative values of V_S reported in the literature range from 0.1 to 0.25 for dead, live and wind load (Nowak 1994, Ellingwood 1999). Hence, the corresponding ratio V_R/V_S for the reported ranges of V_R and V_S range from 0.4 to 5. For values of V_R/V_S between 0.4 and 5, the separation coefficient α takes values within the rather narrow range of about 0.7 to 0.85. Accordingly, a value of 0.75 was assumed for α in our analysis. This value has also been used by Becker (1996) and is consistent with the range as presented in Figure 2.5.1. For comparison, load factor values obtained using α ranging from 0.7 to 0.85 are also examined.

The reliability index, β, is a relative measure of the degree of safety. As shown in Figure 2.4.1, higher values of β are associated with smaller probabilities of failure, and vice versa. By using (2.4.20) and (2.4.21), one can calculate the value of β for given values of the load and resistance factors and statistical parameters. Conversely, the load and the resistance factor can be determined for a given β (i.e., for a target reliability index) and for given statistical parameters. In fact, Code calibration is the process in which the load and resistance factors are adjusted to obtain a desired level of reliability.

The load effects S in Figure 2.4.1 are usually the combination of load effects for several different load types according to the load combinations used. For instance, in a gravity load combination, a load effect S will be the combination of dead load effects and live load effects. In this case, the reliability index β is commonly calculated using the reliability equations, where statistical parameters, such as V_S and V_R, are the statistical parameters representative of the combined load effects (i.e. dead load and live load) and the overall resistance. Based on this approach, Ellingwood et. al. (1980), after careful examination of β for common structural members, such as concrete, steel, and timber, reported that the representative values of reliability index β tend to fall within the range of 2.5 to 3.0 for both the gravity load and the gravity plus wind load combinations. These values for β are representative of the reliability associated with existing designs. He also suggested that, for gravity load, gravity plus wind load, and gravity plus earthquake load combinations, the representative target reliability indices β_T are 3.0, 2.5, and 1.75, respectively. These target reliability indices have been established after consideration of the reliability associated with current designs. Establishing target reliability indices based on current designs will lead to load factors that produce designs that are similar to current designs. This is desirable because the reliability indices can be refined later, if there is a need to refine them at all, in a cautious manner as the Codes evolve. To derive the load factor for a particular load type using (2.4.20), therefore, the selection of different values of β for each load type would be required. In this analysis, based on Ellingwood's work, the values of β equal to 3.0 for dead load, 2.75 for live load, 2.5 for wind load, and 1.75 for earthquake loads were assumed.

For the evaluation of the values of k_S and V_S, extensive research has been performed over several decades of use of LRFD in structural design. For the time-variant loads such as live, wind, and earthquake loads, the values of k_S and V_S are normally obtained from time-stochastic modeling processes based on available recorded data (e.g. traffic survey data, wind speed data or seismic acceleration coefficient). Table 2.5.1 shows the values of k_S and V_S reported by several researchers. As expected, the biases for gravity loads (i.e. dead load and live load) are relatively small. This means that gravity loads tend to be estimated rather accurately. Also note that the coefficient of variation for dead loads is quite low. On the other hand, V_S for earthquake loads are significantly higher than for other loads. Based on the data presented in Table 2.5.1, ranges of values for k_S and V_S are determined for each load type for use in the analysis of the present chapter. The ranges of values used are presented in Table 2.5.2.

2.6 Comparison Between Results and Load Factors in the Codes

Table 2.6.1 and Figure 2.6.1 show the comparisons of the values of the load factors between the analysis and the Codes. The load factors for beneficial dead loads were obtained using equations similar in form to equations (2.4.21) and (2.4.28), namely:

$$LF = k_S e^{-\alpha\beta V_S} \qquad \textbf{(2.6.1)}$$

for the lognormal distribution, and

$$LF = k_S \left(1 - \alpha\beta V_S\right) \qquad \textbf{(2.6.2)}$$

for the normal distribution, based on the reasoning that beneficial dead loads resist failure. These equations are similar to the resistance factor equations, except the bias factor and coefficient of variation are for the beneficial load effects, not the resistances. These

equations also differ from the standard load factor equations, (2.4.20) and (2.4.27), in that they are expressed in terms of $-\alpha\beta V_S$ instead of $\alpha\beta V_S$. This accounts for the beneficial nature of these loads. The values for load factors given in the Codes are found to be reasonably consistent for all loads considered. A relatively wide range in earthquake load factors is mainly due to the values of V_S used in the analysis, which lie within a wide range. In the same table, for comparisons, average values for the ranges of each load are shown. For dead and live load, the values by the analysis are somewhat higher than those in all the Codes. It is interesting to note, however, that when a comparison is made with the US Codes (i.e. AASHTO, ACI, and AISC), the average values from the analysis show relatively good agreement with the values from the Codes, although the ranges given in the analysis are rather large (Table 2.6.1). For α varying from 0.7 to 0.85, the ranges become somewhat larger, but the only load factors affected significantly are those for earthquake loads. In some cases, the analysis supports the use of load factors that are higher than the load factors currently used in the Codes. This can be seen in Figure 2.6.1 for earthquake loads especially. This apparent unconservatism in the current Codes is due to the underlying probability distribution for the loads. The current research is using the least biased distribution considering only the mean and variance of the loads along with the fact that the loads cannot be negative. The Codes are based on more precise, and therefore more biased, distributions of the loads, using more information about the particular loads being considered. Upon considering this extra information, the code developers can arrive at a more precise load factor for a particular case. As can be seen from Figure 2.6.1, these values always lie within the range determined by the current research.

2.7 Future Development of Geotechnical LRFD Design

As demonstrated by equations (2.4.19), (2.4.20), (2.4.21), and (2.5.1), load and resistance factors are inexorably linked through the values of β, V_R, and V_S. This means that each Code will assign different values to resistance factors, because of the different load factor values adopted. This adds to the complexity of LRFD compared with Allowable Stress Design (ASD). In ASD, engineers need only to understand the concept of the global factor of safety, which has been in use for at least a century. The safety factor for a footing, for example, typically would be in the range of 2 to 4, and the engineer selects the value to use in design based on general guidelines. In LRFD, it is essential to use the values of *LF* and *RF* prescribed in the Code, as well as a nominal resistance consistent with the *LF* and *RF* values. This requires understanding of more complex concepts.

Acceptance of the LRFD approach hinges on making the method understandable to and usable by geotechnical engineers. The large array of different load factors currently in existence, which leads to a large number of different resistance factors, adds to the overall complexity of LRFD for the practicing engineer and ultimately discourages the use of this design method. Our analysis shows that, in general, the load factors proposed by different codes are all acceptable from a theoretical standpoint. Ideally, in order to facilitate the use of LRFD in routine practice, the leadership of the organizations responsible for each code would join in adopting a single set of load factors, at least for the primary loads, such as the four load types discussed in this chapter (i.e. dead, live, wind, and earthquake loads). We recognize this is difficult to accomplish, as it involves

overcoming non-technical, political hurdles. The alternative is for engineers to become used to using different load and resistance factors when designing the same type of foundation element depending on the Code controlling design.

2.8 Summary and Conclusions

The load factors proposed by various current structural and foundation LRFD Codes were reviewed. Usually, a larger number of limit states, load types and load combinations are considered in the bridge and offshore foundation design codes, compared with building and onshore foundation design codes. In this study, the load factors for four major load types (i.e. dead, live, wind and earthquake loads) that control most design cases were examined and compared between the Codes.

For ULSs, the load factor values fall within rather consistent ranges for most load types considered. Differences appear in the dead and the live load factors between the building and the bridge Codes. For the bridge Codes, the values of dead load factors lie within a relatively wide range. This is because, for bridge design, more types of loads are usually defined as dead loads, for which different values of load factors are used to account for the different degrees of uncertainty inherent in each load. While the use of a large number of different load factors adds to the complexity of a Code, it also adds to the utility of the Code. When a greater number of load factors are used, the uncertainties due to each load type are better separated. This separation of uncertainties is the ultimate goal of LRFD. The bridge Codes also define different values of live load factors for different load combinations (i.e. different limit states) instead of using load combination factors to account for the reduced probability of simultaneous occurrence of maximum

values of several transient loads. When considering a gravity load combination, however, the values for the dead and the live load factors are reduced to a rather narrow range for all of the Codes, resulting in ranges consistent with other load types examined.

For SLSs, some differences appear again between the bridge and building Codes. While most Codes prescribe the use of unfactored loads, AASHTO (1998) and MOT (1991) use values less than 1.0 for wind and both wind and live load factors, respectively. This reflects the differences in how each Code prescribes the determination of the characteristic wind load, as well as the transient nature of the live load for bridges. However, an argument can be made against using load factors less than one, except when the foundation soil is clay.

A simple FOSM reliability analysis was implemented to find appropriate ranges of the load factor values for each load considered in this study. The analysis produced results consistent with all the Codes reviewed, although the values produced lie in rather wide ranges due to the relatively wide range of the input parameters. The analysis shows even better agreement with the Codes when considering only the US Codes (AASHTO, ACI, and AISC). The values presented in the US Codes lie in the middle of the acceptable range determined by the analysis, as summarized by Figure 2.6.1. As the analysis uses the least biased distribution to model the loads, load factors for use in geotechnical LRFD should not lie outside the range determined by the current research unless that load factor applies to a specific type of load that is not considered in this research.

2.9 Notation

H = entropy

k_R = bias factor of resistance

k_S = bias factor of load effect

LF = load factor

$(LF)_D$= dead load factor

$(LF)_L$= live load factor

$(LF)_W$= wind load factor

p_i = probability of event i

P_f = probability of failure

R = resistance

RF = resistance factor

R_n= nominal resistance

$\overline{R}$ = mean resistance

S = load effects

S_D= nominal dead load effect

S_L= nominal live load effect

S_n= nominal load effect

S_W= nominal wind load effect

$\overline{S}$ = mean load effect

V_R = coefficient of variation of resistance

V_S = coefficient of variation of load effect

α = separation coefficient

β = reliability index

β_T= target reliability index

η_m= material factor

η_f= fabrication factor

η_a= analysis factor

σ = standard deviation

Table 2.3.1. Load factors

	US				Canada		Europe	
Loads	AASHTO (1998)	ACI (1999)	AISC (1994)	API (1993)	MOT (1992)	NRC (1995)	DGI (1985)	ECS (1995)
Dead	1.25-1.95 (0.65-0.9)	1.4 (0.9)	1.2-1.4 (0.9)	1.1-1.3 (0.9)	1.1-1.5 (0.65-0.95)	1.25 (0.85)	1.0 (0.85)	1.0-1.35 (0.95)
Live	1.35-1.75	1.7	1.6	1.1-1.5 (0.8)	1.15-1.4	1.5	1.3	1.3-1.5
Wind	1.4	1.3	1.3	1.2-1.35	1.3	1.5	1.3	1.3-1.5
Seismic	1.0	1.4	1.0	0.9	1.3	1.0	1.0	1.0

Note: Values in parentheses apply when the load effects tend to resist failure for a given load combination.

Table 2.3.2. Load factors and gravity load combinations

Code	Representative gravity load combination
AASHTO (1998)	1.25D+1.75L
ACI (1999)	1.4D+1.7L
AISC (1994)	1.2D+1.6L
API (1993)	1.3D+1.5L
MOT (1992)	1.2D+1.4L
NRC (1995)	1.25D+1.5L
DGI (1985)	1.0D+1.3L
ECS (1995)	1.35D+1.5L

Table 2.3.3. Load factors for SLS

Loads	US			Canada		Europe	
	AASHTO (1998)	ACI (1999)	AISC (1994)	MOT (1991)	NRC (1995)	DGI (1985)	ECS (1995)
Dead	1.0	1.0	1.0	1.0	1.0	1.0	1.0
Live	1.0	1.0	1.0	0.75	1.0	N/A[a]	1.0
Wind	0.3	1.0	1.0	0.7	1.0	N/A[a]	1.0

[a]The values for transient loads are given in the structural Code.

Table 2.5.1. Ratio of mean to nominal load, k_S, and coefficient of variation, V_S

Loads	k_S	References	V_S	References
Dead	1.03-1.05	Nowak 1994; Ellingwood 1999	0.08-0.15	Nowak 1994; Ellingwood 1999
Live	1.0	Ellingwood 1999	0.25	Ellingwood 1999
Wind	0.875	Nowak 1994	0.20	Nowak 1994
Earthquake	0.3	Nowak 1994	0.7 <	Ellingwood, et al. 1980; Nowak 1994

Note: k_S and V_S in transient loads (i.e. live, wind and earthquake loads) are maximum 50-year values

Table 2.5.2. Values of k_S and V_S assumed for the analysis

Loads	k_S	V_S
Dead	1.0-1.05	0.07–0.16
Live	0.95-1.05	0.2–0.3
Wind	0.85-0.9	0.15–0.25
Earthquake	0.25-0.35	0.9-1.1

Table 2.6.1. Comparison of the values of load factors from the analysis and from the Codes

	Dead load	Live load	Wind load	Earthquake load
Analysis ($0.7<\alpha<0.85$)	1.16 - 1.58 (1.34) 0.66 - 0.91[a] (0.79)	1.40 - 2.12 (1.71)	1.11 - 1.53 (1.29)	0.75 - 1.80 (1.17)
Analysis ($\alpha=0.75$)	1.17 - 1.50 (1.33) 0.70 - 0.90[a] (0.79)	1.44 - 1.95 (1.68)	1.13 - 1.44 (1.28)	0.81 - 1.48 (1.12)
All Codes	1.0 - 1.4[b] (1.24) 0.65 - 0.95[a] (0.80)	1.3 - 1.75[b] (1.53)	1.2 - 1.5 (1.36)	0.9 - 1.4 (1.08)
AASHTO, ACI and AISC only	1.2 - 1.4[b] (1.28) 0.65 - 0.9[a] (0.86)	1.6 - 1.75[b] (1.68)	1.3 - 1.4 (1.33)	1.0 - 1.4 (1.13)

Note: Values in parentheses represent average values
[a] Beneficial dead loads
[b]The range for a representative gravity load combination, as presented in Table 2.3.2

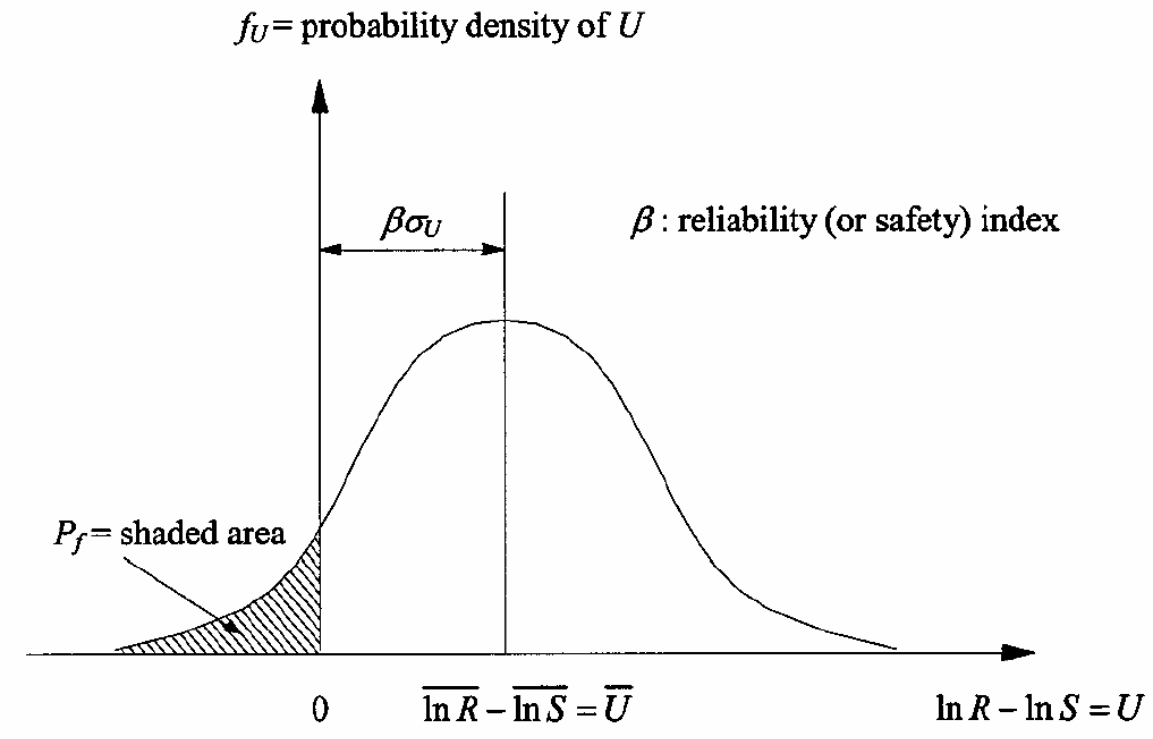

Figure 2.4.1. Load effects, resistance and reliability

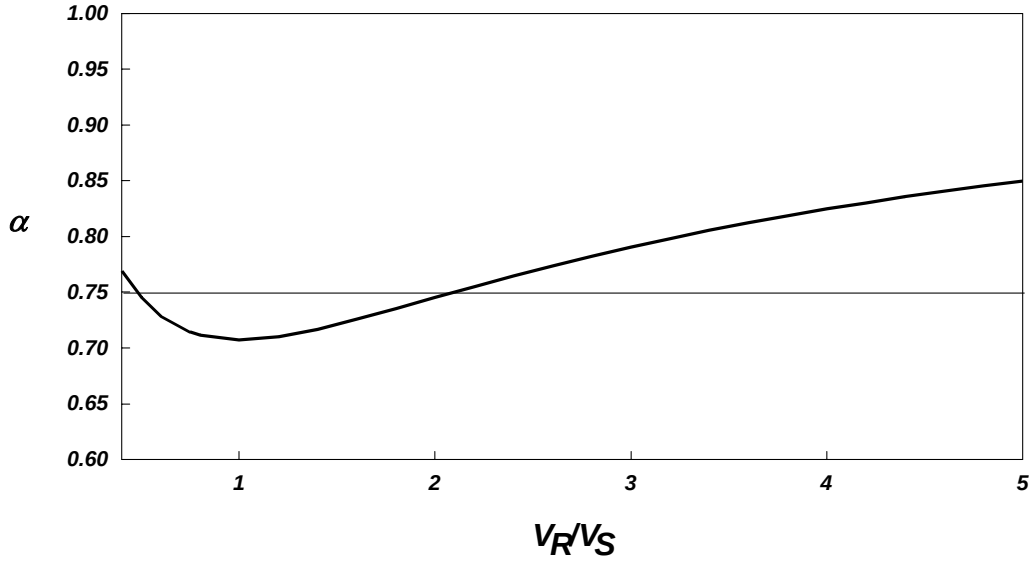

Figure 2.5.1. Variation of separation coefficient, α

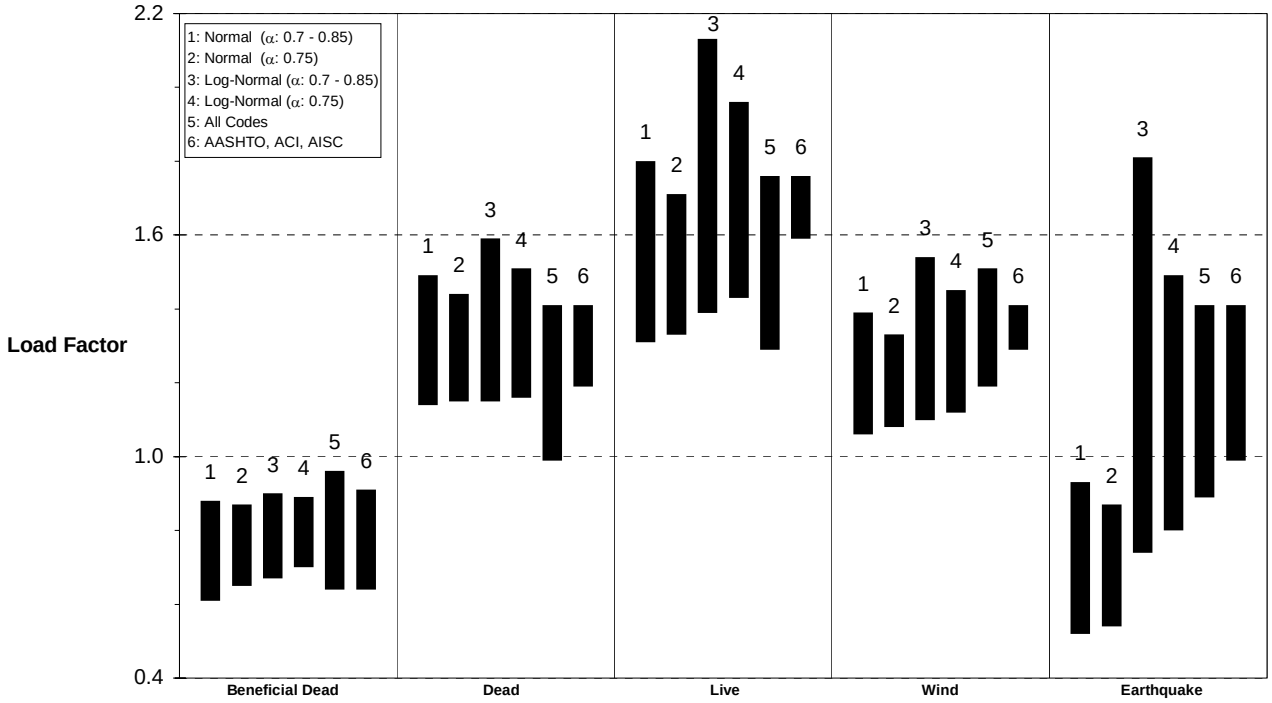

Figure 2.6.1. Comparison of analysis and the Codes

CHAPTER 3. METHODOLOGY TO DETERMINE RESISTANCE FACTORS

Many possible techniques exist to select Resistance Factors (*RFs*) for use in geotechnical LRFD. One very common technique is to "calibrate" *RFs* using existing factors of safety and code-specified Load Factors as input. In this way, *RFs* may be specified to allow the equivalent correction to resistance as results from existing factors of safety. This technique is acceptable as a first step in the adoption of LRFD, but better methods are available. The most rational method available to determine *RFs* is reliability analysis.

Many studies have been published that advocate the use of reliability analysis for LRFD development. However, our study differs significantly in the methods used to assess the uncertainty of design variables input into the reliability analysis. The most widely used techniques involve statistics performed on large databases of indiscriminately combined data. An example of this technique applied to load test databases is the recent NCHRP Report 507 (Paikowsky 2004). An example of this technique applied to soil properties is Phoon and Kulhawy (1999). These methods have the advantage that they are readily applied in the short term. However, they have the disadvantage that there is virtually no control over the quality or applicability of the data collected. In contrast, this study uses very carefully selected data that targets very precisely the uncertainties in design we need to quantify. To ensure the completeness of our uncertainty assessment, we have proposed the following rational framework for evaluating resistance factors. This work is presented as a model for research into the development of complete LRFD methodologies for geotechnical design.

3.1 A Rational Framework for Evaluating Resistance Factors

A consistent framework for evaluating resistance factors is key to successful LRFD implementation. A number of possible approaches exist, such as scaling factors to existing factors of safety; using simple probabilistic analyses considering a select set of uncertainties; and performing more rigorous probabilistic analyses considering all quantifiable uncertainties. Results of a method conforming to this last approach would be highly credible. After the model framework for determining resistance factors for structural design set forth by Ellingwood et al. (1980), the following set of steps is proposed as a geotechnical framework for such a method:

1. identify the equations used to compute foundation resistance;
2. identify the component variables of the resistance equations;
3. identify the measurable quantities (geotechnical tests) associated with each of the input variables;
4. identify all component uncertainties for each variable, including transformations;
5. evaluate the composite uncertainties using available statistics (literature, tests/analysis, current research);
6. use uncertainties to select PDFs for reliability analysis;
7. select representative design variables (dimensions, strengths, loads);
8. execute reliability analysis to obtain resistance factors;
9. adjust resistance factors for governing load factors;
10. repeat reliability analysis to cover a range of representative design conditions.

Steps 1-6 of these guidelines are demonstrated in Chapter 4 for the development of PDFs for shallow foundation bearing capacity in sands and in clays. Steps 7-10 are demonstrated in Chapter 5 for the development of resistance factors for shallow foundation bearing capacity. Steps 1-10 are applied to deep foundations in Chapter 8 for sands and Chapter 9 for clays.

3.2 Tools to Assess Uncertainty

Steps 1-3 of the framework will be explained as they are demonstrated in Chapters 4, 7, 8, and 9. In each of steps 4-6 in these guidelines, operations will be performed on the data describing the uncertainty of geotechnical measurements and transformations. The following tools are used to accomplish these operations.

Standard Deviation and Coefficient of Variation

The scatter or uncertainty in measurements and correlations can be quantified using the standard deviation. The standard deviation (σ) of a random variable X can be estimated using the sample standard deviation (S) when n occurrences of value x_i are known,

$$S_X = \sqrt{\frac{\sum_{i=1}^{n}(x_i - \mu_x)^2}{(n-1)}} \qquad \textbf{(3.2.1)}$$

where S_X is the sample standard deviation of X and μ_X is the mean of X. According to probability theory, S_X has expected value (mean) σ_x, hence it is used to find σ_X. For many random variables in engineering, it is more convenient to express standard deviation using a Coefficient of Variation (*COV*):

$$COV = \frac{\sigma_X}{\mu_X} \qquad \textbf{(3.2.2)}$$

It is especially useful in case where the standard deviation varies with the mean value.

In the assessment of variable uncertainties in the following chapters, there are many instances where a particular relationship between two variables can be determined from data. Suppose we have data indicating a relationship between variables *X* and *Y*. A function $y = f(x)$ can be defined that represents a mean trendline through this data. This task is routinely accomplished using least squares regression. It is necessary to describe the uncertainty of this correlation $f(x)$. The first step is to detrend the data by subtracting $f(x_i)$ from each value y_i. A standard deviation quantifying the uncertainty of this correlation can then be found by applying equation (3.2.1) to all the values of $(y_i - f(x_i))$. Alternatively, if it is observed that the scatter of the data about the mean trend line is proportional to the value of $f(x)$, then a representative *COV* expressing the uncertainty of the correlation can be found by applying equation (3.2.1) to all values of $(y_i - f(x_i))/f(x_i)$.

6σ and modified 6σ method

The scatter in measurements tends to conform to normal distributions. A normal distribution is a type of PDF that can be described completely using its mean and standard deviation. Many geotechnical data such as Standard Penetration Test (SPT) blow count (*N*) and Cone Penetration Resistance (CPT) tip resistance (q_c) have trends with depth. The 6σ method can expedite assessments of the standard deviation of these trended data[1]. The first step is to observe the bounds and mean trend of the data. An

[1] This six standard deviation (6σ) procedure is also recommended for determining the uncertainty of variables by the FHWA (Withiam et. al. 1997).

example mean trend and data bounds are illustrated in Figure 3.2.1 for q_c. For a particular depth, the value of the mean and the range (difference between minimum and maximum bound values) can be computed. The standard deviation is then found using

$$\frac{Range}{6} = \sigma \qquad \textbf{(3.2.3)}$$

where σ is the standard deviation. An implication of Equation (3.2.3) is that the range is taken to represent six standard deviations of the normal distribution – encompassing 99.74% of the possible values of q_c for this measurement. In geotechnical engineering, the standard deviation is frequently expressed using the Coefficient of Variation (*COV*),

$$COV = \frac{\sigma}{\mu} \qquad \textbf{(3.2.4)}$$

where μ is the mean. The value of using the *COV* instead of σ is that, in many cases, the *COV* is independent of μ. It is possible that for some geotechnical quantities, the *COV* varies with the mean value or with depth. In these circumstances, it is conservative to select the greatest computed *COV* value for use in reliability analysis.

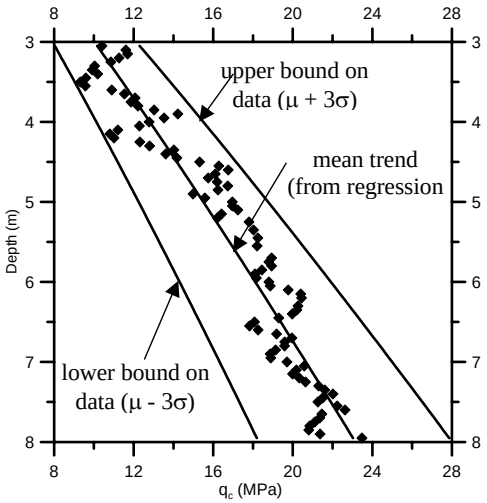

Figure 3.2.1. Mean Trend (power regression) and Bounds of CPT Tip Resistance Data for Sand. The mean and bounds can be used to calculate the COV for q_c using the 6σ procedure.

A modified version of the 6σ procedure is applied when relatively few data points are available. In this procedure, the data's bounds are assumed to represent a number of standard deviations N_σ depending on the number of available data points *n*. Values of N_σ for different values of *n* are tabulated in Table 3.2.1. Table 3.2.1 is derived from work by Tippett (1925). It is applicable to sets of normally distributed data for which the number of data points is limited, the range of data is known, and the average standard deviation of the population based on this data sample is sought. For the modified 6σ approach, (3.2.3) is rewritten as

$$\frac{Range}{N_\sigma} = \sigma \qquad \textbf{(3.2.5)}$$

Table 3.2.1. Values of Number of Standard Deviations (N_σ) Represented by the Range of *n* data points that are Normally Distributed (after Tippett 1925)

n	N_σ	*n*	N_σ
2	1.128379	17	3.587886
3	1.692569	18	3.640066
4	2.058751	19	3.688965
5	2.325929	20	3.734952
6	2.534413	50	4.498153
7	2.704357	100	5.0152
8	2.847201	200	5.492108
9	2.970027	300	5.755566
10	3.077506	400	5.936396
11	3.172874	500	6.073445
12	3.258457	600	6.183457
13	3.335982	700	6.275154
14	3.406765	800	6.353645
15	3.471828	900	6.422179
16	3.531984	1000	6.482942

Assessment of Composite Uncertainties using Numerical Integration

In steps 4 and 5 of the framework, it is necessary to determine the uncertainty of variables, such as relative density (D_R), that are computed from other variables, such as

CPT q_c. An equation (transformation) is used to compute q_c from D_R. Just as for q_c and D_R, the transformation also has uncertainty (Phoon and Kulhawy 1999). Numerical Integration is a technique that allows us to combine the uncertainties of the original variable *X* and the transformation to determine the uncertainty of the final (transformed) variable *Y*. The result of this numerical integration technique is a histogram depicting the uncertainty of the final variable.

The PDF of a random variable *Y* that is a function *f* of a random variable *X* can be expressed as (Ang and Tang 1975)

$$p_Y(y) = p_X\left(f^{-1}(y)\right)\left|\frac{df^{-1}(y)}{dy}\right| \qquad \textbf{(3.2.6)}$$

where $p_X(x)$ is the PDF of *X* and $f^{-1}(y)$ is the inverse of the transformation function from *X* to *Y*. In a numerical scheme, (3.2.6) can be approximated by assuming $dy = \Delta y$ and multiplying both sides of the equation by Δy, yielding

$$p_Y(y)\Delta y = p_X\left(f^{-1}(y)\right)\Delta f^{-1}(y) \qquad \textbf{(3.2.7)}$$

Since transformation *f(x)* has uncertainty, Eq. (3.2.7) needs to be modified to incorporate a PDF representing the transformation uncertainty. The concept of conditional probability is used for that. The conditional PDF of variable *Y* for a given value *x* is written $p_{Y|X}(y \mid x)$. The conditional PDF represents the uncertainty of *Y* when the value of *X* is known exactly. Thus, PDF $p_{Y|X}(y \mid x)$ represents the transformation uncertainty, the uncertainty of *f*(*x*). By this definition, PDF $p_{Y|X}(y \mid x)$ has expected value *y=f(x)*,

meaning this PDF is also a function of *x*. According to probability theory, the independent PDF[2] of *Y* can be found by

$$p_Y(y) = \int_{-\infty}^{\infty} p_{Y|X}(y \mid x)\, p_X(x) dx \qquad \textbf{(3.2.8)}$$

Multiplying both sides by *dy* yields

$$p_Y(y)dy = dy \int_{-\infty}^{\infty} p_{Y|X}(y \mid x)\, p_X(x) dx \qquad \textbf{(3.2.9)}$$

Finally, to facilitate numerical evaluation, as in (3.2.7), an iterative scheme is adopted. The probability of random variable *Y* taking a value *y* contained in the finite range Δy is expressed as $p_Y(y)\Delta y$. To find $p_Y(y)\Delta y$, the integral of (3.2.9) is approximated by a summation where $p_X(x)dx$ and $p_{Y|X}(y \mid x)dy$ are approximated by integrals over small intervals Δx and Δy, respectively, to yield

$$p_Y(y)\Delta y = \sum_{\xi=a}^{b} \left[\int_{\xi-\frac{1}{2}\Delta x}^{\xi+\frac{1}{2}\Delta x} p_X(x)dx \cdot \int_{y-\frac{1}{2}\Delta y}^{y+\frac{1}{2}\Delta y} p_{Y|X}(y \mid x)dy \right] \qquad \textbf{(3.2.10)}$$

where the successive integration limits in *x* are Δx apart, and *a* and *b* are chosen such that

$$\sum_{\xi=a}^{b} \int_{\xi-\frac{1}{2}\Delta x}^{\xi+\frac{1}{2}\Delta x} p_X(x)dx \approx 1 \qquad \textbf{(3.2.11)}$$

This means we are evaluating $p_Y(y)\Delta y$ in essence for all values of *x*, given that we have very closely approximated 100% probability of *x* being between *a* and *b*. The evaluation of (3.2.10) is repeated across a range of *y* values, always Δy apart. The final result is a complete description of PDF $p_Y(y)$ in terms of a histogram with intervals of width Δy.

Assessment of Composite Uncertainties using Monte Carlo Simulation

[2] according to probability theory, the independent PDF of a random variable Y that is jointly distributed with another variable X is the PDF of Y over all possible values of x.

An alternate method of computing (3.2.9) and constructing an approximate histogram representing $p_Y(y)$ is Monte Carlo Simulation. In this method, the PDFs $p_X(x)$ and $p_{Y|X}(y|x)$ are approximated by a very large number of random values *x* and *y*, selected as follows. First, a random number ξ between 0 and 1 is generated[3]. The pseudo-random number generators available in spreadsheet software are suitable for this task. Next, a random value x' is selected such that

$$\int_{-\infty}^{x'} p_X(x)dx = \xi \qquad \textbf{(3.2.12)}$$

Thus, value x' has the same probability of occurrence with respect to its PDF as ξ. This process is repeated until a large number of x' values has been generated. For each random value x', an expected value of $(y|x)$ can be calculated using $E[y|x] = f(x')$. Just as for the numerical integration technique above, distribution $p_{Y|X}(y|x)$ has expected value $E[y|x] = f(x')$. This PDF can then be used to obtain a large number of *y* values using the same technique used to find values of x'. Notice that many values of *y* are determined for each value of x' and many values of x' are required. Each value *y* found using this process is called a simulation. A histogram of *Y* can be computed by counting all of the simulations of *y* that fall within each interval of the histogram.

While Monte Carlo methods are very popular and possibly efficient under some conditions, for calculations involving a large number of transformations, they require many more computations than direct numerical integration for the same resolution of the histogram of $p_Y(y)$.

[3] the random variable corresponding to this value ξ, chosen randomly from 0 to 1, has a uniform distribution with bounds 0 and 1.

Nominal Values, Mean Values, and Bias Factors

Figure 3.2.2 illustrates the PDF for an idealized design parameter that is normally distributed. The mean value corresponds to the expected value (or mean) of the distribution. For measurements, this value is determined by taking the mean of the data, or by finding a mean trend for trended data such as q_c. For transformed variables Y, such as D_R, the mean value μ_Y is taken as the expected value of Y according to PDF $p_Y(y)$ or the histogram representing PDF $p_Y(y)$. In many cases in geotechnical design, the value of the parameter used in design, the "nominal" value, may be different from the mean value. In these cases, a bias factor is used to express the difference. The bias factor is defined as

$$\text{bias factor} = \frac{\mu_Y}{y_{\text{nominal}}} \qquad \textbf{(3.2.13)}$$

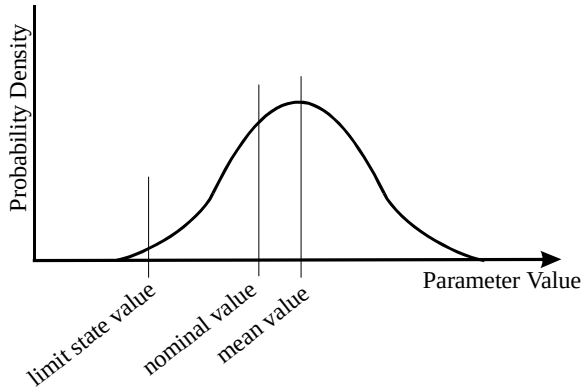

Figure 3.2.2. The mean, nominal, and limit state values of a normally distributed design parameter. Here, limit state value corresponds to the value at which a limit state such as bearing capacity failure is reached. Mean value is the mean of the distribution under consideration. Nominal value is the parameter value used in design. The mean can be calculated from the nominal by (nominal) * (bias factor).

The mean value of a design parameter can be different from the nominal value for one of two reasons. First, some equations used in design are known to be biased. In these cases,

the bias factor is used to correct the value determined using the design equation for the known bias so that the statistical mean of the design parameter reflects our best knowledge of what that parameter should be. Second, nonlinear transformations $y=f(x)$ result in transformed PDFs $p_Y(y)$ with shapes that differ from those of the input PDFs $p_X(x)$. The change in shape also shifts the mean value such that $E[Y] \neq f\left(E[X]\right)$. Bias factors are useful for defining the PDFs for normally and lognormally distributed variables. These PDFs can be described completely with the mean and the COV.

The third value identified in Figure 3.2.2 is the limit state value. This value is the value of the design parameter required for a design to reach a particular limit state. The optimization required to find this value is presented in the following section.

3.3 Tools to Assess Resistance Factors

In the previous section we presented the methodology to develop Probability Density Functions (PDFs) describing the uncertainties of the variables for any limit state design check. In this section, we will present the methodology to perform the reliability analysis and compute resistance factors (steps 7-10 of the framework) for these design checks.

Design, Mean, and Limit State Values and the Reliability Index

For a certain limit state, the limit state equation (the function that separates satisfactory from unsatisfactory performance) can be given as a function of several variables. For example, the limit state equation for the ultimate bearing capacity of rectangular footings on sand under vertical load is

$$\frac{DL+LL}{B\cdot L}-\left(\gamma\cdot D\cdot N_q\cdot s_q\cdot d_q+\frac{1}{2}\gamma\cdot B\cdot N_\gamma\cdot s_\gamma\right)=0 \qquad \textbf{(3.3.1)}$$

In (3.3.1), if the resistance is greater than the load effect, there is some margin of safety. This margin of safety can be expressed through the concept of the reliability index (β) (Cornell 1969, Hasofer and Lind 1974, Low and Tang 1997). The reliability index is dependent on the mean and variance of each of the variables and also on the limit state under consideration. A visual depiction of the reliability index is shown in Figure 3.3.1. In part (a) of Figure 3.3.1, β is expressed for a problem with one normally distributed random variable. In this case, the probability of failure can be simply calculated as the area under the probability density function (PDF) of X to the left of the limit state (LS) value. The reliability index can be seen as the ratio of the distance between the expected value of X (the mean μ) and the limit state value, x_{LS}, to the variable standard deviation σ of X. Thus, β is directly related to the probability of failure. The Hasofer and Lind (1974) definition of the reliability index retains this property of β for multi-variable problems. In part (b) of Figure 3.3.1, a two-variable problem is expressed. A simpler, two-dimensional illustration of Fig. 3.3.1(b) appears in Fig. 3.3.1(c). Here the probability density is indicated by contours. Now the reliability index can be expressed as

$$\beta=\sqrt{\left(\frac{x_{LS}-\mu_X}{\sigma_X}\right)^2+\left(\frac{y_{LS}-\mu_Y}{\sigma_Y}\right)^2} \qquad \textbf{(3.3.2)}$$

For multiple random variables X_i, with i = 1, 2, . . ., n, with corresponding means and standard deviations μ_i and σ_i, a generalization of (3.3.2) is possible,

$$\beta = \sqrt{\left(\frac{x_{1,LS} - \mu_{X_1}}{\sigma_{X_1}}\right)^2 + \left(\frac{x_{2,LS} - \mu_{X_2}}{\sigma_{X_2}}\right)^2 + \Lambda + \left(\frac{x_{n,LS} - \mu_{X_n}}{\sigma_{X_n}}\right)^2} = \sqrt{(\mathbf{x}-\mathbf{m})^{\mathbf{T}}\left[\boldsymbol{\sigma}^{\mathbf{2}}\right]^{-1}(\mathbf{x}-\mathbf{m})} \qquad \textbf{(3.3.3)}$$

where **x** is a vector of limit state values of X_i, **m** is a vector of mean (μ) values of X_i, and [$\boldsymbol{\sigma}^{\mathbf{2}}$] is a diagonal matrix of the variance (σ^2) values of X_i. Equation (3.3.3) holds for uncorrelated normal random variables. A more general expression, considering the possibility that the normal random variables are correlated, was given by Low and Tang (1997):

$$\beta = \sqrt{(\mathbf{x}-\mathbf{m})^T \mathbf{C}^{-1}(\mathbf{x}-\mathbf{m})} \qquad \textbf{(3.3.4)}$$

where **C** is the covariance matrix of the random variables considered where $\mathbf{C}_{kl}$ = covariance(X_k,X_l). Note that covariance(X_k,X_k) is equal to the variance of X_k. When random variables X_i are uncorrelated, non-diagonal terms $\mathbf{C}_{kl}$ are equal to zero, thus **C** is equal to [$\boldsymbol{\sigma}^{\mathbf{2}}$] and (3.3.4) reduces to (3.3.3). Since the minimum β for a given set of mean values is sought, an optimization of **x** that satisfies the limit state equation is required.

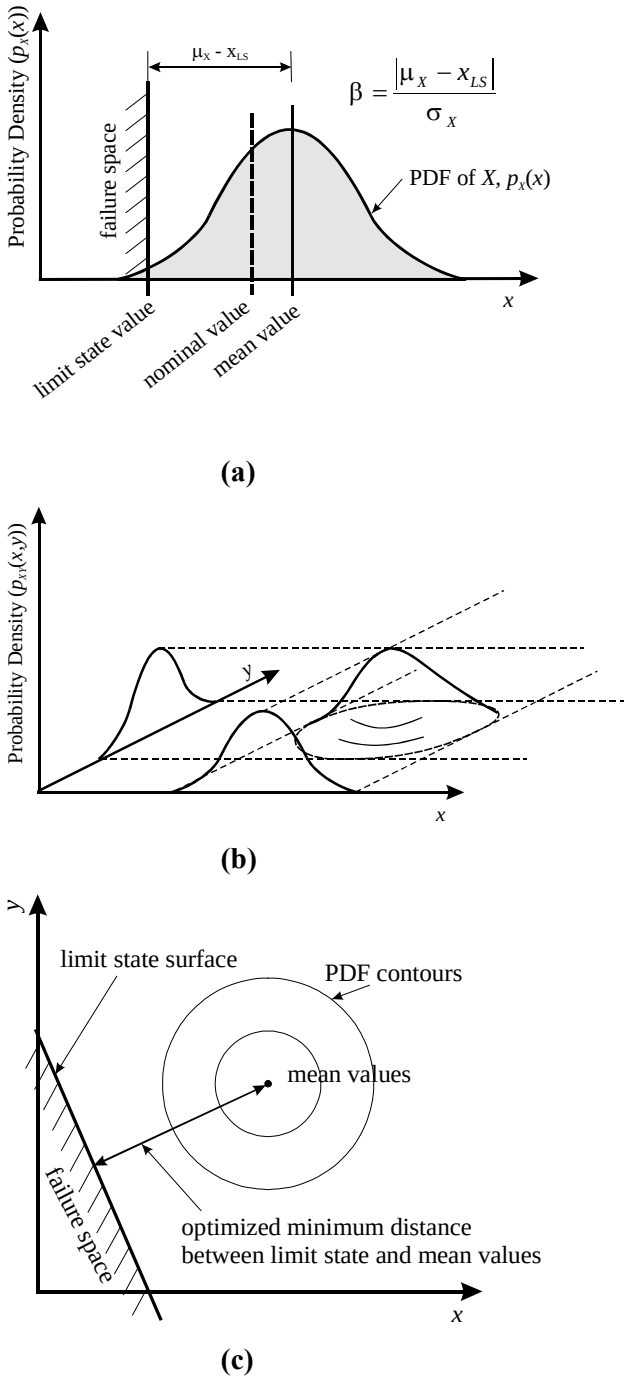

Figure 3.3.1. Depiction of Reliability Index: **(a)** one normally distributed random variable – here reliability index (β) is defined as the distance from the mean parameter value to its limit state value, normalized with respect to its standard deviation; **(b)** two normally distributed random variables; **(c)** a two-dimensional projection of (b) illustrating the concept of "distance" to the limit state surface.

In LRFD, the goal is to have a set of load and resistance factors that will allow the engineer to produce designs with a consistent reliability index. Therefore, in the determination of load and resistance factors, the reliability index must be set equal to a certain value in order to attain uniform reliability throughout a structural and geotechnical system. Ellingwood et al. (1980) argued that this target reliability index should be 3.0 for gravity loading situations. Some structural elements, such as steel connections have target reliability indices greater than 3.0 (Fisher et al., 1978). In these cases, a major driving concern is to provide for a plastic, gradual failure of the overall structure rather than a brittle, sudden one. Vesic (1973) argued that foundations are loaded in a load-controlled mode and that, under some conditions, sudden bearing capacity failures could occur. However, most footings are members of a larger system of redundant footings, with the possibility of settlements and load transfer between footings prior to any structural collapse. Therefore, considering each footing as a component of a structural system, a reliability index of 3.0 is consistent with existing structural practice, even in the relatively few cases where “brittle” foundation failure would be possible.

Computation of resistance values using a target reliability index can be accomplished with an iterative scheme. First, initial mean values of the variables governing a foundation design are selected, defining a point in multi-variable space. The reliability index for this initial trial is computed by finding **x** in (3.3.4) with the requirement that **x** be on the limit state surface and minimize β. These computations can be efficiently executed using the spreadsheet formulation of Low and Tang (1997). In this formulation, non-normal PDFs are substituted by normal distributions such that the cumulative probability at the limit state value is equal to that for the non-normal PDF.

Once a value of β is obtained, it is compared with the target value. Trial mean values are adjusted and reliability indices computed iteratively until the target β is satisfied. The output of this optimization for one design case is a set of limit state and nominal design values for which the minimum β is equal to the target reliability index.

Computing Load and Resistance Factors

With the nominal and limit state points known, load and resistance factors can be determined. The value of resistance is calculated for the point on the limit state surface defined by (3.3.1) as

$$R_{LS} = \left(B_{LS} \cdot L_{LS}\right)\left(\frac{1}{2} \cdot \gamma_{LS} \cdot B_{LS} \cdot N_{\gamma_{LS}} \cdot s_{\gamma_{LS}} + \gamma_{LS} \cdot D_{f_{LS}} \cdot N_{q_{LS}} \cdot s_{q_{LS}} \cdot d_{q_{LS}}\right) \qquad \textbf{(3.3.5)}$$

where R is the resistance and the subscript LS denotes values on the limit state surface. Next, the value of resistance for the design values is found using

$$R_n = \left(B_n \cdot L_n\right)\left(\frac{1}{2} \cdot \gamma_n \cdot B_n \cdot N_{\gamma_n} \cdot s_{\gamma_n} + \gamma_n \cdot D_{f_n} \cdot N_{q_n} \cdot s_{q_n} \cdot d_{q_n}\right) \qquad \textbf{(3.3.6)}$$

where n denotes the nominal resistance values (the values used for design). The resistance reduction factor $(RF)^*$ can then be calculated as

$$(RF)^* = \frac{R_{LS}}{R_n} \qquad \textbf{(3.3.7)}$$

Here, the asterisk is used to denote an optimum RF value determined in analysis. Optimum load factors $(LF)^*$ are also determined as

$$\left(LF\right)_i^* = \frac{Q_{i,LS}}{Q_i} \qquad \textbf{(3.3.8)}$$

where Q_i is the design value of the load and $Q_{i,LS}$ is the value of a load for the corresponding point on the limit state surface. The optimum *RF* is only applicable when considered in conjunction with these load factors.

The resistance reduction factor must be modified to be applicable to load factors – $(LF)_{DL}$ and $(LF)_{LL}$ – developed by code-writing authorities. Prevention of an ultimate limit state requires that the factored resistance must be greater than or equal to the factored load,

$$RF^* \cdot R_n \geq (LF)^*_{DL} \cdot DL + (LF)^*_{LL} \cdot LL \qquad \textbf{(3.3.9)}$$

Inequality (3.3.9) can be maintained when using load factors other than the optimum load factors by multiplying both sides by the least of $(LF)_{DL}/(LF)^*_{DL}$ or $(LF)_{LL}/(LF)^*_{LL}$. This operation yields

$$RF = RF^* \cdot \min\left\{\frac{(LF)_{DL}}{(LF)^*_{DL}}, \frac{(LF)_{LL}}{(LF)^*_{LL}}\right\} \qquad \textbf{(3.3.10)}$$

Note that this correction is conservative for any value of the LL/DL ratio.

3.4 Summary

In this chapter, we proposed a framework for the rational assessment of resistance factors for use in geotechnical LRFD. We presented tools to assess the uncertainty of random variables appearing in design equations. Finally, we presented a methodology to compute resistance factors within the framework. In the next chapter, we demonstrate steps 1-6 of the framework to determine variable uncertainties for shallow foundation design.

CHAPTER 4. ASSESSMENT OF VARIABLE UNCERTAINTY FOR SHALLOW FOUNDATIONS

4.1 Assessment of Uncertainty in Bearing Capacity of Footings on Sand

In this section, each of steps 1-6 of the rational framework for evaluating resistance factors discussed in Chapter 3 is demonstrated for shallow foundations on sand.

Step 1. Identify limit state equation

The equation for fully drained conditions for sand is considered. For rectangular footings on sand, the bearing capacity limit state equation is

$$\frac{DL + LL}{B \cdot L} - \left(\gamma \cdot D \cdot N_q \cdot s_q \cdot d_q + \frac{1}{2} \gamma \cdot B \cdot N_\gamma \cdot s_\gamma \right) = 0 \qquad \textbf{(4.1.1)}$$

where DL is the dead load, LL is the live load, B and L are the footing plan dimensions, γ is the design soil unit weight, D is the footing base depth, N_q and N_γ are bearing capacity factors, and s_q, s_γ and d_q are correction factors for footing shape and depth of embedment of the footing. Equation (4.1.1) represents a design check against the possibility that the foundation will experience a classical bearing capacity failure. A reliability analysis relevant to this design check must consider the probability that the bearing capacity is evaluated to be less than required to support the load placed on the foundation.

Step 2. Identify the component variables

Of the variables in Equation (4.1.1), B, L, and D are selected by the designer; DL and LL are outputs of the design of the superstructure; γ is estimated or measured; and

factors N_q, N_γ, s_q, s_γ and d_q are determined using transformations from friction angle ϕ_p and B, L and D. Friction angle ϕ_p can be computed from Bolton (1986):

$$\phi_p = \phi_c + \xi\left[\frac{D_R}{100}\cdot\left(Q - \ln\left(\frac{\frac{1+\sin\phi_p}{1-\sin\phi_p}+2}{3}\cdot\sigma'_h\right)\right) - R_Q\right] \qquad \textbf{(4.1.2)}$$

where Q and R_Q are constants (typically 10 and 1) and ϕ_c is the critical state friction angle, an intrinsic property for a sand. Coefficient ξ in (4.1.2) is equal to 5 for plane strain and 3 for triaxial compression conditions. Horizontal effective stress σ'_h is a representative value estimated by the designer for a depth approximately 0.5B below the footing base. Relative density D_R can be determined by using correlations with the CPT or SPT.

Step 3. Identify the geotechnical tests associated with each variable

Two geotechnical tests have been identified, the CPT and the SPT. Because of the transformations identified in Step 2, the uncertainties in CPT tip resistance q_c and SPT blow count N influence the uncertainty of factors N_q, N_γ, s_q, and d_q in Equation (4.1.1). The influence of q_c is illustrated in Figure 4.1.1.

Figure 4.1.1 is a schematic representation of the variabilities in Equation (4.1.1), including the component *COVs*. A number appears immediately under each variable in Figure 4.1.1. This number represents the *COV* associated with that variable. The reference (a number in a circle) for this value is presented when the variable is an input variable, not a calculated variable. An arrow between two variables in Figure 4.1.1 represents a transformation. The number inside the arrow represents the *COV* of that particular transformation, calculated with respect to its output. The *COV* of a

transformed variable (the output) is a reflection of both the *COV* of the original variable and of the transformation. Thus, moving from transformation to transformation in sequence, the *COVs* presented are composites of the variabilities introduced by the original variables and the preceding transformations. Details of how these COVs have been determined appear in the following subsections.

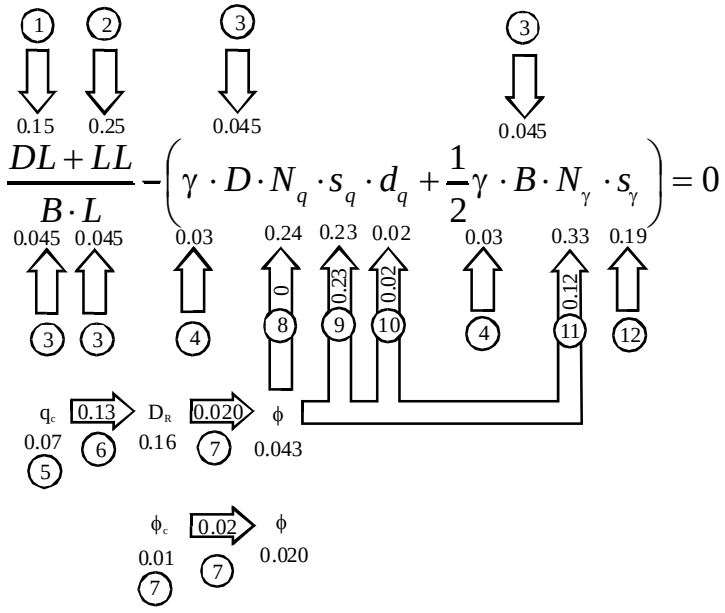

No.	Source	Use of Source
1	Nowak(1994) and Ellingwood(1999)	Reported COV – dead load
2	Ellingwood(1999)	Reported COV – live load
3	ACI (1990)	Standard tolerances – variability of footing dimensions
4	Hammitt (1966)	Reported COV – unit weight
5	Withiam et. al. (1997), Purdue University	Reported COV and CPT logs – variability of q_c
6	Salgado and Mitchell(2003)	Data on q_c predictions from D_r – variability of D_r
7	Bolton(1986)	Equation to calculate ϕ_p from D_r
8	Reissner (1924)	Deterministic relationship for N_q
9	DeBeer (1970)	Data on bearing capcity – variability of s_q
10	Bandini (2003)	Limit analysis results – variability of d_q
11	Sloan and Yu (1994)	Limit analysis results – variability of N_γ
12	DeBeer (1970)	Data on bearing capcity – variability of s_γ

Figure 4.1.1. Sources of Uncertainty with Coefficients of Variation (COVs) for Bearing Capacity in Sand. Numbers below variable symbols represent variable COVs. Numbers in arrows indicate transformation COVs (in terms of result). Numbers in circles indicate references.

Step 4. Identify all component uncertainties for each variable, including transformations

For some variables, the uncertainty is very small, and the contribution of their uncertainty to the overall variability of bearing capacity becomes negligible when compared with other variables. For these variables, namely unit weight γ and footing dimensions *B*, *L*, and *D*, *COV* values from the literature have been used. The *COVs* and distribution types for these variables are reported in Table 4.1.1.

Table 4.1.1. COVs, Bias Factors and Distribution Types for use in a Probabilistic Analysis of Bearing Capacity on Sand and Clay

variable	COV	bias	dist. type
DL	0.15	1.05	normal
LL	0.25	1.15	lognormal
γ	0.03	1	normal
D_f	0.045	1	normal
B	0.045	1.05	normal
L	0.045	1.05	normal

The variability of unit weight has been examined by Hammitt (1966) using the results of nearly 100 different laboratories. The COV for unit weight was reported as 0.03. This value can be seen as quite reasonable by applying the six standard deviation (6σ) procedure. Suppose, for example, that a value for unit weight is guessed between 15 and 22 kN/m^3, an interval that is nearly certain to contain the totality of unit weight values of soils ranging from clay to sand. Suppose also that this unit weight guess follows a normal distribution with the mean representing the actual value of the unit weight. Applying the 6σ procedure using Equations (3.2.3) and (3.2.4), the COV of γ is computed as

$$COV = \frac{\sigma}{\mu} = \frac{Range}{6\mu} = \frac{(22-15)\text{kN/m}^2}{6\times 18.5\text{kN/m}^2} = 0.06 \qquad \textbf{(4.1.3)}$$

It is likely that even a simple measurement will be more accurate than such a guess, validating a COV of 0.03.

ACI 117 (ACI 1990) sets the tolerance for horizontal dimensions (*B*, *L*) of unformed footings with widths between 2ft and 6ft at –1/2 in to +6 in. A conservative estimate of the COV for footing dimensions is desired. Thus, according to (3.2.4), the smallest applicable value for μ should be used (2 ft., in this case). Applying the 6σ procedure and using 2ft as the mean, the COV for footing dimensions is 0.045. This value is also conservatively applied to formed footings since the small uncertainty in *B* and *L* has minimal effect on the reliability analysis.

For a tolerance of this nature specified by ACI – where the upper bound is substantially further from the design value than the lower bound – it is reasonable to assume builders will tend to err on the high side of design values. It is appropriate to apply a bias factor (Equation 3.2.13) to account for this tendency. According to equation (3.2.13), footing dimensions which are built, on average, larger than design(nominal) will have a bias factor greater than 1, as is the case in Figure 4.1.2. Using ACI 117, a conservative estimate of the bias factor for footing dimensions is 1.05. The bias factors for *B* and *L* is also presented with their *COV*s in Table 4.1.1.

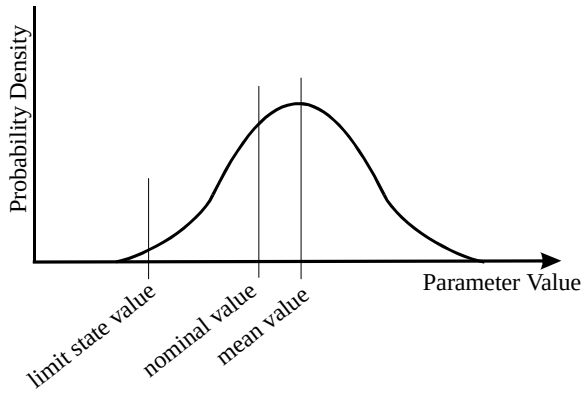

Figure 4.1.2. The mean, nominal, and limit state values of a normally distributed design parameter. Here, limit state value corresponds to the value at which a limit state such as bearing capacity failure is reached. Mean value is the mean of the distribution under consideration. Nominal value is the parameter value used in design. The mean can be calculated from the nominal by (nominal) * (bias factor).

Live Load *LL* and Dead Load *DL* variability has significant impact on the final uncertainty in bearing capacity. It has been examined thoroughly in Chapter 2. Nowak (1994) and Ellingwood (1999) report a COV and bias factor for dead load of 0.15 and 1.05, respectively. Ellingwood (1999) reports a COV and bias factor for live load of 0.25 and 1.15, respectively. These *COVs* and bias factors appear in Table 4.1.1.

As we will show later in Step 5, the uncertainty of capacity factors N_q, N_γ, s_q, and d_q will be determined from the uncertainties of measurement q_c or N and of the transformations from q_c to D_R, D_R to ϕ_p, and ϕ_p to the bearing capacity factors. This progression is illustrated by the arrows in Figure 4.1.1. Thus, in Step 4, it is necessary to find the uncertainty of q_c and of each of these transformations.

First, the assessment of the uncertainty in q_c is presented. The estimation of soil properties from in-situ test data involves uncertainties introduced by the inherent soil variability, the measurement uncertainty, and the transformation model uncertainty

(Phoon and Kulhawy 1999). Tip resistance q_c inherits uncertainty from the variability of the CPT measurements themselves as well as the variability of the soil profile. The variability of the test equipment is difficult to discern since very little human or random error is possible in the test (Kulhawy and Trautmann 1996). However, the variability of the overall measurement is readily observed by examining CPT logs. The value of the coefficient of variation of q_c presented in Withiam et. al. (1997) is 0.07. Values may be expected to be slightly higher for coarser sand and slightly lower for finer sand, but 0.07 was confirmed as reasonable in the current research by considering tip resistance versus depth profiles for various CPT tests in sand. One of these profiles, for a reasonably uniform sand layer (same D_R), is presented in Figure 4.1.3. A power regression was performed on the data, conforming to the relationship expressed by Salgado and Mitchell (2003), according to which q_c varies with a power function of horizontal effective stress. This power function describes the mean line in Figure 4.1.3. The bounds in Figure 4.1.3, also varying with depth, were fit to the actual data points around the mean line. Using the 6σ procedure, the COV can be calculated using (3.2.3) and (3.2.4) as described earlier in the paper.

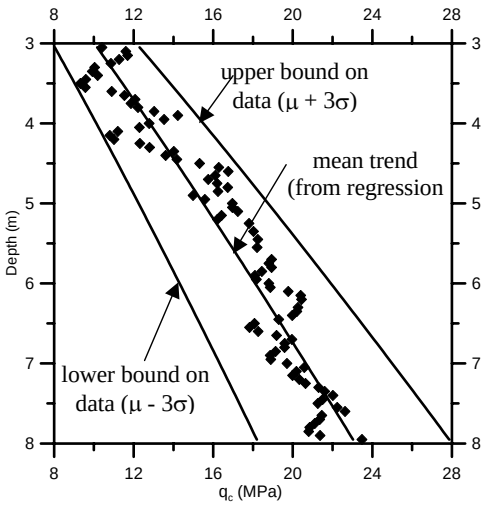

Figure 4.1.3. Mean Trend (power regression) and Bounds of CPT Tip Resistance Data for Sand. The mean and bounds can be used to calculate the COV for q_c using the 6σ procedure.

The SPT is subject to greater test uncertainty than the CPT (Kulhawy and Trautmann 1996). The additional uncertainty introduced by this test can be assessed by considering a transformation from *N* values to q_c values. The relationship between SPT blow count *N* and CPT tip resistance q_c in sand has been studied by Robertson et. al. (1983), Ismael and Jeragh (1986), and the geotechnical engineering group at Purdue University. Using their combined data (Figure 4.1.4), the modified 6σ procedure can be applied to compute the *COV* of the transformation from *N* to q_c using equations (3.2.5) and (3.2.4). The modified 6σ procedure is used since relatively few data points are available. The resulting COV is 0.16. The purpose of finding this transformation uncertainty is so that the cone tip resistance estimated by the SPT, $q_{c,SPT}$, may be used in place of *N* for the remaining transformations illustrated in Figure 4.1.1. Thus, uncertainties representing SPT- and CPT-based designs will be developed within the same framework. What is required, then, is a PDF describing the uncertainty of $q_{c,SPT}$. Note that the results of the side-by-side field CPTs and SPTs performed by Robertson et.

al. (1983) and Ismael and Jeragh (1986) reflect both the uncertainty of the in-situ sand and of the individual tests. Thus, the inherent soil variability and the SPT measurement uncertainty are fully accounted for. Thus, a normal distribution is selected for $q_{c,SPT}$ with a *COV* of 0.16.

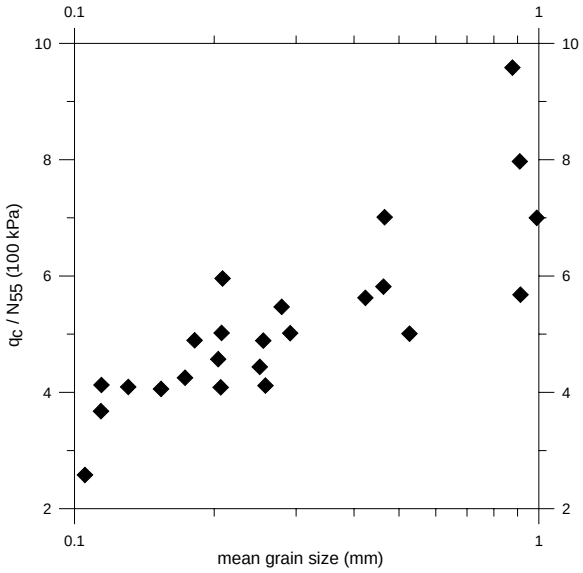

Figure 4.1.4. SPT – CPT correlation (after Robertson et. al.1983, Ismael and Jeragh 1986, and Purdue University)

The transformation from q_c to D_R is that proposed by Salgado and Mitchell (2003) based on the results of the most recent version of the CONPOINT program (Salgado et al. 1997, Salgado 2003),

$$D_R = \frac{1}{c_3}\ln\left[\frac{1}{c_1}\cdot\frac{q_c}{p_A}\cdot\left(\frac{p_A}{\sigma'_h}\right)^{c_2}\right] \qquad \textbf{(4.1.4)}$$

where p_A is a reference stress, σ'_h is the horizontal effective stress, and constants c_1, c_2 and c_3 are related to intrinsic properties of sands. The predictive capability of an equation like (4.1.4) to determine values of q_c from a known D_R in the lab was examined by Salgado, Mitchell and Jamiolkowski (1997). Experimental values of q_c were found to fall

within a ± 30% band of predicted values. The 6σ procedure was applied to find the *COV* of this predicted q_c, yielding a value of 0.10. Taking q_c as normally distributed with a *COV* of 0.10, Equation (3.2.7) can be used to find the PDF of D_R. This PDF, representing the transformation uncertainty from q_c to D_R, was found to be normally distributed with a standard deviation between 3% and 6% depending on the specific value of relative density. The *COV* in Figure 4.1.1 representing the uncertainty of this transformation is that of a representative case.

The transformation from D_R to ϕ_p (Equation 4.1.2) was calibrated against lab-measured values of D_R (Bolton, 1986). With respect to the accuracy of (4.1.2), Bolton reported a ±1º band encompassing all measurements of ϕ_c and a ±2º band capturing all measured values of $\phi_p - \phi_c$ about predicted values. First, the 6σ procedure was applied to find the *COV* of ϕ_c and $\phi_p - \phi_c$. Then, numerical integration of Equation (3.2.9) was used to find the PDF of the D_R to ϕ_p transformation, just as was done for the N to q_c correlation. The resulting transformation PDF was found to be a normal distribution with a *COV* of 0.020. The same *COV* found using Monte Carlo simulation was 0.015.

The bearing capacity factors N_γ, s_q, and d_q have uncertainties due to the transformations required to compute them. The uncertainty of these transformations has been examined using tools such as limit analysis and test data. Factor N_q is calculated from the exact relationship given by Reissner (1924):

$$N_q = e^{\pi \tan\phi} \cdot \tan^2\left(45 + \frac{\phi}{2}\right) \qquad \textbf{(4.1.5)}$$

Since it is exact, the arrow representing the ϕ_p to N_q transformation in Figure 4.1.1 reports a COV of zero.

Factor N_γ is found using Brinch Hansen (1970) expression:

$$N_\gamma = 1.5 \cdot \left(e^{\pi \tan\phi} \cdot \tan^2\left(45 + \frac{\phi}{2}\right) - 1 \right) \cdot \tan\phi \qquad \textbf{(4.1.6)}$$

The results of numerical limit analysis by Sloan and Yu (1996) were used to determine the possible range of the values of N_γ with respect to ϕ_p. Since the true value of N_γ is in fact guaranteed by limit analysis to be within the limit bounds for a given friction angle, the probability of N_γ being so bound is 100%, not the 99.7% associated with the 6σ procedure. However, for practical purposes, the 6σ deviation procedure can be used effectively. Using the 6σ procedure, the *COV* of the ϕ_p to N_γ transformation was found to be 0.12.

Limit analysis was again used to determine the possible range of the values of d_q with respect to *D*/*B* ratio based on results by Bandini (2003). Using the 6σ procedure, the *COV* of the ϕ_p to d_q transformation was found to be 0.02.

The *COVs* for the shape factors s_q and s_γ can be determined by making reference to more than fifty tests performed by DeBeer (1970). The modified 6σ procedure (Equation 3.2.5) is used since relatively few data points are available. The resulting *COVs* are 0.23 and 0.19 for the ϕ_p to s_q transformation and factor s_γ, respectively.

At this point, the uncertainties for all of the relevant geotechnical tests, transformations and other design variables have been described. The next step will be to combine these uncertainties to describe the PDFs for each of the variables that appear in Equation (4.1.1).

Steps 5 and 6. Evaluate the composite uncertainties and select PDFs for reliability analysis

Numerical integration of Equation (3.2.9) was used to find the uncertainty of each of transformed variables D_R, ϕ_p, N_q, s_q, d_q, and N_γ. For example, to compute the histogram representing the uncertainty of D_R using (3.2.9), $p_X(x)$ was defined as a normal distribution with COV = 0.07, representing q_c, and $p_{Y|X}(y \mid x)$ was defined as a normal distribution with σ = 0.06, representing equation (4.1.4). The resulting histogram $p_Y(y)\Delta y$ represents the uncertainty of D_R computed using q_c and equation (4.1.4). Computations of the uncertainty of ϕ_p, N_q, s_q, d_q, and N_γ had comparable results using Monte Carlo simulation.

The *COVs* to be used in reliability analysis are those computed from the numerical integration results, as this is the most accurate technique. Computed values of *COV* for variables N_q, s_q, d_q, and N_γ. are reported in Tables 4.1.2 and 4.1.3 for different values of ϕ_p. Table 4.1.2 is used for reliability analysis of designs relying on the CPT while Table 4.1.3 is for the SPT. *COVs* for N_q and N_γ vary significantly with ϕ_p due to the increasing slope of Equations (4.1.5) and (4.1.6) with ϕ_p. Representative *COVs* from Table 4.1.2 appear in Figure 4.1.1.

The final task to fully describe the uncertainty of each variable is to select a PDF. The shapes of the histograms generated through the numerical integration of (3.2.9) and through Monte Carlo simulation are used to determine representative PDFs with closely matching shapes. Example histograms representing the distributions of ϕ_p, N_q, s_q, and N_γ appear in Figure 4.1.5. The shape of the histograms for ϕ_p, s_q, and d_q resemble normal

distributions. Thus, normal distributions are used to represent these variables. The shape of the histograms for N_q and N_γ suggests the use of lognormal distributions. The distribution type selected for each variable also appears in Tables 4.1.2 and 4.1.3.

Table 4.1.2. COVs, bias factors and distribution types for bearing capacity factors for use in reliability analysis of footings on sand using the CPT

		N_q - lognormal		N_γ - lognormal		d_q - normal		s_q - normal	
Footing type	ϕ_p	COV	bias	COV	bias	COV	bias	COV	bias
Square	36.5	0.21	1.12	0.30	1.17	0.02	1.00	0.23	1.00
	39.5	0.24	1.14	0.33	1.19	0.02	1.00	0.23	1.00
	42.8	0.31	1.16	0.41	1.22	0.03	1.00	0.23	1.00
strip	38.7	0.34	1.24	0.46	1.34	0.03	1.00		
	43.5	0.41	1.28	0.54	1.38	0.03	1.00		
	48.5	0.47	1.30	0.63	1.49	0.03	1.00		

Table 4.1.3. COVs, bias factors and distribution types for bearing capacity factors for use in reliability analysis of footings on sand using the SPT

		N_q - lognormal		N_γ - lognormal		d_q – normal		s_q - normal	
Footing type	ϕ_p	COV	bias	COV	bias	COV	bias	COV	bias
square	39.5	0.32	1.13	0.42	1.19	0.08	1.00	0.24	1.00
	42.8	0.34	1.16	0.45	1.21	0.04	1.00	0.23	1.00
strip	43.5	0.55	1.33	0.70	1.47	0.06	1.00		
	48.5	0.61	1.38	0.72	1.50	0.04	1.00		

Each of these PDFs is not fully described without considering if a bias factor is required. As mentioned in the bias factor subsection, bias factors for N_q and N_γ are needed due to the effect of the non-linear transformations in (4.1.5) and (4.1.6). As seen in Figure 4.1.1, values of the bearing capacity factors ultimately depend on values of q_c. In Chapter 5, we suggest that the designer conservatively select a value of q_c that is 0.84 standard deviations less than the mean. Thus, bias is introduced to every design parameter that is a transformation of q_c. As a result, the means of the bearing capacity factors are different from the biased values used in design (Figure 4.1.2). Thus, bias factors are computed using (3.2.13). Inputs to (3.2.13) are the means, computed from the

histograms found using numerical integration of (3.2.9), and nominal values, determined using the design equations presented earlier with the conservative q_c value. These bias factors are also reported in Tables 4.1.2 and 4.1.3.

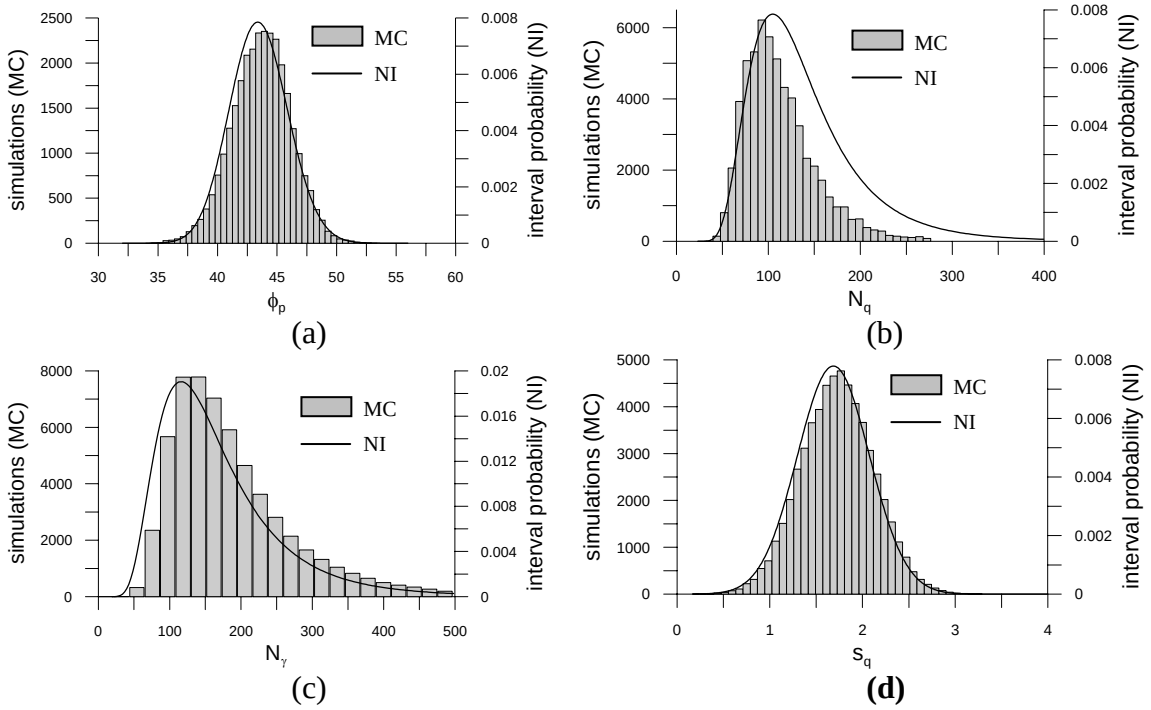

Figure 4.1.5. Example Histograms of Monte Carlo Simulation (MC) and Numerical Integration (NI) Results for ϕ_p, N_q, N_γ, and s_q

4.2 Assessment of Uncertainty in Bearing Capacity of Footings on Clay

Step 1. Identify limit state equation

The equation for fully undrained conditions for clay is considered. The bearing capacity limit state equation is

$$\frac{DL+LL}{B\cdot L}-\left(s_u\cdot N_c\cdot d_c\cdot s_c+\gamma\cdot D\right)=0 \qquad \textbf{(4.2.1)}$$

where s_u is the undrained shear strength.

Step 2. Identify the component variables

Of the variables in Equation (4.2.1), *DL*, *LL*, *B*, *L*, *D*, and γ have already been treated in the sand section (see Table 4.1.1). N_c, d_c, and s_c are factors depending on the problem geometry (described by *B*, *L*, and *D*). The equations defining s_c and d_c for use in design are taken from Salgado et al. (2004),

$$d_c = 1 + 0.27 \cdot \sqrt{\frac{D}{B}} \qquad \textbf{(4.2.2)}$$

and

$$s_c = 1 + 0.12 \cdot \frac{B}{L} + 0.17 \cdot \sqrt{\frac{D}{B}} \qquad \textbf{(4.2.3)}$$

Undrained shear strength s_u can be determined from lab and in-situ test correlations.

Step 3. Identify the geotechnical tests associated with each variable

The CPT or laboratory testing (such as the unconfined compression test) can be used to find values of s_u. Thus, q_c or s_u is the measured test value associated with Equation (4.2.1), depending on the test performed.

Step 4. Identify all component uncertainties for each variable, including transformations

The variability of q_c in clay was estimated using CPT logs from the literature in known uniform clay deposits. By selecting this group of data, the variability of q_c in clay only, not an aggregate profile of clay and other materials, can be assessed. Ten logs from two papers were analyzed – Jacobs and Coutts (1992) and Baligh et. al. (1980) – using the 6σ procedure exactly as performed on the sand q_c data (Figure 4.1.3). As before, only logs or portions of logs for one reasonably uniform layer were considered. From this data, the COV for q_c in clay was found to be 0.06.

From tip resistance q_c, s_u can be determined from

$$s_u = \frac{q_c - \sigma_v}{N_k} \qquad \textbf{(4.2.4)}$$

where σ_v is the vertical stress and N_k is the cone factor. Limit analysis of circular foundations in clay by Salgado et al. (2004) is used to analyze the expected value of the cone factor and its uncertainty. The value of N_k according to Salgado et al. (2004) is between 11.0 and 13.7. Unlike N_γ, no other information concerning the mean value of N_k is used here. Thus, the least biased estimate (Harr 1987) of the PDF of N_k, representing the uncertainty of transformation (4.2.4), is a uniform distribution between 11.0 and 13.7.

The uncertainty of s_u as determined in the lab can be estimated by considering the extreme case of the unconfined compression test, which should be more uncertain than most other lab tests, such as triaxial testing, in common use. Phoon (1995) reports a number of papers addressing the uncertainty of this test. A representative value given by the author is a *COV* of 0.30. This value is confirmed by a paper on undrained testing by Matsuo and Asaoka (1977). Matsuo and Asaoka (1977) examined the uncertainty and spatial variability of undrained laboratory tests on marine clays. They attribute the uncertainty of s_u to inherent soil variability and sample disturbance. Hence, it is natural that the uncertainty found for laboratory testing for s_u is higher than that for in-situ CPT testing since the scatter in q_c measurements is largely controlled by local soil variability.

Since the COV of undrained shear strength from laboratory tests is much higher than that found for CPT determinations, continued use of the normal distribution for s_u is not likely to be realistic. A better suited PDF for strength would include the bounded distributions, such as the beta or lognormal distributions. Lognormal distributions are in

common use for this parameter in the literature. Therefore a lognormal distribution is used to represent the uncertainty of s_u in reliability analysis.

The value of N_c is known exactly as $2 + \pi \approx 5.14$ and therefore has no uncertainty (Prandtl 1920). However, factors s_c and d_c are not known exactly. The uncertainties of these factors can be accounted for using the results of limit analysis. Salgado et al. (2004) report upper and lower bounds on a lumped bearing capacity factor $N_c s_c d_c$ at different embedment ratios for strip and square footings. Applying the same least biased principle as for N_k, these results can be used directly to define a set of uniform distributions for $N_c s_c d_c$. For this type of PDF, the upper and lower bounds define the distribution completely. The distribution bounds are given in Table 4.2.1.

Steps 5 and 6. Evaluate the composite uncertainties and select PDFs for reliability analysis

Numerical integration of Equation (3.2.9) was used to find the uncertainty of s_u determined from q_c. To compute the histogram representing the uncertainty of s_u using (3.2.9), $p_X(x)$ was defined as a normal distribution with COV = 0.06, representing q_c, and $p_{Y|X}(y \mid x)$ was defined as a uniform distribution with bounds 11.0 and 13.7, representing factor N_k from equation (4.2.4). The resulting histogram $p_Y(y)\Delta y$ represents the uncertainty of s_u computed using q_c and equation (4.2.4). From this histogram, s_u was found to be normally distributed with COV = 0.09.

Table 4.2.1. Uniform Distribution Bounds on $N_c s_c d_c$ for varying embedment ratios for use in a Probabilistic Analysis of Bearing Capacity on Clay **(**Salgado et al. 2004)

D/B	Strip footing		Square footing	
0.00	5.132	5.203	5.523	6.221
0.01	5.164	5.271	5.610	6.498
0.05	5.293	5.396	5.886	6.830
0.10	5.448	5.536	6.171	7.129
0.20	5.696	5.802	6.590	7.516
0.40	6.029	6.137	7.194	8.092
0.60	6.240	6.341	7.671	8.577
0.80	6.411	6.508	8.068	9.004
1.00	6.562	6.656	8.429	9.355
2.00	7.130	7.229	9.752	10.861
3.00	7.547	7.655	10.532	12.000
4.00	7.885	7.997	10.941	12.879
5.00	8.168	8.286	11.206	13.603

The PDF representing $N_c s_c d_c$ was defined completely in step 4. The bounds of the uniform distribution desribing the uncertainty of $N_c s_c d_c$ appear in Table 4.2.1. The PDFs for *DL*, *LL*, *B*, *L*, *D*, and γ have been defined in the sand section and are reported in Table 4.1.1.

4.3 Summary

In this chapter, steps 1-6 of the framework were demonstrated to determine the variable uncertainties for ultimate limit state design checks of shallow foundation on sand and clay. The next steps, 7-10, to determine resistance factors for shallow foundation ULS design are demonstrated in the next chapter.

CHAPTER 5. ASSESSMENT OF RESISTANCE FACTORS FOR SHALLOW FOUNDATIONS

5.1 Calculation of Resistance Factors

Input Variables

Before any calculations can take place, the governing limit state equation must be defined and the COVs and bias factors must be established for each variable of the equation. This procedure was demonstrated in Chapter 4. With the variable COVs, target β, and reliability analysis method defined, *RF*s can be computed.

A large number of possible design parameters exist in foundation design. There are also many design and test methods. Each of these will lead to different uncertainties in the overall problem. Therefore, a complete analysis of the problem will consider a range of design parameters. Eight sets of design conditions are considered – strip and square footings on sand using the CPT and SPT, and strip and square footings on clay using the Salgado et al. (2004) and the Meyerhof (1951) shape and depth factors. Resistance factors are computed for different values of the live- to dead-load ratio (LL/DL), strength parameter (expressed as either friction angle ϕ or undrained shear strength s_u), and relative embedment (D/B).

Live load is more uncertain than dead load. Trends observed by Galambos et al. (1982), Milford (1987), and Tabsh (1997) indicate that the influence of the additional uncertainty introduced by live load is greatest for small values of LL/DL and decreases for greater values of LL/DL. This influence becomes negligible for LL/DL $\geq$ 4. Also, results in Ellingwood et al. (1982) indicate that, in calibration, resistance factors also

effectively cease to change for LL/DL ≥ 4. This upper boundary will therefore allow both a thorough analysis and safe RF values for design. A lower bound is taken as LL/DL = 0.5.

For footings on sand, values of friction angle ϕ were considered from 35º to 42º and from 37º to 48º for square and strip footings, respectively. For clay, values of undrained shear strength considered were s_u = 150kPa and s_u = 800kPa. Embedment ratios were considered from D/B = 0 to D/B = 1 since shallow foundations are usually defined for D/B ≤ 1.

Structural design codes using the ASCE-7 (1996) load factors include ACI 318-02 (ACI, 2002) and AISC 3rd ed. (AISC 2001). For the dead- and live- load combination, these load factors are $(LF)_{DL}$ = 1.2 and $(LF)_{LL}$ = 1.6. AASHTO (1998) load factors are $(LF)_{DL}$ = 1.25 and $(LF)_{LL}$ = 1.75.

Sand

The results of the resistance factor computations for footings on sand are shown in Figure 5.1.1 (CPT) and Figure 5.1.2 (SPT) for ASCE-7 load factors. One trend is immediately apparent in all five square footing plots: a sharp increase in resistance factor from D/B = 0 to D/B = 0.1. This trend is due mostly to the difference in COV between N_q and N_γ. At D/B = 0, the 'γ' term of the bearing capacity equation is the only term contributing to resistance. At higher values of D/B, the 'q' term (which has lower uncertainty than the 'γ' term) contributes more to resistance. Hence, for these higher values of D/B, the uncertainty of the overall equation is less than at D/B = 0, causing the *RF* to increase.

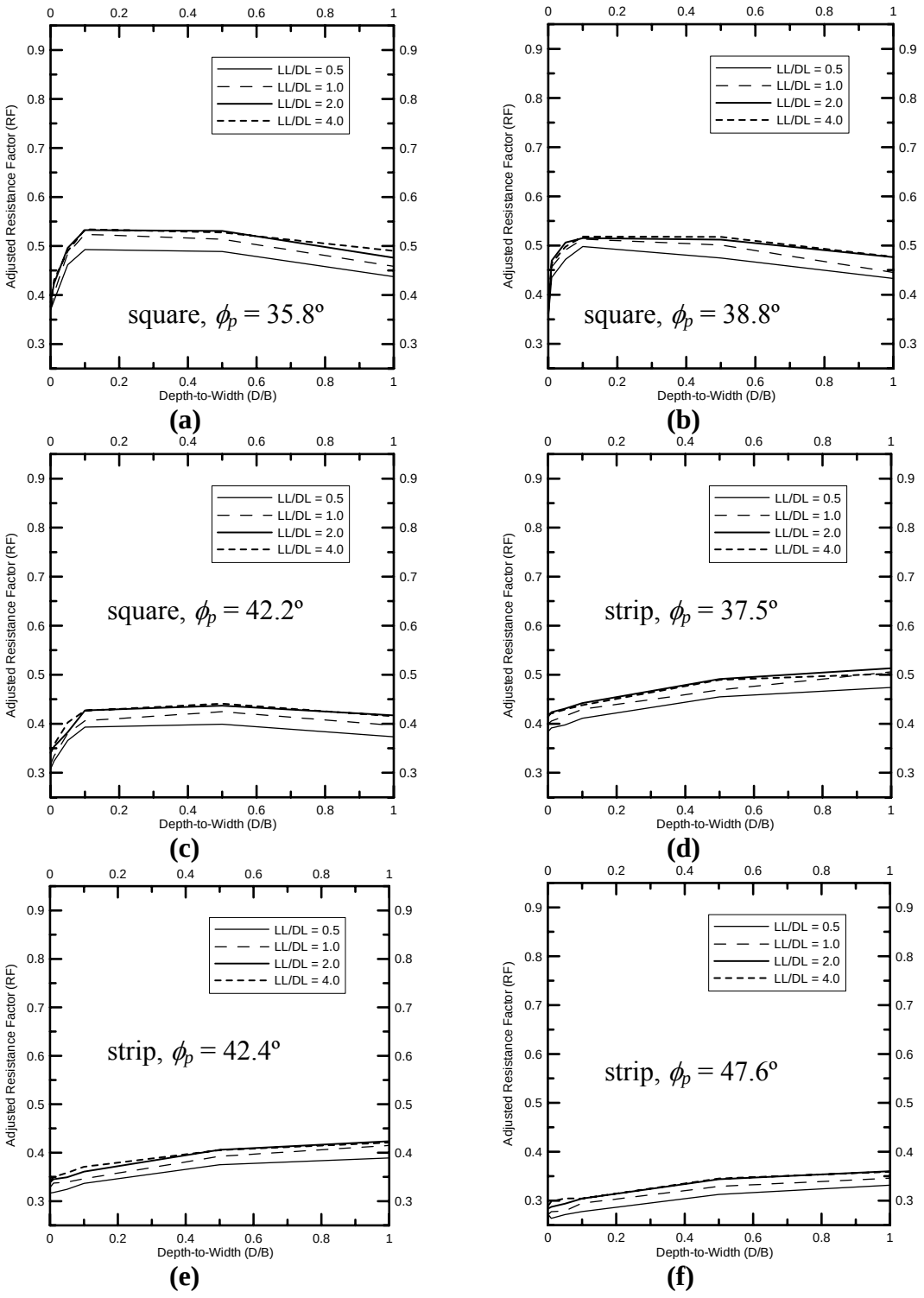

Figure 5.1.1. Adjusted Resistance Factors for Footings on Sand using CPT: Square: (a)ϕ_p = 35.8º, (b)ϕ_p = 38.8º, (c) ϕ_p = 42.2º; Strip: (d)ϕ_p = 37.5º, (e) ϕ_p = 42.4º, (f) ϕ_p = 47.6º

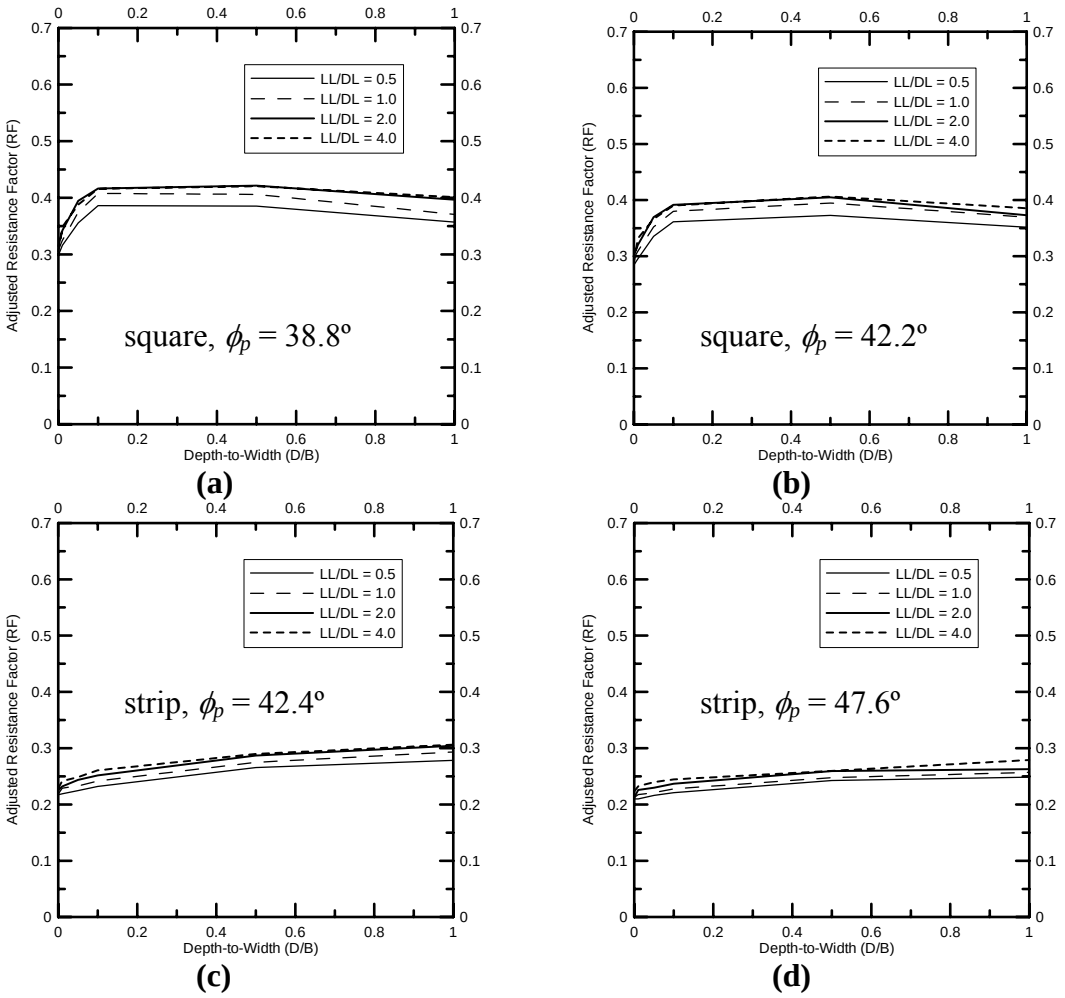

Figure 5.1.2. Adjusted Resistance Factors for Footings on Sand using SPT: Square: (a)ϕ_p = 38.8º, (b) ϕ_p = 42.2º; Strip: (c) ϕ_p = 42.4º, (d) ϕ_p = 47.6º

For square footings, a distinct trend of decreasing *RF* after approximately D/B = 0.5 illustrates another influence on *RF* computations. The optimization of (3.3.4) will yield a point on the limit state surface tangent to some contour of probability density about the mean values. Figure 5.1.3 illustrates a two-variable example where a change in the slope of the limit state curve will affect the calculated resistance factor. Considering the relationship between load capacity and bearing capacity factor N_q, a slope can be

defined for the relationship between N_q and load for a given design condition (values of D, B, s_q, d_q, s_γ). As D/B increases, values of D and d_q increase for a given value of B, indicating an increase in the slope of the limit state surface in N_q-load space. Note that σ_{dq} and σ_D will also increase, but μ_{sq} and σ_{sq} will remain constant, which affects the optimization of (3.3.4). This change in the N_q vs. load slope will move the location of the point of tangency between the limit state surface and the probabilistic distribution about the mean of N_q. As shown in Figure 5.1.3, this increase in slope will cause an increase in the separation between mean and limit state values of N_q, and therefore, a decrease in *RF*.

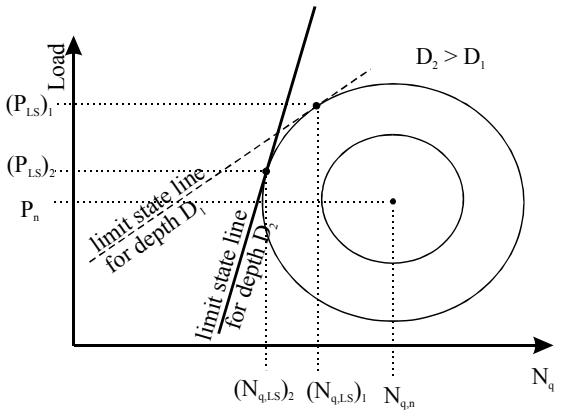

Figure 5.1.3. Two-Dimensional Explanation (similar to Figure 3.2.1c) of *RF* Curve Shapes in Figure 5.1.1(a-c) and Figure 5.1.2(a-b) – when the other bearing capacity variables change, the slope of the limit state surface at the point of consideration from depth 1 to depth 2 also changes – the optimum relative distance between nominal and limit state values is affected.

A very important result presented in Figures 5.1.1 and 5.1.2 is the effect of different friction angles ϕ on the computed value of *RF*. Since values of the bearing capacity factors increase exponentially with increasing ϕ, an overestimate of ϕ will significantly overestimate the nominal resistance of the footing. This possibility is

correctly accounted for in the reliability analyses, showing as decreasing values of *RF* for higher nominal values of ϕ.

Also of interest in Figures 5.1.1 and 5.1.2 are the curves for different *LL*/*DL* ratios. Due to the high uncertainty of live load relative to dead load, the plots could naively be expected to present a sequence of high to low *RF*s for low to high *LL/DL*s. However, this is not the case. The answer lies in the fact that the *RF*s cannot be considered in isolation, but always combined with load factors. Since different *LL/DL* ratios are presented, an assessment of the overall adjustment must consider the *LL/DL*, *LF*s, and *RF*s together. These quantities can be grouped as a factor of safety:

$$FS = \frac{(LF)_{DL} + (LF)_{LL}\left(\frac{LL}{DL}\right)}{\left(\frac{LL}{DL}+1\right)(RF)} \qquad \textbf{(5.1.1)}$$

Referring, for instance, to Figure 5.1.2(a), with a D/B of 0.5, the curves report a *RF* of 0.49 for *LL/DL* = 0.5 and 0.53 for *LL/DL* = 4.0. Considering also the *LF* values (LF_{DL} = 1.2 and LF_{DL} = 1.6) and *LL/DL*, Equation (5.1.1) yields values of factor of safety of 2.72 and 2.87, respectively. This result indicates that the factor of safety is greater for the *LL/DL* = 4.0 case despite the higher *RF*, and thus the greater load uncertainty is accounted for properly.

Two last observations are made. First, due to the uncertainty introduced by the SPT test procedure, RFs for designs using the SPT are lower than those using the CPT. Finally, in all cases for square footings, the change in resistance factor with embedment is greatest from *D/B* = 0 to *D/B* = 0.10. For this reason, recommended values of *RF* for

footings on sand are broken into two categories: $D/B < 0.10$ and $D/B \geq 0.10$. The recommended *RF* values appear in Table 5.1.1.

Table 5.1.1. Recommended Resistance Factors for Bearing Capacity on Sand and Clay**,** applicable for D/B ≤ 1

Design Case		ASCE-7 LFs		AASHTO (1998) LFs	
		D/B < 0.10	D/B ≥ 0.10	D/B < 0.10	D/B ≥ 0.10
Footings on Sand					
Strip Footings using CPT	$\phi \leq 38^o$	0.40		0.42	
	$\phi > 38^o$	0.25		0.26	
Strip Footings using SPT		0.20		0.21	
Rectangular Footings using CPT	$\phi \leq 39^o$	0.40	0.45	0.42	0.47
	$\phi > 39^o$	0.30	0.35	0.31	0.36
Rectangular Footings using SPT		0.30	0.35	0.31	0.36
Footings on Clay					
Strip Footings using Salgado et al. (2003) Factors (CPT)		0.70		0.73	
Strip Footings using Meyerhof (1951) Factors (CPT)		0.72	0.75	0.75	0.78
Rectangular Footings using Salgado et al. (2003) Factors (CPT)		0.73		0.76	
Rectangular Footings using Meyerhof (1951) Factors (CPT)		0.70	0.78	0.73	0.81
Strip Footings using Salgado et al. (2003) Factors (lab)		0.52		0.54	
Strip Footings using Meyerhof (1951) Factors (lab)		0.52	0.55	0.54	0.57
Rectangular Footings using Salgado et al. (2003) Factors (lab)		0.52		0.54	
Rectangular Footings using Meyerhof (1951) Factors (lab)		0.48	0.54	0.50	0.56

Clay

The results of the resistance factor computations for footings on clay designed using the CPT are shown in Figure 5.1.4. In Chapter 3 the concept of bias and the bias factor were presented. One use of the bias factor mentioned was to correct design equations so that they yield values equal to the mean values observed in analysis and testing. The bias introduced by the Meyerhof (1951) shape and depth factors, and the resulting effect on *RF*s is notable in Figure 5.1.4. A difference appears between the *RF*s computed using the Salgado et al. (2004) and by the Meyerhof (1951) factors. The

probability density functions (PDFs) of the composite bearing capacity factor ($N_c s_c d_c$) for clay presented in Chapter 4 were developed on the basis of the limit analysis results by Salgado et al. (2004). Thus the mean value of $N_c s_c d_c$ can be quite different from the nominal design value suggested by the Meyerhof (1951) design factor equations. The end result is that the resistance factors presented here behave partially as adjustment factors. In this study, bias factors have been applied to designs both on sand and on clay, but their use has particularly prominent effect in this example.

Three other noteworthy observations are made. First, *RF* decreases with increasing *LL*/*DL*. Second, unlike sands, the *RF* plots for clays do not show any pronounced change in *RF* over a particular *D/B* range (excluding the Meyerhof (1951) shape and depth factor correction mentioned above). Finally, in striking contrast to sand, the effect of different strength (s_u) values is negligible, as seen from the comparison of Figures 5.1.4(a) and 5.1.4(c).

Effect of Target Reliability Index

An important consideration in the selection of *RF* values for use in design is the appropriate target value of the reliability index to use. A target β of 3.0 was argued earlier as the most appropriate for shallow foundation ULS design. Figure 5.1.5 presents the results of the *RF* computations described above with varying target β values. In both sand and clay, the effect of changing β is quite significant, as expected. Charts such as these can act as valuable tool to assess the acceptable probability of classical ULS failure when compared with established design methodologies and factors. Also of note in

Figure 5.1.5(c) is the possibility of a *RF* greater than 1.0. This condition is due to the reasons discussed in the following section.

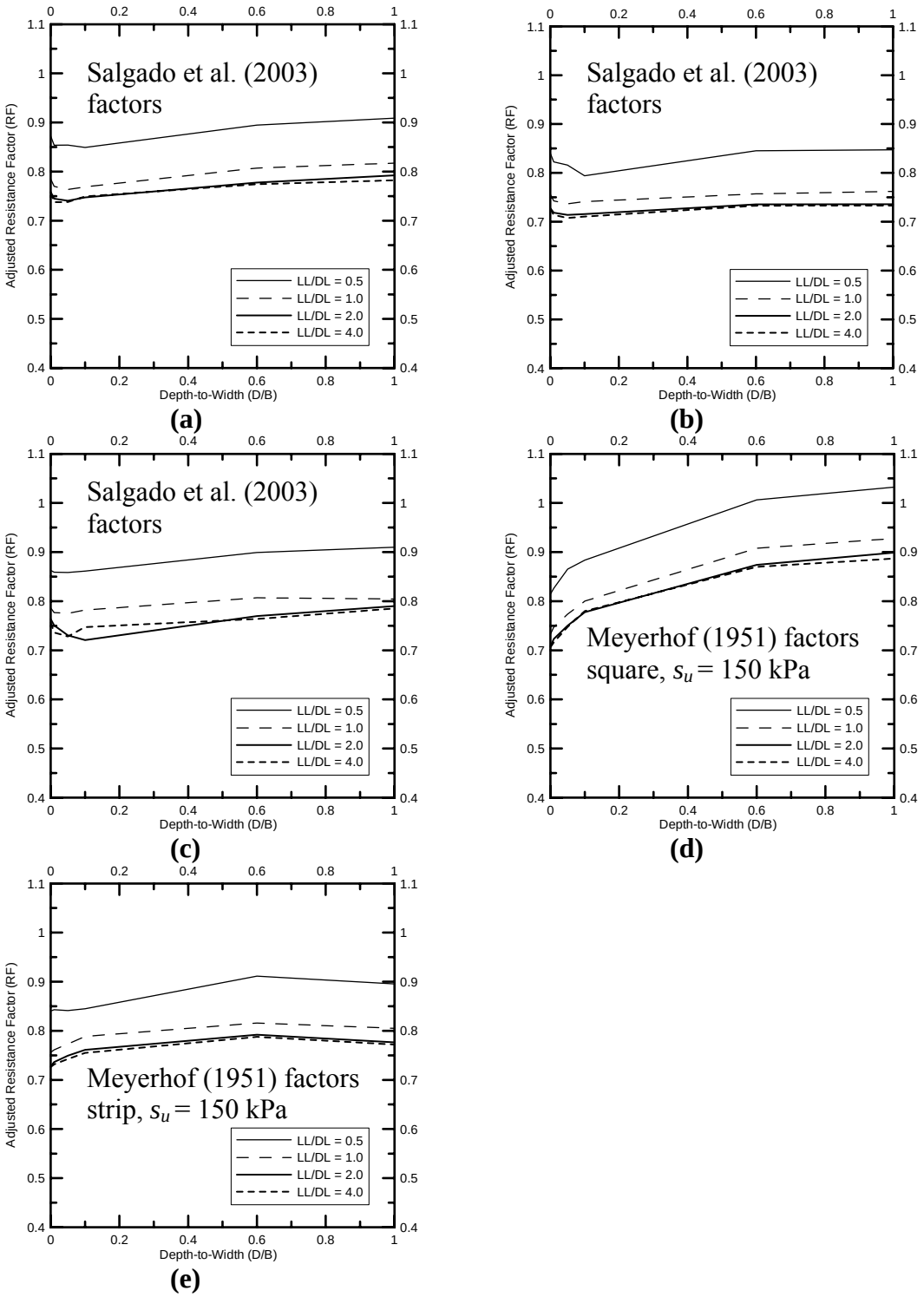

Figure 5.1.4. Adjusted Resistance Factors for Footings on Clay using CPT: Salgado et al. (2003) shape and depth Factors: (a) Square, s_u = 150 kPa, (b) Strip, s_u = 150 kPa, (c) Square, s_u = 800 kPa; Meyerhof (1951) Factors: (d) Square, s_u = 150 kPa, (e) Strip, s_u = 150 kPa

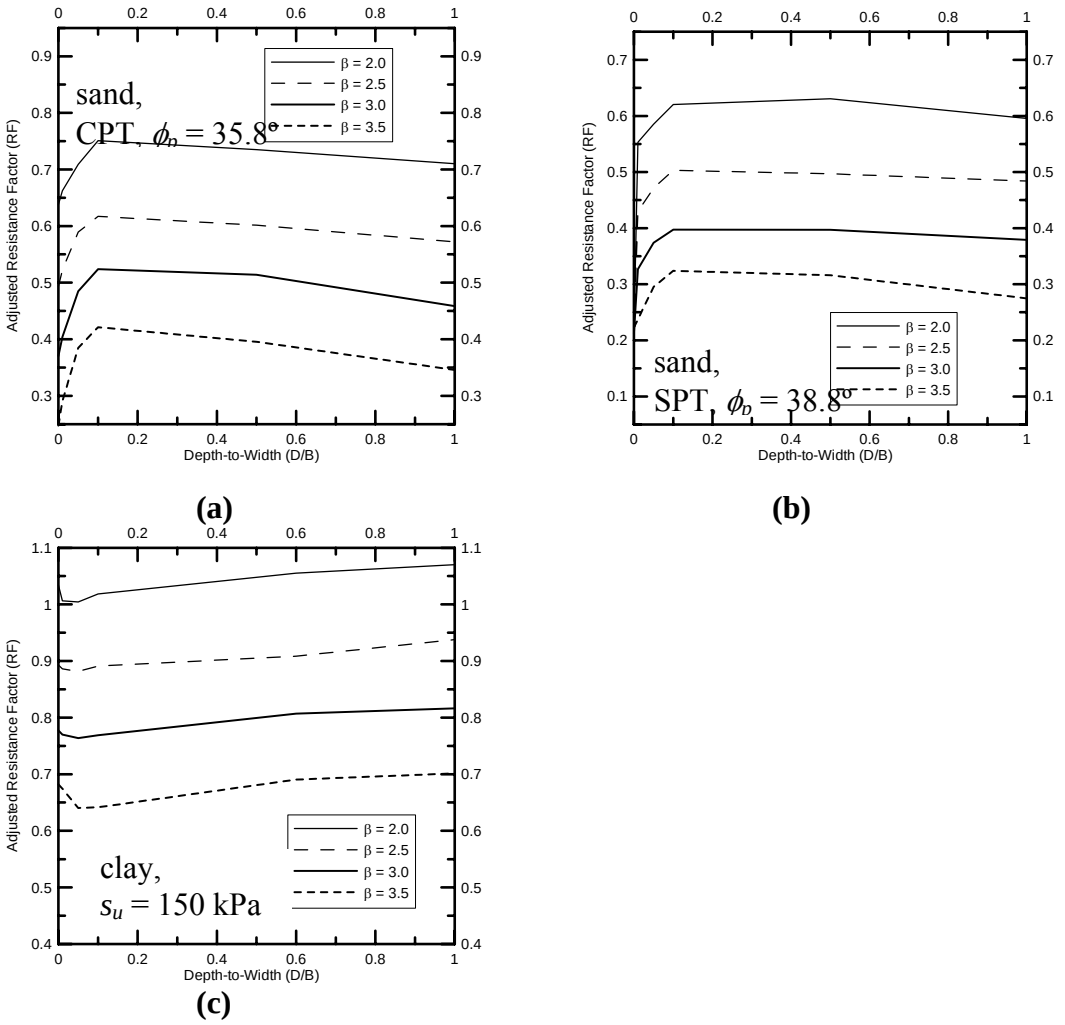

Figure 5.1.5. Adjusted Resistance Factors for a Square Footing, *LL/DL* = 1.0, varying β: (a) sand using CPT, ϕ_p = 35.8º, (b) sand using SPT, ϕ_p = 38.8º, (c) clay using Salgado et al. (2003) Factors, s_u = 150 kPa

5.2 Characteristic Resistance

In-situ tests, such as the CPT or SPT, are used in sands to evaluate the friction angle. To estimate undrained shear strength in clays, the CPT or laboratory tests can be used. Following the collection of soil strength data, the engineer's task becomes selecting an appropriate value of strength for design. This value of strength is referred to

as characteristic strength. The characteristic strength, in turn, is used to determine the characteristic (design) resistance in bearing capacity analysis.

The uncertainties in test correlations are quantifiable. To take advantage of LRFD, a statistically consistent approach to design is necessary. Determination of the characteristic shear strength as a conservatively assessed mean (CAM) is helpful in this regard. The first step in determining the CAM is to determine the mean value of the data. Since shear strength tends to increase with depth because of the higher effective confining stress, a mean trend of the data with depth is found. Once this mean function is determined, it must be reduced by some amount to conservatively assess the mean. One reduction method is a percent exceedance criterion (Becker 1996), in which the value above which 80% of the data lay is determined.

Characteristic Values in Sand

Characteristic values for friction angle in sand can be determined using both the CPT and SPT. For each CPT performed, the individual layers of soil are first identified. A layer in this context is defined as a volume of soil with approximately the same relative density. For each soil that is of interest, the values of q_c are normalized using the following relationship from Salgado and Mitchell (2003):

$$\frac{q_c}{p_A} = e^{c_3 D_R} \cdot c_1 \left(\frac{\sigma'_h}{p_A} \right)^{c_2} \qquad \textbf{(5.2.1)}$$

where p_A is a reference stress of 100kPa, D_R is relative density, σ'_h is the lateral effective stress, and c_1, c_2, and c_3 are coefficients related to intrinsic sand properties. The equation

can also be rewritten with depth in place of σ'_h. Using a power regression, the resulting equation will be consistent with (5.2.1), where q_c is a function of depth raised to a power.

Unless a very large number of data points is available, the sample (data) set is relatively small compared to the size of the population (all possible values). Thus, the modified 6σ procedure (Chapter 3) is an applicable statistical tool to determine the standard deviation. Taking the mean of the sample (a regression line with depth) as a close representation of the population mean, the 80% exceedance value line can be determined as a value 0.84 standard deviations below the regression line. This value can be determined by operating on detrended data. When a large number of data points is available, the procedure can also be approximated visually. Figure 5.2.1 illustrates an example where the CAM line for an approximately linear q_c profile can be drawn visually such that 80% of the data points lie above the CAM line.

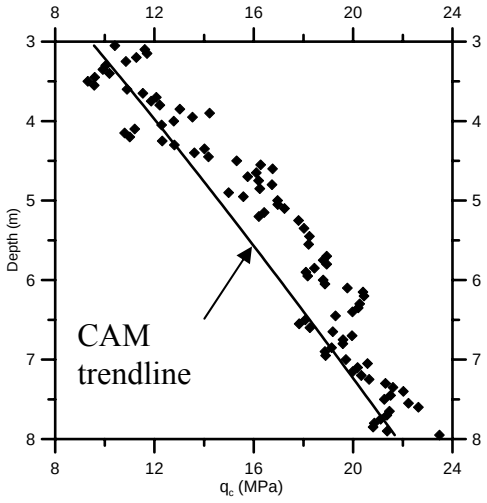

Figure 5.2.1. Visual Approximation of CAM Function for a CPT Profile – The trend line is drawn so that 80% of the data points occur to the right of the line.

An assessment of the validity of the 80% exceedance criterion is in order. Considering equation (1.1.1), it is necessary that the evaluation of $(RF)R_n$ correspond to a consistent level of reliability regardless of the value of q_c *COV* existing in the field. Thus, either *RF* or R_n must vary with $COVq_c$ so that the target reliability index β is always achieved. In this chapter, it has already been shown that for a given target reliability index and q_c uncertainty, an optimum *RF* can be found. Thus, it is necessary that, if R_n is to be a function of $COVq_c$,

$$\left[RF\left(COV_{qc}\right)\right]\left[R_{n,mean}\right]=\left[RF\right]\left[R_{n,CAM}\left(COV_{qc}\right)\right] \qquad \textbf{(5.2.2)}$$

where $RF(COV_{qc})$ is the optimum resistance factor that varies with COV_{qc} and is multiplied with a nominal resistance $R_{n,mean}$ found using the mean trend of q_c with depth; and $R_{n,CAM}(COV_{qc})$ is a nominal resistance R_n that varies with COV_{qc}. In the approach followed in this report, the variation of R_n with the COV_{qc} is captured by defining R_n as a CAM of the resistance. This nominal resistance is then multiplied by a constant *RF* value (the value determined using reliability analysis).

Geotechnical designers routinely determine representative values of R_n in practice. Thus, the determination of $R_{n,CAM}$ adds no burden to the engineer. Values of *RF* are usually selected according to design codes or established practice. Detailed reliability analyses may be used to determine *RF* values at the time of code development or in other *RF* studies. However, detailed reliability analyses are highly uncommon for specific projects. Thus, it is more reasonable to establish one value of *RF* for a type of design than to specify the use of $RF(COV_{qc})$.

Note that the reinforced concrete code (ACI 1999) makes use of $R_{n,CAM}(COV)$ rather than $RF(COV)$ for concrete design. In this code, ACI specifies 95% exceedance as

a criterion for evaluating concrete compressive strength. However, given the values of *COV* encountered in geotechnical design, this criterion would yield physically unrealistic values when applied to q_c. Thus, an 80% criterion has been selected.

To assess the ability of this 80% criterion-based resistance $R_{n,CAM}$ to satisfy equation (5.2.2), values of $RF(COV_{qc})$ and *RF* for a square foundation on sand and on clay were determined for different values of COV_{qc}. The results of this assessment appear in Figure 5.2.2. These plots are presented in the same relative *RF* scale as Figures 5.1.1, 5.1.2 and 5.1.4 to highlight the relative influence of the *COV* of q_c. Of note in Figure 5.2.2(b) is the negligible change in *RF* with *COV*. Thus, in this case, the application of $R_{n,CAM}(COV_{qc})$ is successful since a constant *RF* is desired. The application of this CAM method to sands is less successful. Referring to Figure 5.2.2(a), although the decrease in *RF* (based on the CAM q_c) with increasing q_c *COV* is less than the decrease in $RF(COV_{qc})$ (based on the mean q_c), the decrease is still significant. Thus, the CAM method proposed only partly accounts for a higher uncertainty than that assumed in the development of the proposed RF values in the case of sands.

Taking the CAM value after normalizing sounding data accounts for the deviation of the data from the mean trend with depth – the spatial variability of the soil in the vertical direction. To account for the lateral variability of the soil, the traditional approach of using the worst applicable sounding appears to be the best solution. A statistical treatment of the soil variability in the lateral direction is far too complicated and in most cases not feasible, given the information available.

In summary, the conservatively assessed mean (CAM) procedure is a valuable tool in selecting design values for two reasons: first, and most importantly, it provides a

statistically consistent method to analyze data from a particular soil layer, replacing arbitrary selection with a consistent procedure; second, the CAM procedure tends to stabilize the reliability of design checks completed using particular *RF* values. This method does not replace the engineer's responsibility to determine which data are relevant to the design problem, but rather supplements the tools available to analyze them.

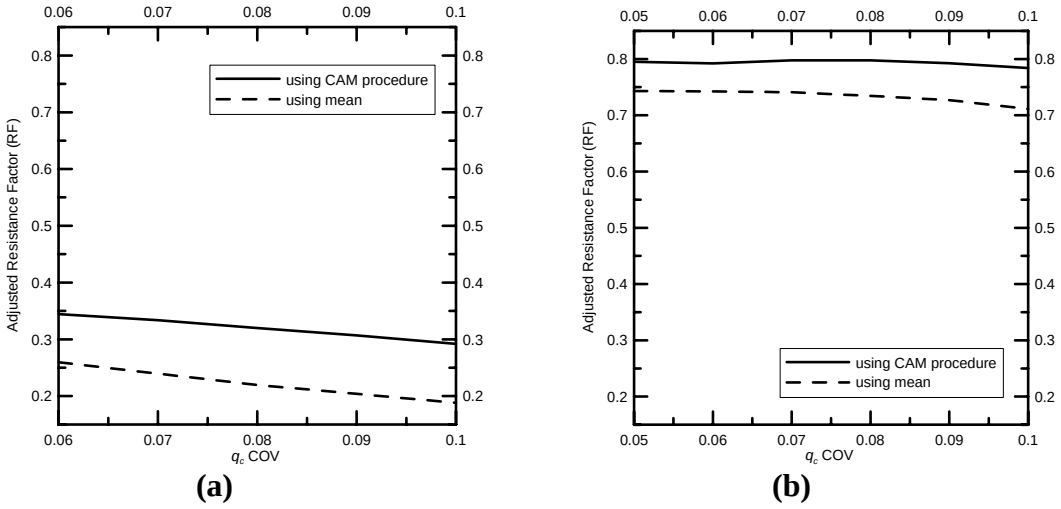

Figure 5.2.2. Adjusted Resistance Factors Computed Using CPT Profiles with Different Variabilities, with and without the CAM procedure, *LL/DL* = 1.0: (a) strip on sand surface, ϕ_p = 42.4º, (b) Square Footing on Clay using Salgado et al. (2003) Factors, s_u = 150 kPa, *D/B* = 0.4

CHAPTER 6. DESIGN EXAMPLES FOR SHALLOW FOUNDATIONS

Design Philosophy

In general, all geotechnical designs follow the flow of design tasks outlined in Figure 6.1.

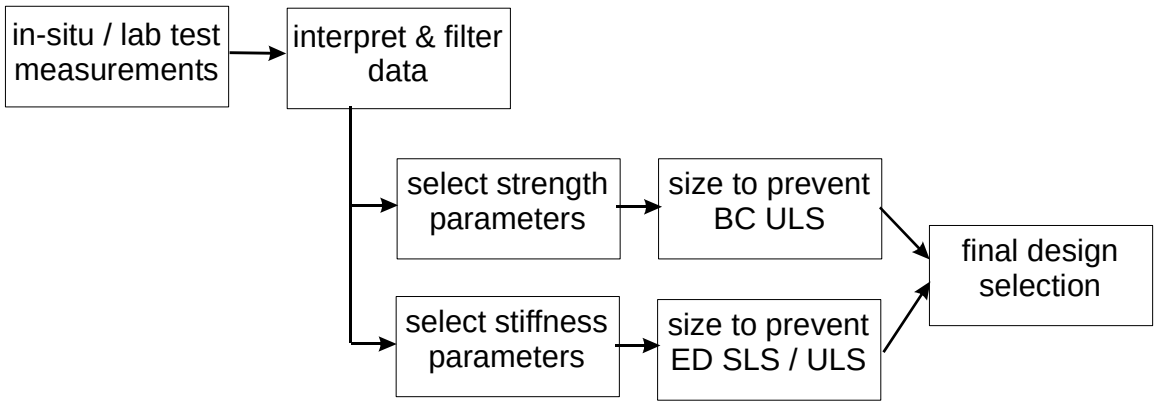

Figure 6.1. General design flow for geotechnical engineering. ULS = ultimate limit states, BC = bearing capacity, SLS = serviceability limit states, ED = excessive deformation.

In the LRFD method advocated in this report, the selection of the CAM value of strength parameters starts with the interpretation of geotechnical tests. For example, after the relevant CPT soundings have been selected, a CAM value of q_c is determined by finding the trend of the data with depth and adjusting the trend according to the CAM procedure. This process is illustrated in the examples below.

Since we are addressing ULS design checks specifically here, the following flow chart (Figure 6.2) illustrates the process in more detail.

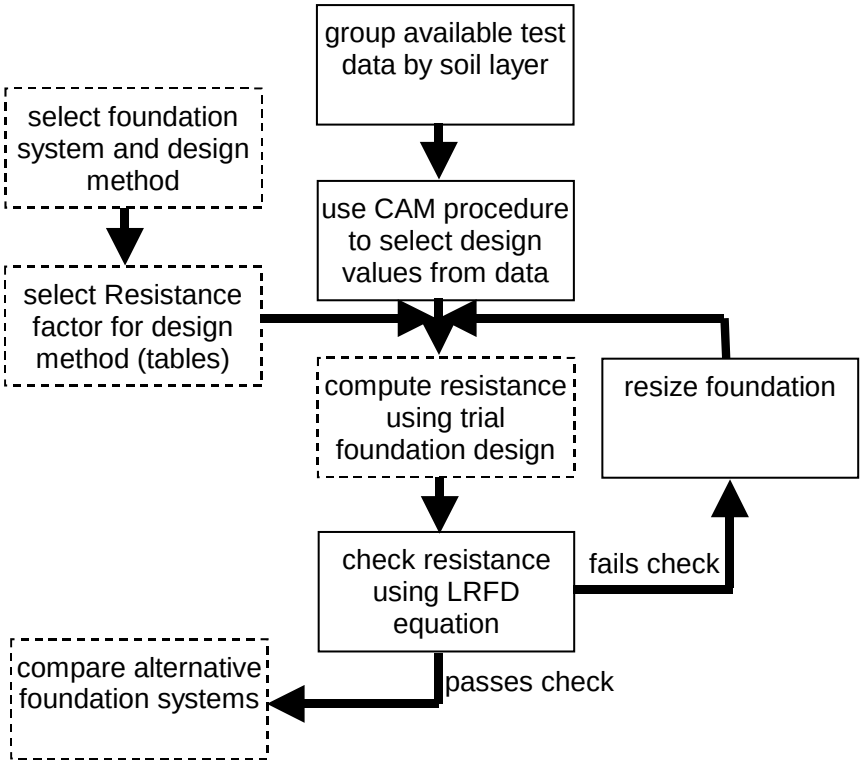

Figure 6.2. LRFD flow chart for ULS checks for foundation design. Dashed line boxes indicate steps specific to a particular design method, solid line boxes indicate steps common to all foundation types.

Notice in Figure 6.2 that the selection of CAM values for in-situ and laboratory tests only needs to be done once. These values can subsequently be used in any of the design methods available for a particular foundation element. The designer must take care to make sure that the Resistance Factor used to check a design matches the particular design method used. Tables of suggested resistance factors have been developed. The design example below illustrates their use.

Example Design Case

Two sites are considered. One is a primarily sand soil profile. The other is a clay site. A number of CPT soundings were taken at each site and the measured tip resistance (q_c) profiles are presented in Figure 6.3. For each site, a square column footing with 440 kN (99 kip) live load and 600 kN (135 kip) dead load will be designed against ultimate limit states. Using live load and dead load factors of 1.6 and 1.2 (ASCE-7 factors), respectively, the design load is 1,420 kN (319 kip). The basement is to extend to a depth of 1 m (3.3 ft). The water table is very deep. Based on the available logs, a reasonable foundation should be possible at a depth of 2.0 m (6.6 ft) (1 m below basement elevation).

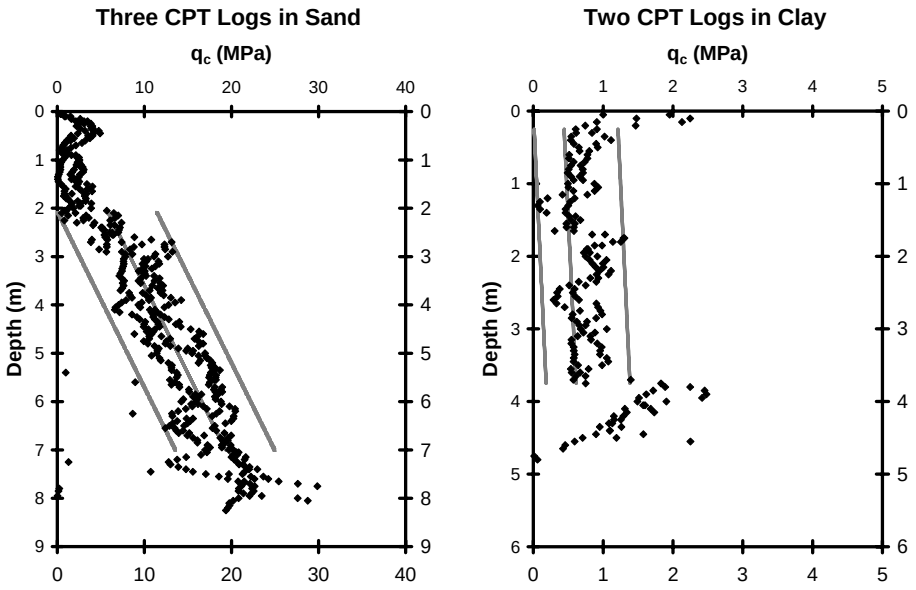

Figure 6.3. CPT logs with Best Fit Lines and Range Lines

The first step to design the foundations is to establish trial footing dimensions and use these to find applicable soil strength parameters from the CPT logs. A CAM method using an 80% exceedence criterion is illustrated using linear regression – a tool readily

available to engineers in spreadsheet applications. These lines represent the mean function of a soil parameter with depth for the soils. Lines can also be drawn bounding the q_c data points, representing the entire range of q_c data for those depths. Both sets of lines are included in Figure 6.3. Table 6.1 presents the statistics used to find the 80% exceedance criterion CAM line using the modified 6σ procedure, effectively shifting the mean line to the left on the plots. In the sand layer, the CAM line is given by the equation

$$q_{c,CAM} = 2.7497(MPa/m)\cdot z - 1.6151(MPa) \quad , 2\text{m} < z < 7\text{m} \qquad \textbf{(6.1)}$$

For the clay layer,

$$q_{c,CAM} = 0.049042(MPa/m)\cdot z + 0.23656(MPa), \; 0.2\text{m} < z < 3.8\text{m} \qquad \textbf{(6.2)}$$

Table 6.1. CPT q_c log statistics

	Sand Profile	Clay Profile
Range (MPa) (R)	11.7	1.2
Data Points in Range (n)	294	142
Standard Deviations Represented (from Tippett 1925) ($R_{\sigma=1}$)	5.743	5.261
One Standard Deviation (MPa) ($\sigma = R / R_{\sigma=1}$)	2.037	0.2281
Number of Standard Deviations for 80% Exceedance	0.84	0.84
Adjustment for 80% Exceedance (MPa)	1.71	0.192

Design in Sand using CPT

Considering the base depth of 2 m and trial footing width of 1.5 m (4.9 ft), a depth of interest to soil strength evaluation will be at 2.75 m (9.0 ft) (0.5B below the footing base). Using (6.1), the CAM q_c at 2.75 m is 5.9 MPa (123 ksf). To use the Salgado and

Mitchell (2003) charts to interpret q_c, a value for horizontal effective stress (σ_h') must be found. Assuming a unit weight and lateral earth pressure coefficient at rest (K_0) of 20 kN/m^3 (127 pcf) and 0.45, respectively, a depth of 2.75 m gives a σ_h' of 25 kPa (522 psf). Assuming a critical state friction angle of 33°, the Salgado and Mitchell (2003) charts yield a relative density and peak friction angle (ϕ_p) of 40% and 37°, respectively. Table 6.2 presents the equations used to compute the bearing capacity factors.

Table 6.2. Bearing capacity factors in sand example

Factor	**Equation**
Overburden[a]	$N_q = \frac{1+\sin\phi}{1-\sin\phi} e^{\pi \tan\phi}$
Unit Weight[b]	$N_\gamma = 1.5(N_q - 1)\tan\phi$
Shape[b]	$s_q = 1 + \frac{B}{L}\sin\phi$
Shape[b]	$s_\gamma = 1 - 0.4\frac{B}{L}$
Depth[b]	$d_q = 1 + 2\tan\phi(1-\sin\phi)^2 \frac{D_f}{B}$
Depth[b]	$d_\gamma = 1$

[a]after Reissner (1924)
[b]after Brinch Hansen (1970)

The factored bearing capacity in sand for this example can be expressed as

$$(RF)R_n = RF\left[B^2\left(\gamma D N_q s_q d_q + \frac{1}{2}\gamma B N_\gamma s_\gamma d_\gamma\right)\right] \quad \textbf{(6.3)}$$

where RF is the resistance reduction factor; R_n is the nominal resistance (a force); B is the foundation width; γ is the soil unit weight; D is the foundation depth; N_q, N_γ are bearing capacity factors, s_q, s_γ are shape factors; and d_q, d_γ are depth factors. Since the footing is located 1m below basement elevation, 1m depth of soil is available to resist bearing

capacity failure. Since $D/B = 1/1.5 > 0.10$, Table 5.1.1 yields a recommended resistance factor of 0.45. Using the $RF = 0.45$, the value of $(RF)R_n$ is 1,840 kN (414 kip). Considering the calculated design load of 1,420 kN (319 kip) and the requirement to satisfy inequality (1.1.1), this is an acceptable design. However, another design iteration is attempted.

For the next iteration, a trial footing width of 1.4m is used. This B yields a $(RF)R_n$ of 1,590 kN (357 kip), an optimized design. If a highly optimized design is desired, Figure 5.1.1(a & b) can be used instead of Table 5.1.1 to obtain a value of RF for the specific design situation. In this case, the optimal RF for this D/B and LL/DL ratio obtained from Figure 5.1.1 is still 0.45, so no further optimization is possible.

Design in Sand Using SPT

The same design procedure can be applied to the problem using SPT data. The only difference in this approach is the interpretation of the test data. The available data for this example are corrected SPT blow counts (N_{60}) of 8, 6, 9, 7, 10, and 9 at depths of 2, 2.5, 3, 3.5, 4, and 4.5 m, respectively. The depth of influence considered earlier, 2.75m, falls within these measurements. Using the Liao and Whitman (1986) stress-normalization, blow counts can be corrected to stress-normalized values $(N_1)_{60}$,

$$\left(N_1\right)_{60} = N_{60}\sqrt{\frac{p_A}{\sigma'_v}} \qquad \textbf{(6.4)}$$

where p_A is the reference stress 100 kPa (2089 psf) and σ'_v is the vertical effective stress. This stress-normalization essentially accounts for the trend of N_{60} with depth. Thus, the mean of the data can be found by taking the mean of the normalized blow count values

$(N_1)_{60}$. The mean and range of the resulting $(N_1)_{60}$ values is 10.3 and 4.3, respectively. Only 6 data points are available, so the modified 6σ procedure is applied, yielding a standard deviation σ_N of 1.7 blow counts. To determine the 80% exceedance CAM $(N_1)_{60}$ value, 0.84 standard deviations are subtracted from the mean. The resulting CAM $(N_1)_{60}$ value is 8.9.

The transformation from N_{60} to D_R can be expressed as (Skempton 1986):

$$D_R = \sqrt{\frac{N_{60}}{A + BC\dfrac{\sigma'_v}{p_A}}} \qquad \textbf{(6.5)}$$

where *A*, *B* and *C* are coefficients related to overconsolidation, taken here as 30, 27 and 1, respectively. Since the CAM $(N_1)_{60}$ value represents data normalized for σ'_v = 100 kPa (2089 psf), (6.5) becomes

$$D_R = \sqrt{\frac{(N_1)_{60}}{A + BC}} \qquad \textbf{(6.6)}$$

For an $(N_1)_{60}$ value of 8.9, (6.5) yields D_R = 40%. The design process can then proceed as described for the CPT example – finding the ϕ_p value using D_R and calculating $(RF)R_n$ using (6.3). For this case ϕ = 37º, and *RF* = 0.30 (Table 5.1.1, D/B > 0.10). An optimized design occurs for a footing width B of 1.7m having a $(RF)R_n$ = 1,600kN (360 kip). The additional uncertainty associated with the SPT led to a larger footing (B = 1.7 vs. 1.4m) in comparison with the CPT design.

Design in Clay using CPT

In clay, the first step is to find the undrained shear strength. A depth of interest to determine a representative value of shear strength is 2.75m (0.25B below the footing). This depth appears conservative since the slip surface (extending to approximately 1*B* below the footing) will pass into a stronger layer. Using (6.2), the CAM value of q_c is 371 kPa (7750 psf). Undrained shear strength can be calculated from

$$s_u = \frac{q_c - \sigma_v}{N_k} \quad \textbf{(6.7)}$$

where N_k is the cone factor – taken here as 10 (Yu et al., 2000). Assuming a soil unit weight of 16 kN/m^3 (102 psf), (6.7) yields an s_u of 33 kPa (690 psf). For B = 3.0m, factors s_c and d_c can be found using Salgado et al. (2004),

$$d_c = 1 + 0.27 \cdot \sqrt{\frac{D}{B}} \quad \textbf{(6.8)}$$

$$s_c = 1 + 0.12 \cdot \frac{B}{L} + 0.17 \cdot \sqrt{\frac{D}{B}} \quad \textbf{(6.9)}$$

The bearing capacity equation is

$$(RF)R_n = (RF)\left[B^2\left(s_u N_c s_c d_c + \gamma D\right)\right] \quad \textbf{(6.10)}$$

Using the recommended resistance reduction factor of 0.73 and substituting the values found above, (6.10) yields a factored resistance of 1,670 kN (375 psf) – a conservative design. For the next iteration, the trial footing width, *B*, is set to 2.8 m, giving a $(RF)R_n$ of 1,470 kN (330 kip) – an optimized design. Results of the two trial designs are presented in Table 6.3.

Table 6.3. Results of CPT Design Example on Sand and Clay

	B	ϕ_p	N_q	s_q	d_q	N_γ	s_γ	RF	$(RF)R_n$	R_n	F.S.
Sand	1.5m	37°	42.9	1.60	1.16	47.4	0.6	0.45	1,840kN	4,090kN	3.93
	1.4m	37°	42.9	1.60	1.16	47.4	0.6	0.45	1,590kN	3,540kN	3.41

	B	s_u	s_c	d_c	RF	$(RF)R_n$	R_n	F.S.
Clay	3.0m	33kPa	1.22	1.16	0.73	1,670kN	2,290kN	2.21
	2.8m	33kPa	1.23	1.16	0.73	1,470kN	2,010kN	1.94

Design in Clay using Unconfined Compression Test

In clay, the first step is to find the undrained shear strength. To determine a CAM value of s_u from laboratory tests, a group of relevant tests must be selected first. Relevant tests are those that were performed on soil samples taken from the same soil layer that is being designed against. If several soil layers are involved, separate CAM values can be determined for each layer. If samples are taken from different depths and the soil properties are expected to vary with depth, then measures to normalize the data before applying CAM statistics are necessary.

In this example, several soil samples from the same depth were tested to estimate s_u for use in design. The available data for this example are unconfined compression test measurements of s_u of 30, 37, 40, 45, and 52 kPa (627, 773, 835, 940, and 1090 psf). Now, we determine the standard deviation of the data. Only 5 data points are available, so the modified 6σ procedure is applied (equation 3.2.5), yielding a standard deviation σ_{su} of 9.46 kPa. To determine the 80% exceedance CAM s_u value, 0.84 standard deviations are subtracted from the mean. The resulting CAM s_u value is 32.9 kPa (687 psf).

Design of shallow foundations on clay proceeds as before for ULS design checks using in-situ test data, taking care to use the correct value of *RF* from Table 5.1.1 (0.52 for the present example since we are designing a square footing using the Salgado et al. 2004 factors).

Comparison with Working Stress Design

Since comparison of these results with traditional Working Stress Design methods is of interest, values of the factor of safety are also given in Table 6.3. Factor of safety is defined here as

$$F.S. = \frac{R_n}{LL + DL} \qquad \textbf{(6.11)}$$

It should be noted that, for design on clay using the CPT, the optimized designs have values of factor of safety less than 2.5. This result would suggest that use of FS values greater than 3 (a practice often seen) is overly conservative with respect to an ULS calculation. Within the Limit States Design (LSD) framework, the Ultimate Limit State and serviceability limit states are treated separately. The traditional practice of using factors of safety greater than 2.5 in stability calculations may have served a purpose in avoiding serviceability limit states, but, as pointed out by Becker (1996), this is not an appropriate use of safety factors. Safety factors in WSD or load and resistance factors in LRFD must be used only to prevent a specific ULS. The practice of inflating FS values to account for anything else should be discouraged.

The factors of safety found for sand (in excess of 3) were quite high. This result is expected since the uncertainties associated with the transformations from q_c measurements to design factor values are much larger than for clay. This comparison between traditional factors of safety and reliability-based factors offers an opportunity to examine acceptable risk in current practice. Reference to Figure 5.1.5 facilitates this discussion. In this figure, adjusted resistance factors for footing designs on sand and clay are presented for different target reliability indices. For a given resistance factor and value of D/B, a corresponding value of β can be obtained from Figure 5.1.5. Higher

reliability indices are related to lower probabilities of failure. For different resistance factors, equivalent factors of safety can be computed using either equation (6.11) or (5.1.1). These factors of safety can then be compared to existing practices.

CHAPTER 7. ASSESSMENT OF DESIGN METHODS FOR DEEP FOUNDATIONS

In this chapter, an appraisal of some available design methods is made and design equations are selected for reliability analysis and resistance factor calculation. In the course of the literature review, it was often discovered that the experimental and theoretical support for many design methods is incomplete. Bustamante and Gianeselli (1982) addressed this issue by stating that "the discrepancies observed between real and theoretical bearing capacities are explained by the fact that present design methods have been developed on the basis of questionable and often insufficient experimental data." Thus, many design methods can be expected to produce unpredictable deviations between measured and predicted load capacities. This means that we are unable to rationally assess the uncertainty for some design methods within the framework established in Chapter 3. In the following development, only design equations with strong experimental support and thorough theoretical development are considered.

7.1 LRFD Design of Piles

In terms of limit states design (LSD), pile foundations are typically designed against an ultimate limit state (ULS). For shaft resistance, the full load capacity of the shaft is often mobilized at relatively small pile displacements. Franke (1993) states that side resistance is fully mobilized well before maximum base resistance is reached. Thus, an ULS is clearly the most pertinent check for shaft resistance. For base resistance, it is possible to have very large relative settlements before the pile enters a plunging mode. The unit base load at plunging is q_{bL}. However, to consistently define an ultimate limit

bearing pressure, a settlement-based criterion for limit bearing capacity is often adopted. Most of the methods considered in this section use the settlement-to-pile diameter ratio of 10% (s/B = 10%) definition of ultimate limit bearing capacity, $q_{b,10\%}$. Thus, although an ULS is defined, there is an implied serviceability limit state (SLS) check in these design methods that should be sufficient in the majority of projects. For foundations of particularly sensitive buildings, a more strict tolerable settlement criterion may need to be imposed to ensure serviceability.

The basic Load and Resistance Factor design (LRFD) equation is

$$(RF)R_n \geq \sum (LF)_i Q_i \qquad \textbf{(7.1.1)}$$

In pile design, both base and shaft resistance contribute to the overall load-carrying capacity of the pile. There are two possible approaches to implementing an axial load limit state design check in LRFD:

$$(RF)(R_s + R_b) \geq \sum (LF)_i Q_i \qquad \textbf{(7.1.2)}$$

or

$$(RF)_s R_s + (RF)_b R_b \geq \sum (LF)_i Q_i \qquad \textbf{(7.1.3)}$$

where R_s and R_b are the shaft and base resistances, respectively, and $(RF)_s$ and $(RF)_b$ are the shaft and base resistance factors, respectively. In reality, the shaft and base resistances are not independent. However, given that in practice we do calculate them separately, it must be recognized that the uncertainties in their prediction are very different. Therefore the likelihood of overestimating shaft resistance by a certain factor is very different than it is for base resistance. Thus, it is more accurate to apply $(RF)_s$ and $(RF)_b$ as separate resistance factors, as in (7.1.3), since the uncertainty of shaft and base resistance estimates is so different. However, in the case of some direct design methods,

it may not be possible to calibrate separate resistance factors for base and shaft resistance depending on the available data to validate the method. Therefore, (7.1.2) is applicable to some circumstances, but (7.1.3) offers better control over design reliability.

Reliability analysis is used to find suitable resistance factors for use with (7.1.2) and (7.1.3). In the case of (7.1.3), the reliabilities for shaft and base resistance are computed separately. By doing so, we assume that the two are independent and, as a consequence, the likelihood of the designer overestimating one resistance is not affected by the likelihood of the designer overestimating the other. This approach is in a way similar to reinforced concrete design, where separate design checks are used for both shear and bending limit states even though both design checks depend on the strength properties of the concrete.

Pile design methods can be broadly classified as either direct or property-based. Direct design methods rely on direct correlations between in-situ tests and measured pile capacity. Property-based design methods compute pile capacity using various soil parameters as input. These parameters are computed from in-situ and/or laboratory tests. A major difference between property-based methods and direct methods is that property-based methods tend to have higher uncertainty (lower *RF*), but apply to general cases, while direct methods tend to have lower uncertainty (higher *RF*) but apply only to cases resembling the specific piles and soils they were developed for. One implication of this difference is that it may be riskier to apply a direct method to a design situation that is different from the pile load test database supporting the method, even though the method may show excellent agreement with measured values in the database.

In Chapters 8 and 9 we will assess the uncertainty of the design methods selected in this Chapter for use in reliability analysis. Resistance factors will be determined in this analysis.

7.2 Design of Piles in Sand

Fundamental Load Response Mechanisms and Property-Based Design

First, studies of shaft capacity design are discussed. Perhaps the most well-known issue in shaft capacity design is the notion of a limiting value of shaft friction at some limit depth. The literature on the subject reveals the following:

- Vesic (1964, 1970, 1977), Meyerhof (1964, 1976) and Kerisel (1964) discussed for the first time the critical depth concept;
- Kulhawy (1984) states that limiting unit shaft capacity is a fallacy;
- Kraft (1991), Randolph (1994), and Kulhawy (1984) explain the factors that caused the concept of critical depth as follows:
    a. For side resistance: the apparent limiting value of shaft resistance is caused by the simultaneous decrease in lateral earth pressure coefficient at-rest (K_0) with depth and decrease in ϕ_p with increase in $\sigma'_{v.}$
    b. For tip resistance: the apparent limiting value of base resistance is caused by decreasing values of ϕ_p and rigidity index with increasing σ'_v (Rigidity index = stiffness/strength)
- Fellenius and Altaee (1995) claim that the critical depth concept resulted from a misinterpretation of pile load tests where residual load effects were neglected;

- Salgado (1995) shows that there is no critical depth, but rather a decreasing rate of increase of bearing capacity with depth.

The literature search revealed a few notable attempts to account for this knowledge of the causes of an apparent limiting shaft and base resistance:

- Fleming et al. (1992) attempted to incorporate in their design the effect of decreasing ϕ as σ increases. They defined K = 0.02 N_q with $\delta = \phi_c$. This method overestimates shaft friction for long piles but compares well with the method presented by Vesic (1970);
- To allow for the degradation of friction due to pile length, Toolan et al. (1990) presented a new method. Their aim was to account for the well-established observation that local shaft friction at any fixed level varies with pile penetration, as discussed by Vesic (1970), Hanna and Tan (1973), Lehane et al. (1993). They proposed an exponential decay function of shaft friction with length of pile in terms of local value;
- Randolph (1994), Kulhawy (1984), Toolan et al. (1990), Vesic (1967), Hettler (1982) and Kraft (1991) explained the trend of limiting values by K_0 depth profiles, friction fatigue processes, local shear-stress distributions and sand dilation;
- Salgado (1995) shows that the limit unit base resistance q_{bL} increases non-linearly, at decreasing rates, with increasing σ'_v. The limit base resistance q_{bL} is

approximately equal to the cone penetration resistance q_c (Salgado 2004),

$$\frac{q_{bL}}{p_A} = C_1 \exp(C_2 D_R)\left(\frac{\sigma'_h}{p_A}\right)^{C_3} \qquad \textbf{(7.2.1)}$$

where p_A is reference stress (100 kPa), C_1, C_2 and C_3 are constants, D_R is relative density, and σ'_h is the horizontal effective stress.

In their study of open ended pile shaft capacity, Paik and Salgado (2003) where able to show very clearly the dependency of shaft capacity on K_0 for driven piles. Therefore, it is important that the designer account for K_0 in the property-based methods. In the uncertainty evaluation in the following section, limit state equations are expressed in terms of K_0 for this reason.

The literature search revealed a number of observations concerning the pile design method recommended by the American Petroleum Institute (API). The API guidelines are in wide use and are supported by considerable research, so assessments of these guidelines allow some insight into the quality of pile design in sand. We are using these results to identify key issues in pile design in sand when considering other design equations. Note the following observations regarding the API method:

- Toolan et al. (1990) reveal a number of limitations of the API codes (several supporting tests are unreliable, the method overpredicts capacity, the method cannot account for loose and very dense sites);
- Randolph (1994) states that API guidelines limit values of shaft and toe resistances at an absolute stress level or depth independently of pile diameter. He

explains that limiting values on end-bearing and shaft capacities are an idealization;

- Randolph (1994) concludes that "There is a need for new, high-quality field data on pile driveability and axial capacity in sand, particularly from piles in field scale, in order to help resolve uncertainties regarding limiting values of shaft friction and end-bearing, the treatment of partial displacement piles, and potential differences in tensile and compressive shaft capacity.";
- With respect to "partial displacement piles," design of open ended piles has traditionally been accomplished through the use of general recommendations for the lateral earth pressure coefficient of the shaft K_s (e.g. Kraft 1990) that do not take the degree of plugging into account. However, it has been shown by Paik and Salgado (2003) that open ended pile resistance depends on degree of plugging during driving, as measured by the incremental filling ratio (IFR). IFR is defined as:

$$IFR = \frac{dL_p}{dL} \qquad \textbf{(7.2.2)}$$

where L_p is the plug length and L is the pile penetration length.

From these observations, it can be seen that much progress is still needed in pile design in sand with respect to accuracy and number and quality of data used to support design methods. The assessment of design equation uncertainty in the following section exposes some areas where pile design can benefit from targeted investigation and better data.

The available knowledge concerning shaft interface friction is much better than that for overall pile design in sand. A large amount of research has been conducted on

the subject of the interface friction between steel and sand, including recent contributions by Kishida and Uesugi (1987), Jardine et al. (1993), Rao et al. (1998), and Jardine and Chow (1998).

Surface roughness is an important factor in interface friction. Two different measures of the surface roughness are commonly encountered in the literature: average roughness (R_a) and maximum roughness (R_{max}). Average, or "center-line average" roughness is an industry standard in the United States and also a very common measure. Average roughness (expressed in μm) is defined as (Outokumpu Stainless, 2004)

$$R_a = \frac{1}{l}\int_0^l |z(x)|dx \qquad \textbf{(7.2.3)}$$

where l is the evaluation length of the measurement (typically 8mm) and $z(x)$ is the measured surface profile. The surface profile $z(x)$ is expressed such that the area under the profile above the mean line is equal to that below. Maximum roughness is the maximum difference in height between a "peak" and a "trough" for a surface profile over a certain gauge length. Thus R_{max} is always expressed for a certain gauge length. R_{max} (L = 2.5mm) is a common measure according to the Japanese Standards Association (Kishida and Uesugi, 1987). However, R_a is a more common measure of surface roughness, and the results by Rao et al. (1998), which are reported with reference to R_a, are used to support the reliability analysis in this chapter.

Rao et al. (1998) and Kishida and Uesugi (1987) have shown that both R_{max} (L = D_{50}) and R_a/D_{avg}. are useful measures of roughness for finding correlations between interface friction angle δ and roughness for different pile materials. D_{avg} is the total area beneath the particle size distribution curve divided by 100%, where particle size is plotted on a linear scale. Values of D_{avg} are approximately equal to D_{50} for sands tested by Rao

et al. Values of R_a for steel piles and D_{50} for sands are easily obtained in practice. For steel piles, R_a is typically 8-10 μm.

Sand sheared along the sides of a pile reaches large strains such that critical state is achieved. Thus, critical state friction angle ϕ_c and the corresponding interface friction angle δ_c are relevant friction angle values to use in design. Interface friction tests results by Jardine et al. (1993), Rao et al. (1998), and Jardine and Chow (1998) are used in the next section to evaluate the uncertainty of δ_c / ϕ_c.

Direct Design Methods

Most of the direct design methods are based on either the standard penetration test (SPT) or the cone penetration test (CPT). The SPT does not relate well to the quasi-static pile loading process. In contrast, the CPT resembles a scaled-down pile load test (Lee and Salgado 1999). The main difference between the CPT and a larger diameter pile base is the size of the zone of soil influencing the base capacity. Thus, spatial variability of soil parameters is the main source of uncertainty in comparisons between CPT tip resistance q_c and pile load tests. White (2003) shows that q_{bL}, on average, tends to q_c.

Direct design methods have been developed for most pile types. Load settlement curves are different depending on pile installation procedure (in general terms, on whether the pile is a displacement or non-displacement pile. However, q_{bL} is mobilized at large settlement levels and is identical for displacement and non-displacement piles.

Lee and Salgado (1999) developed a design method based on analysis of non-displacement piles. They observed that there is a good agreement between load tests performed on steel H-piles, precast concrete piles, and drilled shafts and the predicted

values using their proposed design method. They suggest their design method to be considered a direct method to determine base resistance for displacement piles (H-piles and close-ended piles) and non-displacement piles (drilled shafts). Lehane and Randolph (2002) recommend that the base capacity of displacement piles be estimated, conservatively, using the values of Lee and Salgado (1999) for non-displacement piles.

The design methods we chose for reliability analysis are summarized in Table 7.2.1. These methods were chosen for the completeness of their supporting data. Various sources were used to develop the design methods for closed-ended piles and the complete list of references will be provided in Chapter 8.

Table 7.2.1 – Summary of selected design methods for reliability analysis in sands

Driven Closed-Ended Pipe Piles		
	Base	Shaft
Property-Based Methods	$\frac{q_{b,10\%}}{q_{bL}} = 1.02 - 0.0051 D_R(\%)$ (Various sources)	$f_s = \frac{K_s}{K_0} K_0 \tan\left(\frac{\delta_c}{\phi_c}\phi_c\right)\sigma'_v$ (Various sources)
Direct Methods	$\frac{q_{b,10\%}}{q_c} = 1.02 - 0.0051 D_R(\%)$ (Various sources)	$f_s = \left(\frac{f_s}{q_c}\right) q_c = 0.002 q_c$ (Various sources)
Driven Open-Ended Pipe Piles		
	Base	Shaft
Property-Based Methods	$\frac{q_{b,10\%}}{\sigma'_h} = \alpha\left(326 - 295\frac{\text{IFR}(\%)}{100}\right)$ (Paik and Salgado 2003)	$f_s = \frac{K_s}{K_0} K_0 \tan\left(\frac{\delta_c}{\phi_c}\phi_c\right)\sigma'_v$ (Paik and Salgado 2003)
Direct Methods	$\frac{q_{b,10\%}}{q_c} = -0.00443 IFR(\%) + 0.557$ (Paik and Salgado 2003)	$f_s = \left(\frac{f_s}{q_c}\right) q_c = 0.002 q_c$ (Paik and Salgado 2003)
Drilled Shafts		
	Base	Shaft
Property-Based Methods	$\left(\frac{q_{b,10\%}}{q_{bL}}\right) = 0.225 - 0.0011 D_R(\%)$ (Lee and Salgado 1999)	
Direct Methods	$\left(\frac{q_{b,10\%}}{q_c}\right) = 0.225 - 0.0011 D_R(\%)$ (Lee and Salgado 1999)	

Note that precast concrete piles are the same as closed ended pipe piles in terms of base capacity and shaft resistance since they are both displacement piles. The only difference is the possibility of a greater value for δ_c/ϕ_c due to the higher surface roughness of concrete.

7.3 Design of Piles in Clays

In this section, we present and explain the selected methods and equations for design of driven closed-ended piles in clay soils that are used for reliability analysis and resistance factor calculation. We did not assess the uncertainty for design methods of open-ended pipe piles because we had insufficient data to complete a satisfactory analysis. However, the use of open-ended piles in clay is not as common as in sands.

As for sands, it is important to have a specific definition for the ultimate base bearing capacity in clays. This is often accomplished using the $q_{b,10\%}$ definition (s/B = 10%). For soft to medium stiff clays, q_{bL} is nearly equal to $q_{b,10\%}$ since the bearing capacity of piles in these clays is fully mobilized at small settlements, less than 0.10B in most cases. We did not assess the uncertainty of design methods in stiff clays since there are not enough load testing data.

The base resistance of drilled shafts could be compared with driven closed-ended piles since the load-settlement curves will also lead to q_{bL} at small settlements. This is a consequence of the undrained load-settlement behavior of clay. So for both driven piles and drilled shafts in clay, the base resistance is q_{bL}, which is determined using the same equations for both pile types. Thus the same uncertainty will be applied to the base resistance of drilled shafts. We did not assess the uncertainty for design methods of shaft capacity for drilled shafts since instrumented pile load tests are relatively new, and few load test databases have been presented in the literature.

The base bearing capacity of piles in clay has traditionally been taken as the plunging bearing capacity:

$$q_{bL} = N_c s_u = 9 s_u \qquad \textbf{(7.3.1)}$$

where s_u is the undrained shear strength of the clay near the pile base. Stark and Juhrend (1989) have shown that the bearing capacity factor N_c is likely to be greater than 9 based on a comparison of results from several different studies. Limit analysis of circular foundations in clay by Salgado et al. (2004) is used to analyze the expected value of factor N_c and its uncertainty. The value of N_c according to Salgado et al. (2004) is between 11.0 and 13.7. An average N_c value of 12 is used for the proposed resistance factor.

The American Petroleum Institute API (1991) recommends the following equation for unit shaft resistance using the α method for clays,

$$f_s = \alpha s_u \qquad \textbf{(7.3.2)}$$

where α is an empirical factor which can be related to clay properties. Values of α are determined using the recommendations by Randolph and Murphy (1985), written as a relationship with strength ratio:

$$\alpha = \begin{cases} \left(\frac{s_u}{\sigma'_v}\right)_{NC}^{0.5} \left(\frac{s_u}{\sigma'_v}\right)^{-0.5}, \text{for} \frac{s_u}{\sigma'_v} \le 1 \\ \left(\frac{s_u}{\sigma'_v}\right)_{NC}^{0.5} \left(\frac{s_u}{\sigma'_v}\right)^{-0.25}, \text{for} \frac{s_u}{\sigma'_v} > 1 \end{cases} \qquad \textbf{(7.3.3)}$$

Discussing this method, Randolph and Murphy (1985) state that "the strength ratio may be related both to the value of OCR for a given soil, and also the value of K_0. However, α is a more fundamental (and directly measurable) quantity than either of the other two, and also reflects the full stress history of the soil." Knowing that the API α method is in

wide use and accounts for the factors that affect shaft resistance, we considered it for LRFD.

For direct methods, we considered the method proposed by Aoki and de Alencar Velloso (1975) based on SPT for piles in a variety of soils ranging from sands to clays. In this method, base capacity is computed as:

$$q_b = n_b N_{SPT} \quad \textbf{(7.3.4a)}$$

$$n_b = \frac{K}{F_1} \quad \textbf{(7.3.4b)}$$

where empirical factors K and F_1 are found in Tables 7.3.1 and 7.3.2. These factors are based on the results of 63 pile load tests performed on Franki, Cased Franki, Precast, and Steel piles. At their bases, these piles can all be expected to behave as large-displacement, driven close-ended piles due to their method of installation.

Shaft capacity is computed as:

$$f_s = n_{si} N_{SPT} \quad \textbf{(7.3.5a)}$$

$$n_{si} = \frac{\alpha_1 K}{F_2} \quad \textbf{(7.3.5b)}$$

where empirical factors K, α_1 and F_2 are found in Tables 7.3.1 and 7.3.2.

Table 7.3.1 – Values of α_1 and K for use with Aoki and Velloso (1975) direct design method

Soil type	$\frac{K}{p_A}$	α_1 (%)
Gravel	-	-
Sand	10.	1.4
Silty sand	8.0	2.0
Silty sand with clay	7.0	2.4
Clayey sand with silt	5.0	2.8
Clayey sand	6.0	3.0
Sandy silt	5.5	2.2
Sandy silt with clay	4.5	2.8
Silt	4.0	3.0
Clayey silt with sand	2.5	3.0
Clayey silt	2.3	3.4
Sandy clay	3.5	2.4
Sandy clay with silt	3.0	2.8
Silty clay with sand	3.3	3.0
Silty clay	2.2	4.0
Clay	2.0	6.0

Table 7.3.2 – Values of F_1 and F_2 for use with Aoki and de Alencar Velloso (1975) direct design method

Pile Type	F_1	F_2
Drilled Shafts	3.5	7.0
Franki	2.5	5.0
Steel	1.75	3.5
Precast concrete	1.75	3.5

A comparison of the measured total capacities with those computed using (7.3.4) and (7.3.5) appears in Figure 7.3.1 as given by Aoki and de Alencar Velloso (1975). Like most direct methods, this data set is the same data set used to calibrate the method. Examples of such other methods include Chow (1997) and Eslami and Fellenius (1997). The fact that such design methods were developed for specific design situations limits their wide applicability. This is a limitation of all direct design methods and not only the method we considered in our reliability analysis. Accordingly, these methods can only be used under the same testing circumstances. Later in Section 9.2.1 we will demonstrate how to select different resistance factors for different design methods based on data similar to Figure 7.3.1.

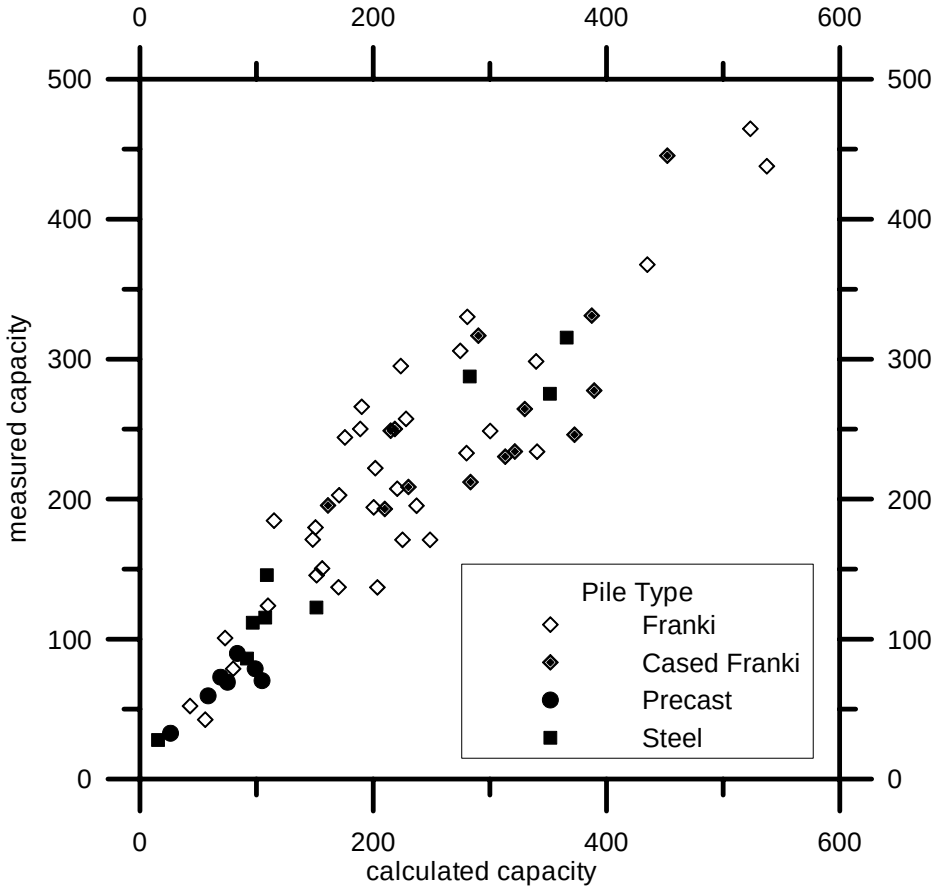

Figure 7.3.1 – Measured vs. calculated total pile resistance in study by Aoki and Velloso (1975) for Franki, Cased Franki, Precast, and Steel piles.

Table 7.3.3 is a summary of the selected design equations for clays.

Table 7.3.3 – Summary of selected design methods for reliability analysis in clays

	Base	Shaft
Property-Based Methods	$q_{bL} = N_c s_u$ (Salgado et al. 2004)	$f_s = \alpha s_u$ (Randolph and Murphy 1985)
Direct Methods	$q_b = n_b N_{SPT}$ (Aoki and de Alencar Velloso 1975)	$f_s = n_{si} N_{SPT}$ (Aoki and de Alencar Velloso 1975)

CHAPTER 8. RESISTANCE FACTORS FOR DEEP FOUNDATIONS ON SAND

8.1 Assessment of Variable Uncertainties for Deep Foundations on Sand

Many design methods are available for consideration. In this section, a few design equations are selected from the literature, or inferred from a database of available instrumented pile load tests. In every case, a limit state equation, quantifying an ULS design check, is expressed in terms of the applied load and design variables. Each limit state equation contains the expression for design resistance, and thus reflects directly the design equation to be used.

Piles are often designed on the basis of in-situ tests prior to any pile driving activity. Occasionally, a pile design may be verified for a particular project by performing dynamic or static load testing on an installed pile. In these cases, a measure is being made of pile capacity for those specific design circumstances: pile length, pile cross-section, and soil profile. From this measurement, the designer has better knowledge of the actual pile capacity, hence reducing the uncertainty of production pile capacity. Thus, it is possible to consider two cases: 1) the uncertainty of a pile's predicted capacity in the absence of any confirming measurements, and 2) the uncertainty of a pile's predicted capacity after a similar pile at the same site has been tested. In the following development, the first case is considered. Thus, the resistance factors developed in this chapter are applicable to the routine design of piles, where the designer will not be able to revise the design on the basis of a verification test program. The data used to support this assessment consists of paired sets of in-situ test or soil property data

and pile load capacity data. By considering this data set, the relationship between soil test measurements and likely outcomes of pile capacity is sought.

8.1.1 Design of Closed-Ended Driven Piles in Sand

Property-Based Design of Shaft Capacity

Step 1. Identify limit state equation

The limit state equation for shaft capacity is written

$$\left[\frac{K_s}{K_0} K_0 \tan\left(\frac{\delta_c}{\phi_c}\phi_c\right)\sigma'_v\right] a_s dL - DL - LL = 0 \qquad \textbf{(8.1.1)}$$

where (K_s/K_0) is the ratio of earth pressure coefficient acting on the driven pile to the assumed at-rest coefficient K_0, (δ_c/ϕ_c) is the ratio of skin interface friction angle to measured critical-state friction angle ϕ_c for the soil, σ'_v is the effective overburden pressure at the depth where unit skin friction is estimated, a_s is the shaft area per unit pile length, *dL* is a unit length of pile, *DL* is the dead load acting on the unit length of pile, and *LL* is the live load acting on the unit length of pile.

Step 2. Identify the component variables

Of the variables in Equation (8.1.1), K_0, σ'_v, and a_s are selected by the designer; *DL* and *LL* are outputs of the design of the superstructure; ϕ_c is estimated or measured; and the ratios (K_s/K_0) and (δ_c/ϕ_c) are based on published results (i.e., values recommended for design).

Step 3. Identify the geotechnical tests associated with each variable

Of the identified variables, only ϕ_c can be measured in routine practice. Variable K_0 cannot be measured independently of D_R or ϕ_p in the field, and thus no systematic uncertainty in its determination can be defined. This means that the designer must have some other information, such as geologic history, from which to make an estimate of K_0. Since no measurement is made, any uncertainty assigned to this variable is arbitrary and does not reflect the specific design circumstance.

Step 4. Identify all component uncertainties for each variable, including transformations

The uncertainty for variables ϕ_c, *DL*, and *LL* have been identified previously (refer to Table 4.1.1). Variable a_s is specified by the designer and has negligible uncertainty since driven pile sections are fabricated at relatively small tolerances. Variable *dL* is used only for design purposes and has no effect on the final design prediction. Variable K_0 is estimated by the designer, but no systematic uncertainty can be determined for it.

We select the relationship from Paik and Salgado (2003) to choose values of ratio (K_s/K_0) for use in design. One strength of this relationship is the fact that it is supported by a focused calibration chamber study where most variables are strictly controlled. Thus, the nature of the relationship is not obscured by testing errors or other erroneous inferences about the stress states or soil properties around the pile shaft – errors that are redundant to those already accounted for in other aspects of the design. This relationship

is plotted in Figure 8.1.1 for closed-ended piles (PLR = 0) and fully unplugged open-ended piles (PLR = 1).

Note that the plot shows the intuitive trend that the change in lateral earth pressure coefficient will be greater for piles installed in dense sand than for loose sand. The accuracy of this trend is corroborated by some of the results of high-quality, instrumented pile load test results by Vesic (1970), BCP Committee (1971), Gregersen et al. (1973), Beringen et al. (1979), Briaud et al. (1989), Altaee et al. (1992, 1993), Paik et al. (2003) and Lee et al. (2003), also plotted in Figure 8.1.1. However, it should be noted that due to the highly sensitive nature of the parameters we are trying to back-calculate from these results, there should be a great deal of scatter in the plotted points, which can be observed in the figure. The most severe deviations from the computed trend in the figure are for Briaud et al. (1989), Paik et al. (2003), and Lee et al. (2003). All three of these studies incorporated adjustments for residual loads, which is outside the scope of this study. Such an adjustment will cause estimates of shaft friction to be reduced, which can be observed in the figure.

Uncertainty in the ratio (K_s/K_0) can be assessed by considering the results of high-quality, calibration-chamber instrumented pile load test results by Paik and Salgado (2003), as is done in the section on open ended piles below (section 8.1.2). Assuming (K_s/K_0) to be normally distributed, the PDF for (K_s/K_0) is defined as a normal distribution with $COV = 0.22$.

Uncertainty in ratio (δ_c/ϕ_c) can be assessed by considering the results of high quality, direct interface shear tests by Lehane et al. (1993), Jardine and Chow (1998), and Rao et al. (1998). A plot of ratio (δ_c/ϕ_c) for steel and concrete surfaces with different

average roughnesses R_a in contact with different sands appears in Figure 8.1.2. Note that at values of R_a greater than 4μm, there is no appreciable change in (δ_c/ϕ_c). Typical values of R_a for steel piles are greater than 8μm. Figure 8.1.3 is a histogram of the data in Figure 8.1.2 for values of R_a greater than 2μm. Based on these results, a normal distribution with mean 0.9 and COV 0.10 represents the uncertainty in (δ_c/ϕ_c).

Steps 5 and 6. Evaluate the composite uncertainties and select PDFs for reliability analysis

Equation (8.1.1) does not include variables that are computed from other variables. Hence, there is no transformation uncertainty to integrate into a composite uncertainty. The PDFs for (K_s/K_0) and (δ_c/ϕ_c) are selected in Step 4 and the PDF of ϕ_c is found in Section 4.1. These PDFs can be used directly with Equation (8.1.1) in reliability analysis.

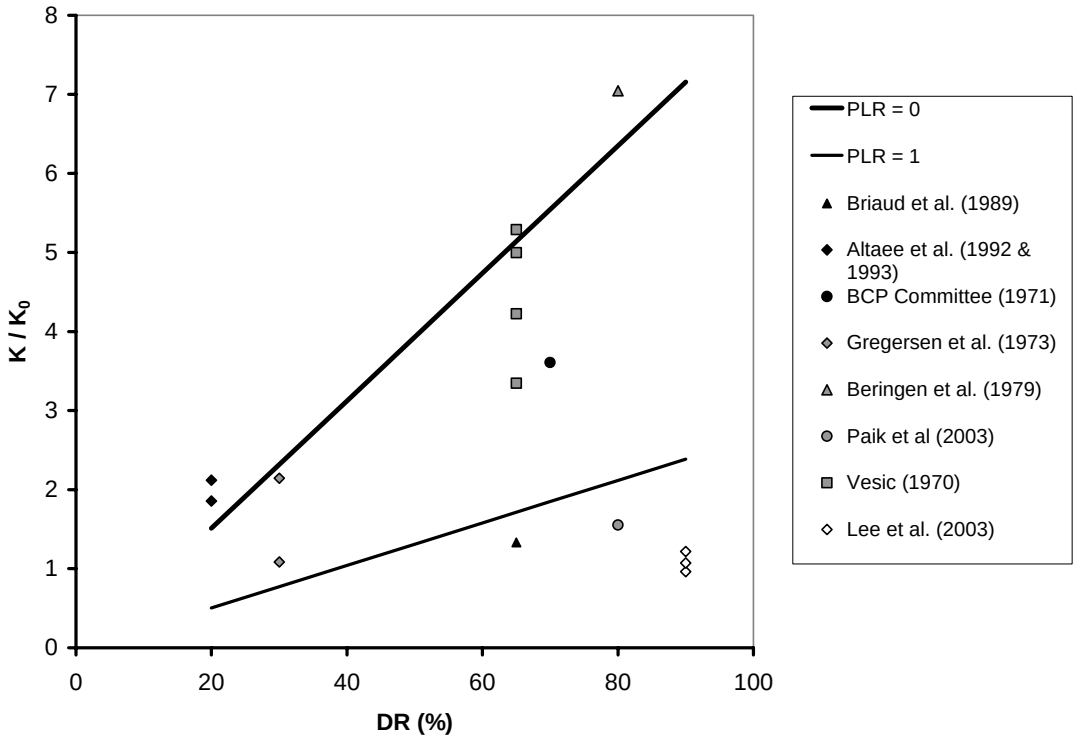

Figure 8.1.1. Relationship by Paik and Salgado (2003) for closed-ended piles (PLR = 0) and fully unplugged open-ended piles (PLR = 1). The results of several high-quality instrumented pile load tests on closed-ended piles are plotted for comparison.

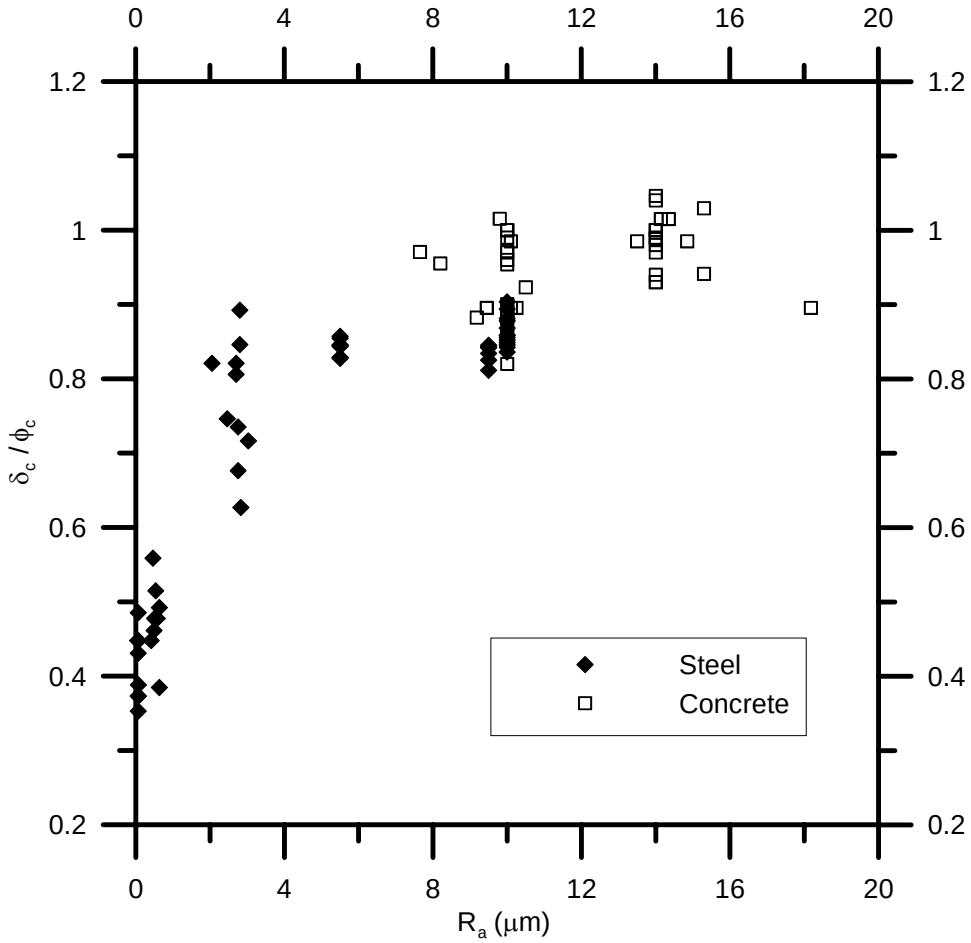

Figure 8.1.2 – δ_c/ϕ_c values based on results from high quality, direct interface shear tests.

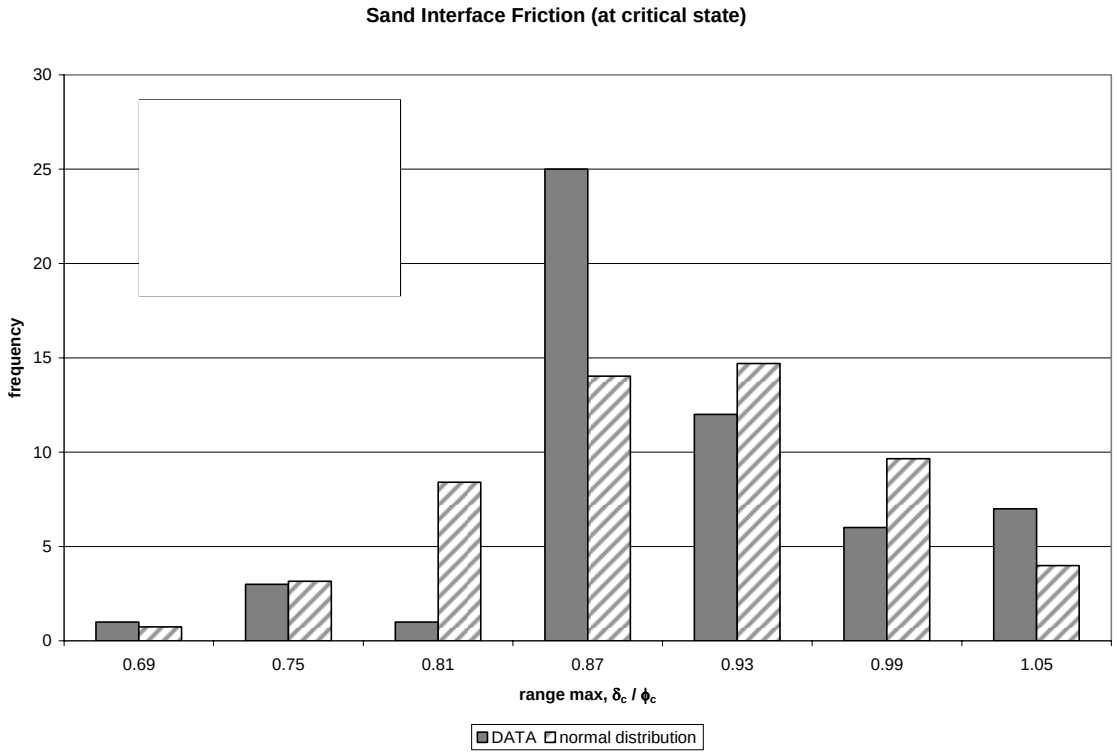

Figure 8.1.3 – Histogram of δ_c/ϕ_c values for R_a > 2μm, based on results from high quality, direct interface shear tests

Property-Based Design of Base Capacity

Step 1. Identify limit state equation

The limit state equation for base capacity is written

$$\left(\frac{q_{b,10\%}}{q_{bL}}\right) q_{bL} A_b - DL - LL = 0 \qquad \textbf{(8.1.2)}$$

where ($q_{b,10\%}/q_{bL}$) is the ratio of the base pressure at s/B = 10% to plunging base resistance q_{bL}, A_b is the pile base area, DL is the dead load acting on the base of the pile, and LL is the live load acting on the base of the pile.

Step 2. Identify the component variables

Of the variables in Equation (8.1.2), A_b is selected by the designer; *DL* and *LL* are outputs of the design of the superstructure; q_{bL} is computed from relative density D_R; and ratio ($q_{b,10\%}/q_c$) is based on published results.

Step 3. Identify the geotechnical tests associated with each variable

Of the identified variables, q_{bL} is computed from D_R, and D_R can be estimated using the CPT, the SPT, or field sampling (although special sampling procedures would be required to obtain a reliable estimate of D_R). Limit bearing pressure q_{bL} is computed from D_R using Salgado and Mitchell (2003):

$$\frac{q_{bL}}{p_A} = C_1 \exp\left(C_2 D_R\right)\left(\frac{\sigma'_h}{p_A}\right)^{C_3} \qquad \textbf{(8.1.3)}$$

where p_A is reference stress (100 kPa), C_1, C_2 and C_3 are constants, D_R is relative density, and σ'_h is the horizontal effective stress.

Step 4. Identify all component uncertainties for each variable, including transformations

The uncertainty for variables *DL*, and *LL* have been identified previously (refer to Table 4.1.1). Variable A_b is specified by the designer and has negligible uncertainty since driven pile sections are fabricated at relatively small tolerances. Uncertainty in ratio ($q_{b,10\%}/q_{bL}$) can be assessed by considering the results of high quality, instrumented pile load test results by Vesic (1970), BCP Committee (1971), Gregersen et al. (1973), Beringen et al. (1979), Briaud et al. (1989), Altaee et al. (1992, 1993), Paik et al. (2003) and Lee et al. (2003). A plot of ratio ($q_{b,10\%}/q_c$) for sand layers with different relative

densities appears in Figure 8.1.4. The uncertainty of ratio ($q_{b,10\%}/q_{bL}$) can be inferred from Figure 8.1.4 because, on average, the plunging load q_{bL} is equal to the cone tip resistance q_c (see discussion is Chapter 7). A significant trend of decreasing ($q_{b,10\%}/q_c$) with increasing D_R is noted from these results. The following trend for ratio ($q_{b,10\%}/q_c$) has been found and is plotted with the data in Figure 8.1.4.

$$\frac{q_{b,10\%}}{q_c} = 1.02 - 0.0051\, D_R(\%) \qquad \textbf{(8.1.4)}$$

The scatter in ratio ($q_{b,10\%}/q_c$) can be assessed by considering the data after it has been detrended and normalized with respect to Equation (8.1.4). This detrending is accomplished by

$$error_{q_{b,10\%}/q_c} = \frac{\left(\frac{q_{b,10\%}}{q_c}\right)_{data} - \frac{q_{b,10\%}}{q_c}(D_R)}{\frac{q_{b,10\%}}{q_c}(D_R)} \qquad \textbf{(8.1.5)}$$

where $error_{qb,10\%/qc}$ expresses the relative position of a particular data point around the trend line and function $q_{b,10\%}/q_c(D_R)$ represents the trend line (8.1.4) evaluated for D_R equal to that for the $q_{b,10\%}/q_c$ data point. When $error_{qb,10\%/qc}$ is computed for all data points, the distribution of the data points around the trendline can be depicted using the histogram in Figure 8.1.5. Since we divide by the mean trend value in (8.1.5), the standard deviation of $error_{qb,10\%/qc}$ is equal to the *COV* of $q_{b,10\%}/q_c$. Assuming ($q_{b,10\%}/q_c$) to be normally distributed, the data in Figure 8.1.4 indicate a *COV* of 0.17 when equation (3.2.1) is applied to the detrended data. This normal distribution is also depicted using a histogram in Figure 8.1.5. Since Equation (8.1.4) defines a mean value for ($q_{b,10\%}/q_{bL}$) a PDF representing the uncertainty of ($q_{b,10\%}/q_{bL}$) is a normal distribution with *COV* of 0.17.

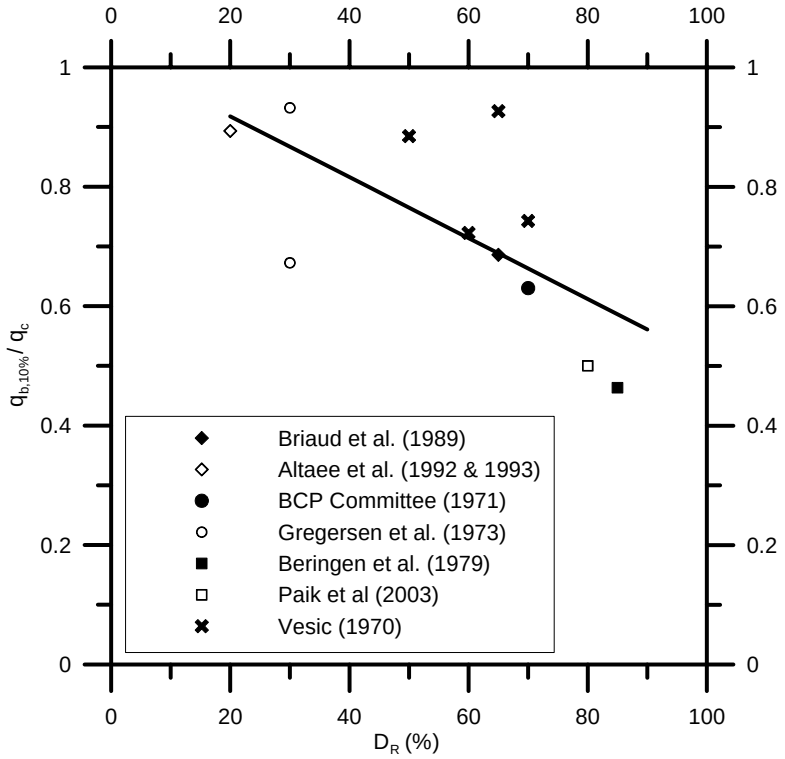

Figure 8.1.4 – $q_{b,10\%}/q_c$ values based on results from high quality, instrumented pile load tests on driven, full scale piles in sand. q_c values were measured using the CPT; $q_{b,10\%}$ was determined from load settlement curves from compression testing; q_b was measure directly from strain gauges in the pile; all piles were closed-ended steel piles or precast concrete; the trendline shown is $q_{b,10\%/qc} = -0.0051D_R(\%) + 1.02$

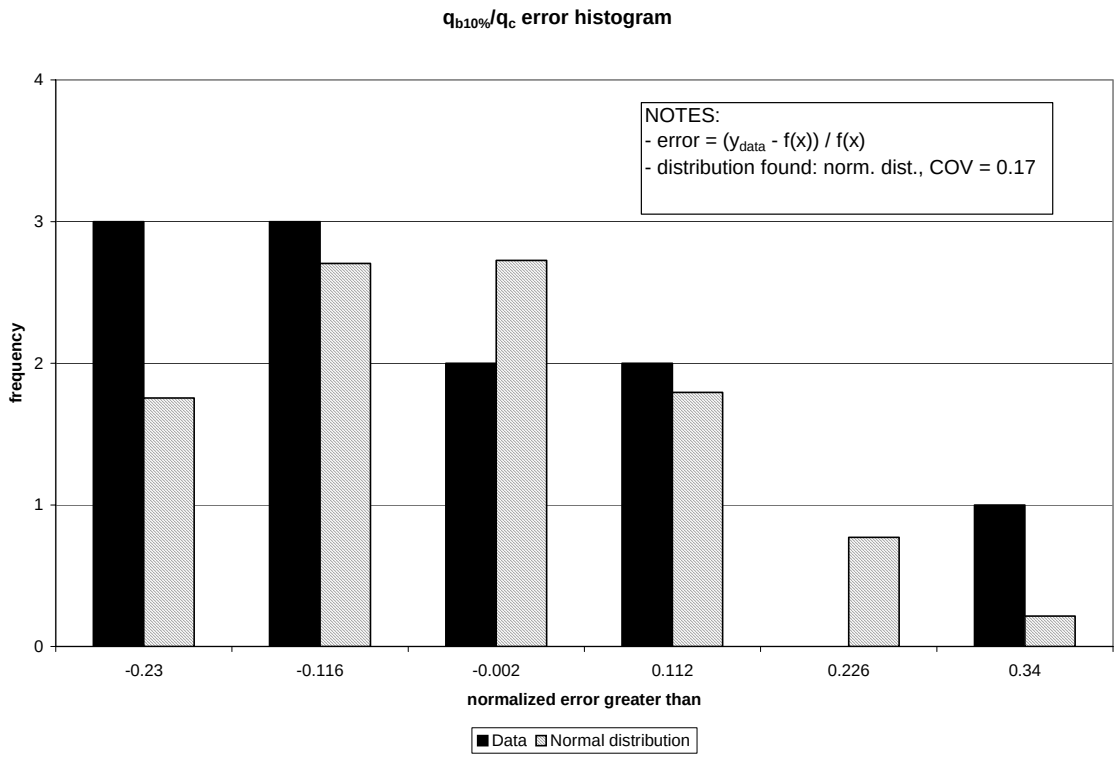

Figure 8.1.5 – Histogram of $error_{qb,10\%/qc}$ (detrended $q_{b,10\%}/q_c$ values) for closed-ended piles in sand

The predictive capability of an equation like (8.1.3) to determine values of q_{bL} from a known D_R in the lab was examined by Salgado et al. (1997). Experimental values of q_{bL} were found to fall within a ± 30% band of predicted values. The 6σ procedure was applied to find the *COV* of this predicted q_{bL}, yielding a value of 0.10. In the absence of other data, we consider the uncertainty of D_R measurements using the uncertainty of D_R determined from the CPT. In Section 4.1, the standard deviation of D_R was found to be 8% or less.

Steps 5 and 6. Evaluate the composite uncertainties and select PDFs for reliability analysis

Numerical integration of Equation (3.2.7) was used to find the uncertainty of transformed variable q_{bL}. To compute the histogram representing the uncertainty of q_{bL} using (3.2.7), $p_X(x)$ was defined as a normal distribution with σ = 8%, representing $D_{R(}\%)$, and transformation $y=f(x)$ is Equation (8.1.3). Note that numerical integration of (3.2.9) is not used here, and thus the uncertainty of transformation (8.1.3) is only included once, since it has already been accounted for in the uncertainty of D_R. The alternative would have been to integrate the uncertainty of (8.1.3) twice, which is not sensible because the same model is being used and thus no additional uncertainty is introduced through its use to find q_{bL}. The resulting histogram of q_{bL} is closely matched by a normal distribution with COV = 0.16. This histogram appears in Figure 8.1.6 for the case where D_R = 80%. A bias factor is needed for q_{bL} because it depends on the CAM method used to find D_R. For example, if the CPT is used to find D_R the bias factor on q_{bL} will be 1.06.

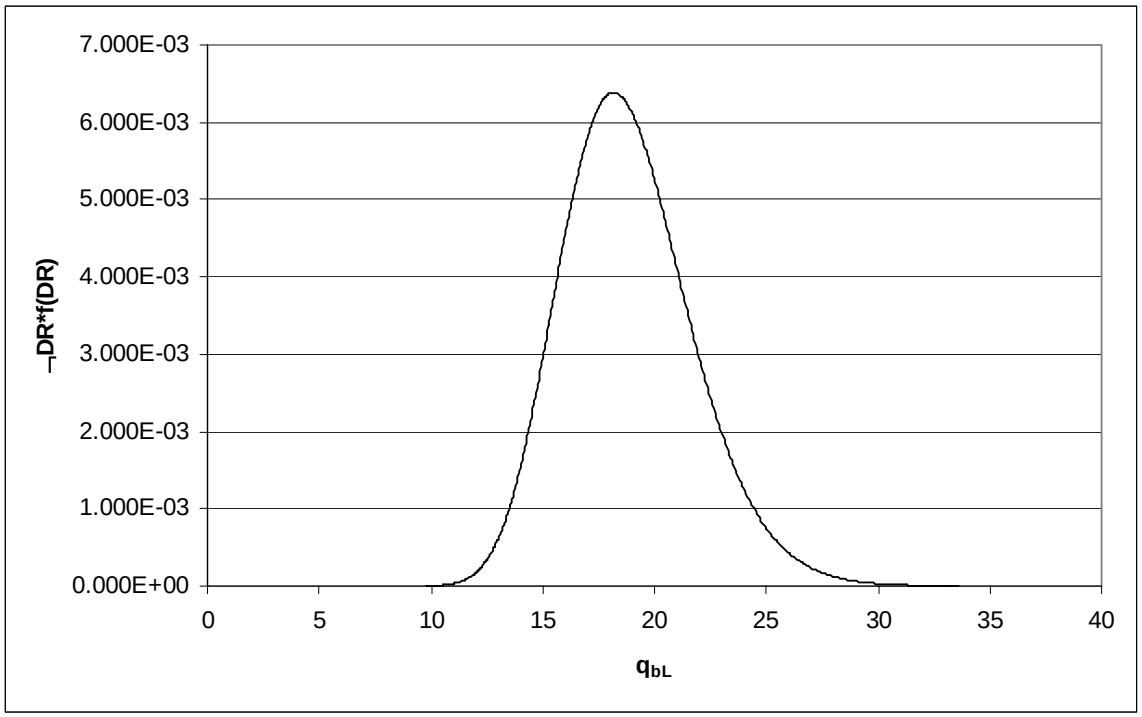

Figure 8.1.6 – Histogram of q_{bL} for D_R = 80% for closed-ended piles in sand

Direct Design of Shaft Capacity

We did not assess the uncertainty for direct design of shaft capacity because we had insufficient data to complete a satisfactory analysis. In Section 8.2, resistance factors for property-based shaft capacity are conservatively adopted for direct design.

Direct Design of Base Capacity

Step 1. Identify limit state equation

The limit state equation for base capacity is written

$$\left(\frac{q_{b,10\%}}{q_c}\right) q_c A_b - DL - LL = 0 \qquad \textbf{(8.1.6)}$$

where ($q_{b,10\%}/q_c$) is the ratio of the base pressure at s/B = 10% to cone tip resistance q_c, A_b is the pile base area, DL is the dead load acting on the base of the pile, and LL is the live load acting on the base of the pile.

Step 2. Identify the component variables

Of the variables in Equation (8.1.6), A_b is selected by the designer; DL and LL are outputs of the design of the superstructure; q_c is measured directly; and the ratio ($q_{b,10\%}/q_c$) is based on published results.

Step 3. Identify the geotechnical tests associated with each variable

Of the identified variables, q_c can be measured in routine practice. The uncertainty of q_c has been examined in Section 4.1.

Step 4. Identify all component uncertainties for each variable, including transformations

The uncertainty for variables q_c, DL, and LL have been identified previously (refer to Table 4.1.1). Variable A_b is specified by the designer and has negligible uncertainty since driven pile sections are fabricated at relatively small tolerances. Uncertainty in ratio ($q_{b,10\%}/q_c$) was assessed for property-based design of closed-ended piles and was found to be normally distributed, with a *COV* of 0.14 and mean equal to Equation (8.1.4).

Steps 5 and 6. Evaluate the composite uncertainties and select PDFs for reliability analysis

Equation (8.1.6) does not include variables that are computed from other variables, with the exception of ($q_{b,10\%}/q_c$) because D_R appears in Equation (8.1.4). Figure 8.1.4 inherently includes the uncertainty of D_R since these values were estimated from the field. Hence, there is no transformation uncertainty to integrate into a composite uncertainty. PDFs for ($q_{b,10\%}/q_c$) and q_c are selected in Step 4 and Section 4.1, respectively, and can be used directly with Equation (8.1.6) in reliability analysis.

8.1.2 Design of Open-Ended Driven Piles in Sand

Property-Based Design of Shaft Capacity

Step 1. Identify limit state equation

The limit state equation for shaft capacity is written

$$\left[\frac{K_s}{K_0}K_0\tan\left(\frac{\delta_c}{\phi_c}\phi_c\right)\sigma'_v\right]a_s dL - DL - LL = 0 \qquad \textbf{(8.1.7)}$$

where (K_s/K_0) is the ratio of earth pressure coefficient acting on the driven pile to the assumed at-rest coefficient K_0, (δ_c/ϕ_c) is the ratio of skin interface friction angle to measured critical-state friction angle ϕ_c for the soil, σ'_v is the effective overburden pressure at the depth where unit skin friction is estimated, a_s is the shaft area per unit pile length, *dL* is a unit length of pile, *DL* is the dead load acting on the unit length of pile, and *LL* is the live load acting on the unit length of pile.

Step 2. Identify the component variables

Of the variables in Equation (8.1.7), K_0, σ'_v, and a_s are selected by the designer; *DL* and *LL* are outputs of the design of the superstructure; ϕ_c is estimated or measured; and ratios (K_s/K_0) and (δ_c/ϕ_c) are based on published results. The value of (K_s/K_0) to use in design is found using Paik and Salgado (2003):

$$\frac{K}{K_0} = \beta(7.2 - 4.8\text{PLR}) \qquad \textbf{(8.1.8a)}$$

$$\beta = 0.0002D_R{}^2(\%) - 0.0089D_R + 0.329,\ 20\% < D_R(\%) < 90\% \qquad \textbf{(8.1.8b)}$$

where *PLR* is the plug length ratio, which can be measured or estimated.

Step 3. Identify the geotechnical tests associated with each variable

Of the identified variables, only ϕ_c and *PLR* can be measured in routine practice. Variable K_0 cannot be measured independently of D_R or ϕ_p in the field, and thus no systematic uncertainty in its determination can be defined. This means that the designer

must have some other information, such as geologic history, from which to make an estimate of K_0. However, since no measurement is made, any uncertainty assigned to this variable is arbitrary and does not reflect the specific design circumstance. Plug length ratio *PLR* can be measured for a test pile before production piling starts or can be estimated from charts presented by Lee et al. (2003).

Step 4. Identify all component uncertainties for each variable, including transformations

The uncertainty for variables ϕ_c, *DL*, and *LL* have been identified previously (refer to Table 4.1.1). Variable a_s is specified by the designer and has negligible uncertainty since driven pile sections are fabricated at relatively small tolerances. Variable *dL* is used only for design purposes and has no affect on the final design prediction. Variable K_0 is estimated by the designer, but no systematic uncertainty can be determined for it.

Uncertainty in ratio (K_s/K_0) can be assessed by considering the results of high-quality, calibration chamber, instrumented pile load test results by Paik and Salgado (2003). A plot of ratio (K_s/K_0) for sand with different relative densities appears in Figure 8.1.7. Note that, in contrast to closed-ended piles, there is a trend of increasing K_s/K_0 with increasing D_R. This is due to the effect of plugging. Denser sands exhibit more plugging, increasing the displacement of the surrounding soil during driving. Increased displacement caused by pile driving increases the stress against the pile shaft, hence higher values of K_s/K_0 are observed. Closed-ended piles behave as a fully plugged open-ended pile for any relative density. Thus, there is no variation in displacement with relative density for closed-ended piles. The scatter in ratio (K_s/K_0) can be assessed by

considering the data after it has been detrended and normalized with respect to equation (8.1.8). This detrending is accomplished by

$$error_{K_s/K_0} = \frac{\left(\frac{K_s}{K_0}\right)_{data} - \frac{K_s}{K_0}(PLR, D_R)}{\frac{K_s}{K_0}(PLR, D_R)} \qquad \textbf{(8.1.9)}$$

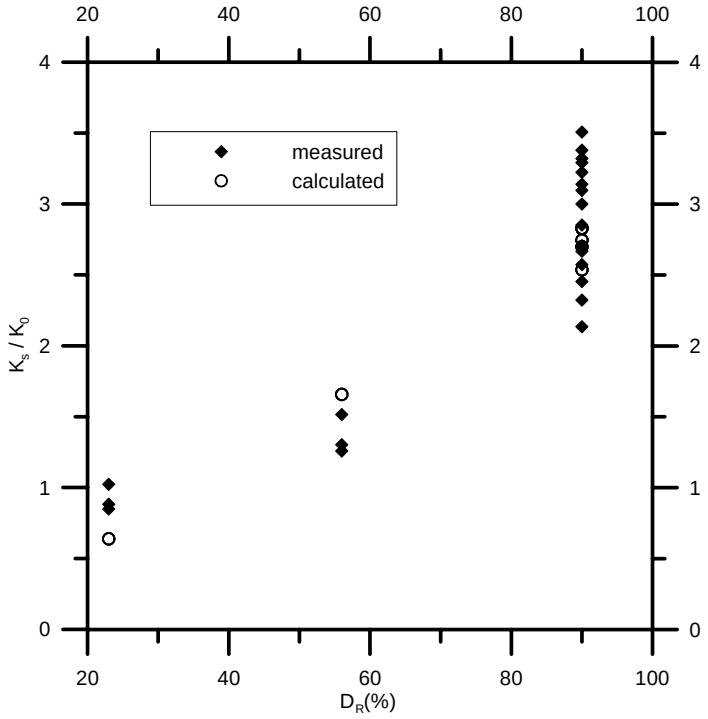

Figure 8.1.7 – Average K_s/K_0 values from Paik and Salgado (2003) for open-ended piles in sand; calculated points indicate values computed using (8.1.8).

where $error_{Ks/Ko}$ expresses the relative position of a particular data point around the trend line and function $K_s/K_0(PLR,D_R)$ represents the trend line (8.1.8) evaluated for *PLR* and

D_R equal to that for the K_s/K_0 data point. When $error_{Ks/Ko}$ is computed for all data points, the distribution of the data points around the trendline can be depicted using the histogram in Figure 8.1.8. Since we divide by the mean trend value in (8.1.9), the standard deviation of $error_{Ks/Ko}$ is equal to the *COV* of K_s/K_0. Assuming (K_s/K_0) to be normally distributed, the data in Figure 8.1.7 indicate a *COV* of 0.22 when equation (3.2.1) is applied to the detrended data. This normal distribution is also depicted using a histogram in Figure 8.1.8.

The uncertainty of (δ_c/ϕ_c) has been determined in Section 8.1.1.

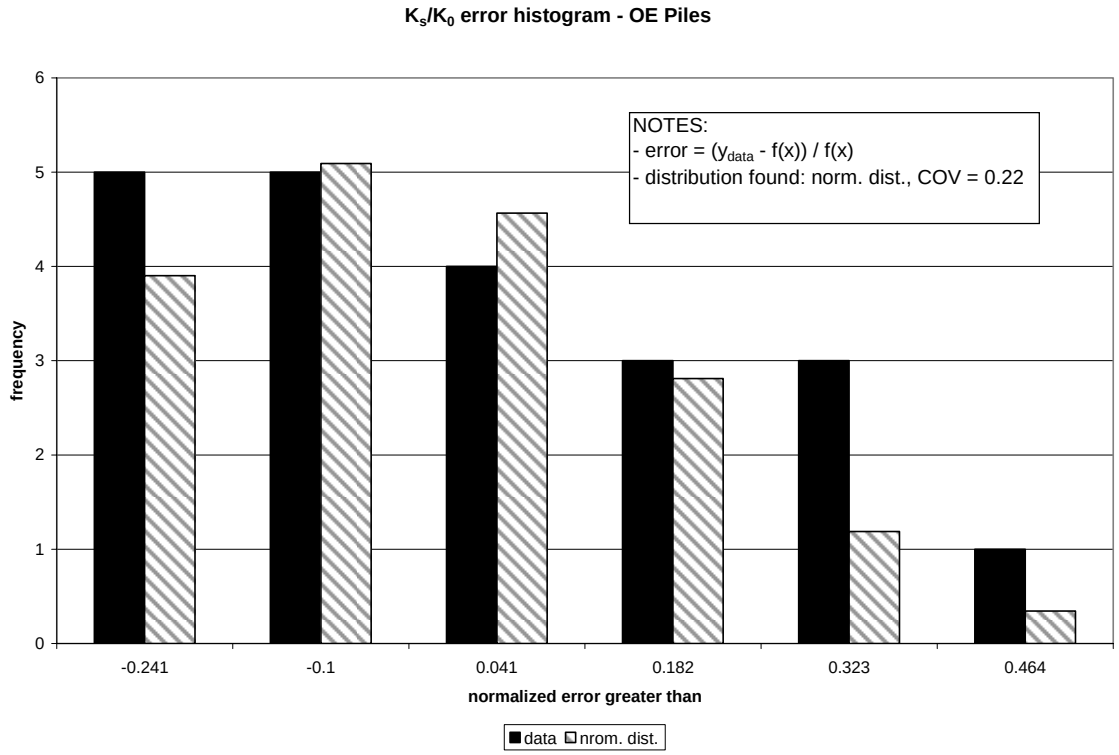

Figure 8.1.8 – Histogram of $error_{Ks/Ko}$ (detrended K_s/K_0 values) for open-ended piles in sand

Steps 5 and 6. Evaluate the composite uncertainties and select PDFs for reliability analysis

Equation (8.1.7) does not include variables that are computed from other variables. Hence, there is no transformation uncertainty to integrate into a composite uncertainty. The PDFs for (K_s/K_0) and (δ_c/ϕ_c) are selected in Step 4 and the PDF of ϕ_c is found in Section 4.1. These PDFs can be used directly with Equation (8.1.7) in reliability analysis.

Property-Based Design of Base Capacity

Step 1. Identify limit state equation

The limit state equation for base capacity is written

$$\left(\frac{q_{b,10\%}}{\sigma'_h}\right)\sigma'_h A_b - DL - LL = 0 \qquad \textbf{(8.1.10)}$$

where ($q_{b,10\%}/\sigma'_h$) is the ratio of the base pressure at s/B = 10% to horizontal effective stress σ'_h, A_b is the pile base area, *DL* is the dead load acting on the base of the pile, and *LL* is the live load acting on the base of the pile.

Step 2. Identify the component variables

Of the variables in Equation (8.1.10), *DL* and *LL* are outputs of the design of the superstructure; σ'_h is estimated by the designer, A_b is calculated using the outside pile diameter d_o,

$$A_b = \pi\left(d_o\right)^2 / 4 \qquad \textbf{(8.1.11)}$$

and the ratio ($q_{b,10\%}/\sigma'_h$) is based on published results by Paik and Salgado (2003) as follows:

$$\frac{q_{b,10\%}}{\sigma'_h} = \alpha\left(326 - 295\frac{\text{IFR}(\%)}{100}\right) \qquad \textbf{(8.1.12a)}$$

$$\alpha = 0.0112 D_R(\%) - 0.0141,\ 20\% < D_R(\%) < 90\% \qquad \textbf{(8.1.12b)}$$

where *IFR*(%) is the incremental filling ratio, which can be measured or estimated.

Step 3. Identify the geotechnical tests associated with each variable

Values of ($q_{b,10\%}/\sigma'_h$) depend on D_R, which can be estimated using the CPT, the SPT, or field sampling. Incremental filling ratio *IFR*(%) can be measured or estimated from charts presented by Lee et al. (2003).

Step 4. Identify all component uncertainties for each variable, including transformations

The uncertainty for variables *DL* and *LL* have been identified previously (refer to Table 4.1.1). Variable A_b is specified by the designer and has negligible uncertainty since driven pile sections are fabricated at relatively small tolerances.

Uncertainty in ratio ($q_{b,10\%}/\sigma'_h$) can be assessed by considering the results of high quality, calibration chamber, instrumented pile load test results by Paik and Salgado (2003). The scatter in ratio ($q_{b,10\%}/\sigma'_h$) can be assessed by considering this data after it has been detrended and normalized with respect to equation (8.1.12). This detrending is accomplished by

$$error_{q_{b,10\%}/\sigma'_h} = \frac{\left(\frac{q_{b,10\%}}{\sigma'_h}\right)_{data} - \frac{q_{b,10\%}}{\sigma'_h}(IFR, D_R)}{\frac{q_{b,10\%}}{\sigma'_h}(IFR, D_R)} \qquad \textbf{(8.1.13)}$$

where $error_{qb,10\%/\sigma'h}$ expresses the relative position of a particular data point around the trend line and function $q_{b,10\%}/\sigma'_h$ (*IFR*,*DR*) represents the trend line (8.1.12) evaluated for *IFR*(%) and D_R equal to that for the $q_{b,10\%}/\sigma'_h$ data point. When $error_{qb,10\%/\sigma'h}$ is computed for all data points, the distribution of the data points around the trendline can be depicted using the histogram in Figure 8.1.9. Since we divide by the mean trend value in (8.1.12), the standard deviation of $error_{qb,10\%/\sigma'h}$ is equal to the *COV* of $q_{b,10\%}/\sigma'_h$. Assuming transformation ($q_{b,10\%}/\sigma'_h$) to be normally distributed, the data indicate a *COV* of 0.11 when equation (3.2.1) is applied to the detrended data. This PDF represents the variability of corrected values of $q_{b,10\%}$ for a given value of σ'_h. This normal distribution is also depicted using a histogram in Figure 8.1.9.

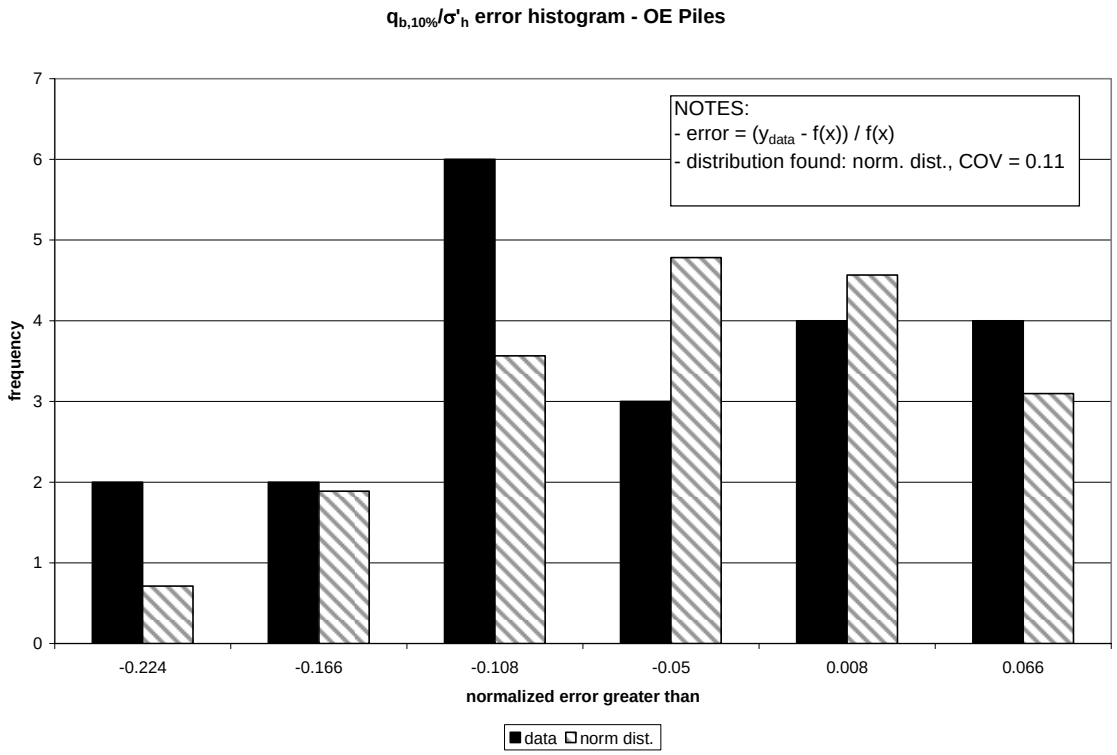

Figure 8.1.9 – Histogram of $error_{qb,10\%/\sigma'h}$ (detrended $q_{b,10\%}/\sigma'_h$ values) for open-ended piles in sand

Due to chamber-to-field size effects, $q_{b,10\%}$ was corrected by Paik and Salgado (2003) based on the results of Salgado et al. (1998). This work is based on penetration resistance analysis described by Salgado et al. (1997). Salgado et al. (1997) examined the predictive capability of this analysis to determine values of q_c from a known D_R in the lab. Experimental values of q_c were found to fall within a ± 30% band of predicted values. The 6σ procedure was applied to find the *COV* of this predicted q_c, yielding a value of 0.10. Thus, a normal distribution with *COV* = 0.10 represents the uncertainty of corrected values of $q_{b,10\%}$ since the same theoretical model was used to make the correction as was assessed in the study by Salgado et al. (1997).

Steps 5 and 6. Evaluate the composite uncertainties and select PDFs for reliability analysis

The composite uncertainty of $(q_{b,10\%}/\sigma'_h)$ due to transformation uncertainty and the uncertainty of the correction to field values of $q_{b,10\%}$ must be assessed. Numerical integration of (3.2.9) is used to accomplish this task. To compute the histogram representing the composite uncertainty of $(q_{b,10\%}/\sigma'_h)$, $p_X(x)$ was defined as a normal distribution with *COV* = 0.10, representing $q_{b,10\%}$, and $p_{Y|X}(y|x)$ was defined as a normal distribution with *COV* = 0.11, representing the transformation uncertainty $(q_{b,10\%}/\sigma'_h)$. The resulting histogram $p_Y(y)\Delta y$ represents the uncertainty of $(q_{b,10\%}/\sigma'_h)$ assessed by Paik and Salgado (2003) using calibration chamber tests. This histogram appears in Figure 8.1.10. A matching PDF is a normal distribution with *COV* = 0.15. Note that the uncertainty of D_R introduced by in-situ test correlation to $(q_{b,10\%}/\sigma'_h)$ through the use of Equation (8.1.12) is accounted for by this PDF. This is because the model used to assess the field correction for $q_{b,10\%}$ is the same model used to correlate CPT q_c values to D_R. Thus, any variation in the prediction of the model for a specific case will have been accounted for. For example, suppose that for a given D_R, the Salgado et al. (1998) model predicts a field value of $q_{b,10\%}$ that is too high. In the same instance, it will also predict a D_R that is too low when applied to a q_c measurement. Thus, the variability of this model should only be integrated once into the composite uncertainty of $(q_{b,10\%}/\sigma'_h)$. Redundant integration of its uncertainty will overestimate the uncertainty of $(q_{b,10\%}/\sigma'_h)$.

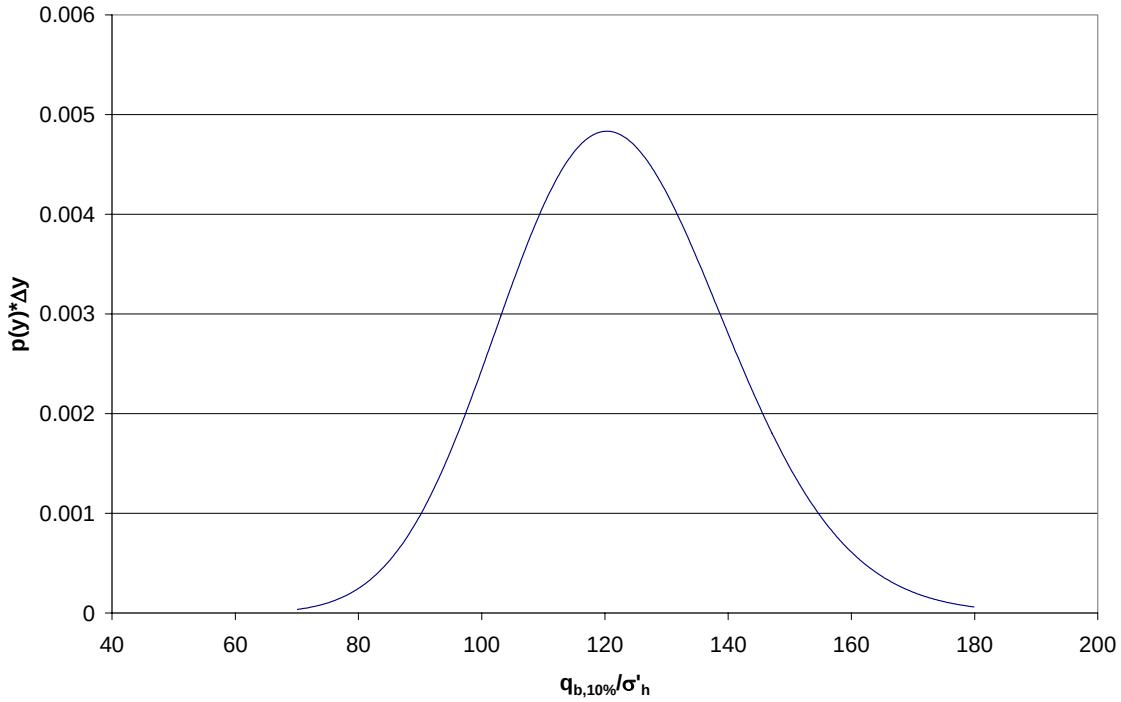

Figure 8.1.10 – Histogram representing the composite uncertainty for $q_{b,10\%}/\sigma'_h$ when D_R = 90% and *IFR* = 70% for open-ended piles in sand

Direct Design of Shaft Capacity

Step 1. Identify limit state equation

The limit state equation for shaft capacity is written

$$\left(\frac{f_s}{q_c}\right) q_c a_s dL - DL - LL = 0 \qquad \textbf{(8.1.14)}$$

where (f_s/q_c) is the ratio of unit shaft friction to CPT tip resistance q_c, a_s is the shaft area per unit pile length, *dL* is a unit length of pile, *DL* is the dead load acting on the unit length of pile, and *LL* is the live load acting on the unit length of pile.

Step 2. Identify the component variables

Of the variables in Equation (8.1.14), a_s is selected by the designer; *DL* and *LL* are outputs of the design of the superstructure; q_c is measured; and ratio (f_s/q_c) is based on published results. Lee et al. (2003) recommend a value between 0.0015 and 0.004 for (f_s/q_c). Analysis of the data from Paik and Salgado (2003) indicates a mean value of 0.002.

Step 3. Identify the geotechnical tests associated with each variable

Of the identified variables, q_c can be measured in routine practice. The uncertainty of q_c has been examined in Section 4.1.

Step 4. Identify all component uncertainties for each variable, including transformations

The uncertainty for variables *DL* and *LL* have been identified previously (refer to Table 4.1.1). Variable a_s is specified by the designer and has negligible uncertainty since driven pile sections are fabricated at relatively small tolerances. Variable *dL* is used only for design purposes and has no affect on the final design prediction.

Uncertainty in ratio (f_s/q_c) can be assessed by considering the results of high quality, calibration chamber, instrumented pile load test results by Paik and Salgado (2003). Assuming (K_s/K_0) to be normally distributed, the data from Paik and Salgado (2003) indicate a mean of 0.002 and a *COV* of 0.23 when equation (3.2.1) is applied.

Steps 5 and 6. Evaluate the composite uncertainties and select PDFs for reliability analysis

Equation (8.1.14) does not include variables that are computed from other variables. Hence, there is no transformation uncertainty to integrate into a composite uncertainty. The PDFs for (f_s/q_c) and q_c are selected in Step 4 and Section 4.1, respectively, and can be used directly with Equation (8.1.14) in reliability analysis.

Direct Design of Base Capacity

Step 1. Identify limit state equation

The limit state equation for base capacity is written

$$\left(\frac{q_{b,10\%}}{q_c}\right)q_c A_b - DL - LL = 0 \qquad \textbf{(8.1.15)}$$

where ($q_{b,10\%}/q_c$) is the ratio of the base pressure at s/B = 10% to CPT tip resistance q_c, A_b is the pile base area, *DL* is the dead load acting on the base of the pile, and *LL* is the live load acting on the base of the pile.

Step 2. Identify the component variables

Of the variables in Equation (8.1.15), *DL* and *LL* are outputs of the design of the superstructure; q_c is measured directly, A_b is calculated using the outside pile diameter (8.1.11), and the ratio ($q_{b,10\%}/q_c$) is based on published results by Paik and Salgado (2003) and Lee et al. (2003). The value of $q_{b,10\%}/q_c$ to use in design is found using Lee et al. (2003):

$$\frac{q_b}{q_c} = -0.00443IFR(\%) + 0.557 \qquad \textbf{(8.1.16)}$$

where *IFR*(%) is the incremental filling ratio, which can be measured or estimated.

Step 3. Identify the geotechnical tests associated with each variable

Of the identified variables, q_c can be measured in routine practice. The uncertainty of q_c has been examined in Section 4.1. Incremental filling ratio *IFR*(%) can be measured or estimated from charts presented by Lee et al. (2003).

Step 4. Identify all component uncertainties for each variable, including transformations

The uncertainty for variables *DL*, and *LL* have been identified previously (refer to Table 4.1.1). Variable A_b is specified by the designer and has negligible uncertainty since driven pile sections are fabricated at relatively small tolerances.

Uncertainty in ratio ($q_{b,10\%}/q_c$) can be assessed by considering the results of high quality, calibration chamber, instrumented pile load test results by Paik and Salgado (2003). A plot of ratio ($q_{b,10\%}/q_c$) for different values of incremental filling ratio IFR(%) appears in Figure 8.1.11. A significant trend of decreasing ($q_{b,10\%}/q_c$) with increasing IFR(%) is noted from these results. The trendline defined by (8.1.16) is plotted with the data in Figure 8.1.11. The scatter in ratio ($q_{b,10\%}/q_c$) can be assessed by considering the data after it has been detrended and normalized with respect to equation (8.1.16). This detrending is accomplished by

$$error_{q_{b,10\%}/q_c} = \frac{\left(\frac{q_{b,10\%}}{q_c}\right)_{data} - \frac{q_{b,10\%}}{q_c}(IFR)}{\frac{q_{b,10\%}}{q_c}(IFR)} \qquad \textbf{(8.1.17)}$$

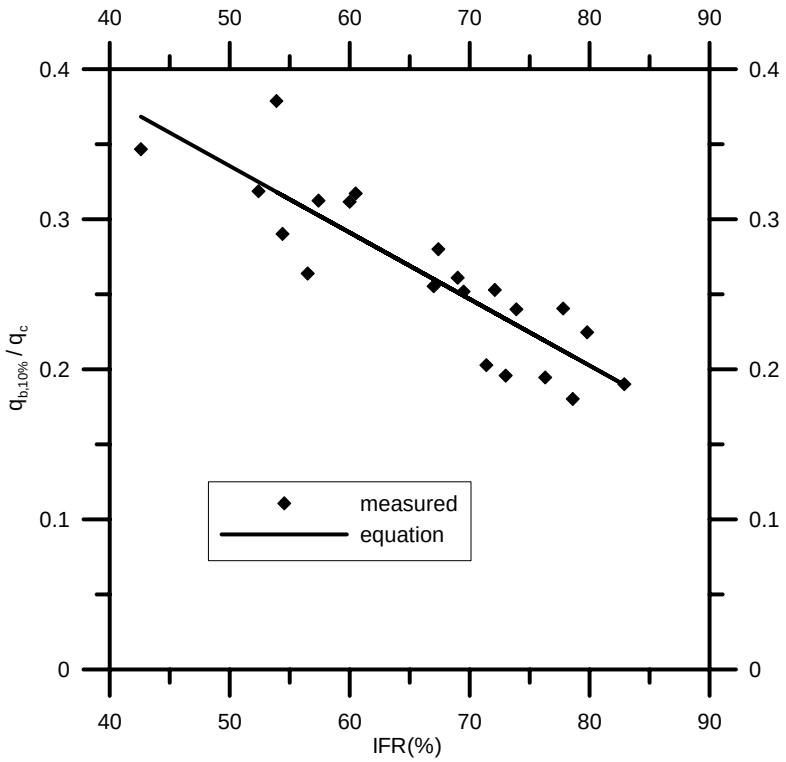

Figure 8.1.11 – $q_{b,10\%}/q_c$ vs. *IFR*(%) for Open-Ended piles from Paik and Salgado (2003) with trend line proposed by Lee et al. (2003)

where $error_{qb,10\%/qc}$ expresses the relative position of a particular data point around the trend line and function $q_{b,10\%}/q_c(IFR)$ represents the trend line (8.1.16) evaluated for *IFR*(%) equal to that for the $q_{b,10\%}/q_c$ data point. When $error_{qb,10\%/qc}$ is computed for all data points, the distribution of the data points around the trendline can be depicted using the histogram in Figure 8.1.12. Since we divide by the mean trend value in (8.1.17), the standard deviation of $error_{qb,10\%/qc}$ is equal to the *COV* of $q_{b,10\%}/q_c$. Assuming $(q_{b,10\%}/q_c)$ to be normally distributed, the data in Figure 8.1.11 indicate a *COV* of 0.10 when equation (3.2.1) is applied to the detrended data. This normal distribution is also depicted using a histogram in Figure 8.1.12.

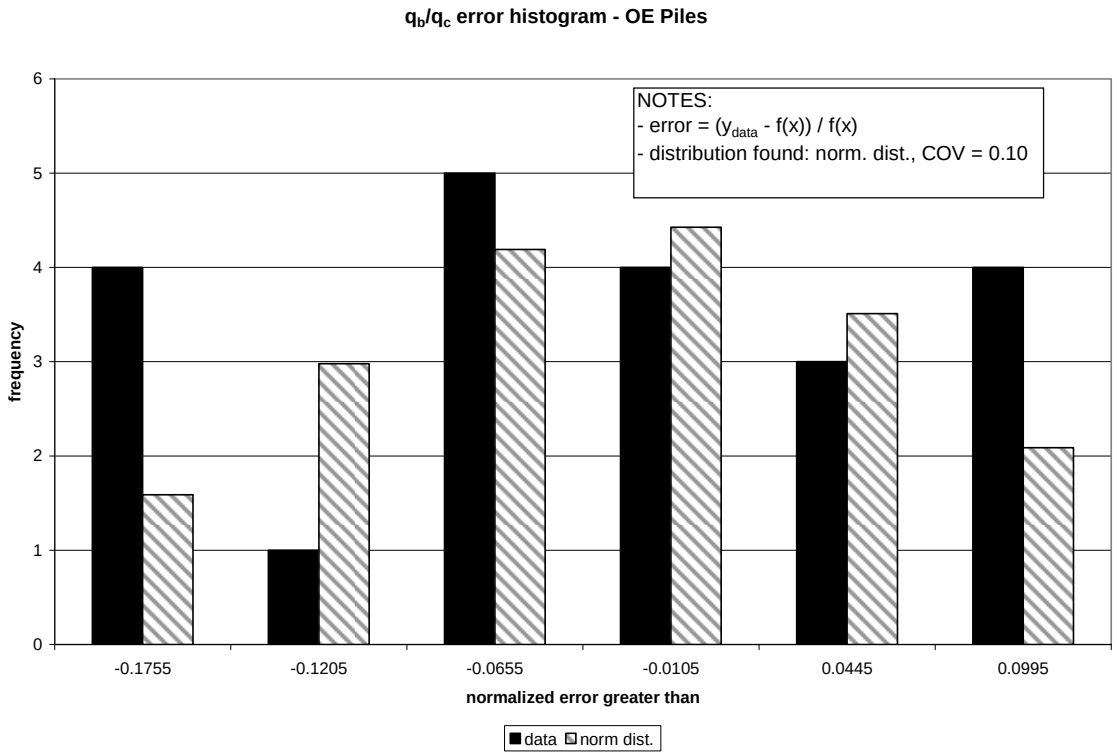

Figure 8.1.12 – Histogram of $error_{qb,10\%/qc}$ (detrended $q_{b,10\%}/q_c$ values) for open-ended piles in sand

Steps 5 and 6. Evaluate the composite uncertainties and select PDFs for reliability analysis

The uncertainty in values of IFR(%), which depends on σ'_h and D_R, is present in both the designer's estimate and in the data used to assess the uncertainty of ratio ($q_{b,10\%}/q_c$). Thus a normal PDF with *COV* = 0.10 represents the transformation uncertainty of (8.1.16) and *IFR*(%). The PDFs for q_c, *DL*, and *LL* have been defined previously.

8.1.3 Design of Drilled Shafts in Sand

Property-Based Design of Shaft Capacity

We did not assess the uncertainty for property-based design of shaft capacity because we had insufficient data to complete a satisfactory analysis.

Property-Based Design of Base Capacity

Step 1. Identify limit state equation

The limit state equation for base capacity is written

$$\left(\frac{q_{b,10\%}}{q_{bL}}\right) q_{bL} A_b - DL - LL = 0 \qquad \textbf{(8.1.18)}$$

where ($q_{b,10\%}/q_{bL}$) is the ratio of the base pressure at s/B = 10% to the plunging value of base pressure q_{bL}, A_b is the pile base area, DL is the dead load acting on the base of the pile, and LL is the live load acting on the base of the pile.

Step 2. Identify the component variables

Of the variables in Equation (8.1.18), A_b is selected by the designer; DL and LL are outputs of the design of the superstructure; q_{bL} is estimated from relative density D_R and an estimated value of σ'_h using (8.1.3); D_R can be estimated from the CPT, the SPT, or field sampling; and ratio ($q_{b,10\%}/q_{bL}$) is based on published results by Lee and Salgado (1999).

The load-settlement response of a pile base can be expressed simply as

$$w = \frac{q_b D}{E_s}\left(1 - \mu_s^2\right) I_p \qquad \textbf{(8.1.19)}$$

where w is the settlement, q_b is the unit base load, E_s and μ_s are the soil Young's modulus and Poissons's ratio, respectively, and I_p is an influence factor. Even though the soil response cannot be expected to be linear elastic as is implied by (8.1.19), if the modulus is adjusted for the strain level, this is an acceptable approximation. For use in design circumstances, E_s in Equation (8.1.19) can be calibrated with the results from ABAQUS as was done by Lee and Salgado (1999, 2002). If sufficient convergence checks are performed, the calibration performed using ABAQUS introduces little uncertainty beyond that of the material model. Thus, if the uncertainty for E_s in (8.1.19) can be found, the uncertainty of q_b is found. Rewriting (8.1.19) with the assessment of uncertainty in mind, the following expression for q_b results:

$$q_b = \frac{E_s w}{D} c_s \qquad \textbf{(8.1.20)}$$

where c_s is a constant accounting for the problem mechanics and geometry. Equation (8.1.20) clearly shows that q_b is directly proportional to E_s. Thus the uncertainty in q_b is directly proportional to that of E_s.

Lee and Salgado (1999) developed a non-linear elastic constitutive model to investigate the load-settlement response at the base of a drilled shaft. With this load-settlement model, Equation (8.1.20) can be used to estimate E_s using D_R as an input parameter. Thus, the uncertainty of the constitutive model used by Lee and Salgado (1999) must be considered to evaluate the uncertainty of E_s. Figure 8.1.13 illustrates the complete series of transformations required to move from relative density to modulus E_s. The numbers beneath each variable represent the COV for that variable. The numbers in each arrow represent the uncertainty for that transformation in terms of the resulting variable.

The work of Hardin and Black (1966) led to the following empirical relationship for G_0,

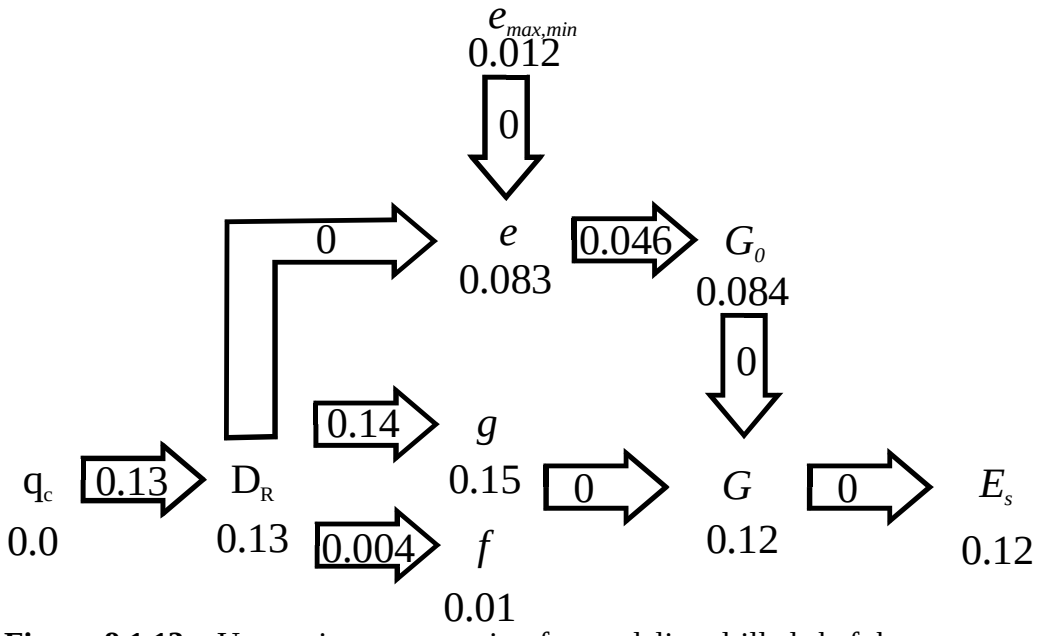

Figure 8.1.13 – Uncertainty propagation for modeling drilled shaft base movement, from CONPOINT estimates of D_R to modulus E_s

$$G_0 = C_g \frac{(e_g - e_0)^2}{1 + e_0} P_a^{(1-n_g)} (\sigma'_m)^{n_g} \qquad \textbf{(8.1.21)}$$

where C_g, n_g, and e_g are intrinsic material variables; e_o is the initial void ratio; P_a is a reference pressure of (100 kPa); and σ'_m is the initial mean effective stress in the same units as P_a. The initial void ratio can be determined from relative density using the fundamental equation

$$D_R = \frac{e_{\max} - e}{e_{\max} - e_{\min}} \qquad \textbf{(8.1.22)}$$

The modulus degradation with stress level is modeled with the expression

$$\frac{G}{G_0} = \left[1 - f\left(\frac{\sqrt{J_2} - \sqrt{J_{2o}}}{\sqrt{J_{2max}} - \sqrt{J_{2o}}}\right)^g\right]\left(\frac{I_1}{I_{1o}}\right)^{n_g} \qquad \textbf{(8.1.23)}$$

where J_2 = second invariant of the deviatoric stress tensor, f and g are curve fitting parameters, and I_1 and I_{1o} are the first variants of the stress tensor at the current and initial states, respectively.

Step 3. Identify the geotechnical tests associated with each variable

Of the identified variables, D_R can be estimated using the CPT, the SPT, or unit weight from field sampling. The CPT, SPT, or unit weight can be measured in routine practice. The uncertainty of q_c and N_{SPT} has been examined in Section 4.1.

Step 4. Identify all component uncertainties for each variable, including transformations

The first consideration is the uncertainty in ratio ($q_{b,10\%}/q_{bL}$). The uncertainty of this ratio is due to the uncertainties in the numerical model used to represent the soil. Starting at the left side of Figure 8.1.13, the influence of D_R uncertainty is considered. Since the curves presented by Lee and Salgado (1999) for base resistance use cone penetration as the input concerning the state of the soil, the ability of CONPOINT to predict q_c from D_R is a pertinent measure of the variability of D_R in the analysis. Values of q_c at this point are not measured, but computed by CONPOINT, so the inherent soil variability measured by the CPT is not introduced at this stage.

To find values of G_0 for use in the analysis, e_0 is found using (8.1.22) from D_R, e_{min}, and e_{max}. The uncertainty of void ratios e_{min} and e_{max} can be approximated from ASTM standard tolerances. The uncertainty of the transformation represented by

equation (8.1.21) can be assessed by considering the data presented by Hardin and Black (1966).

Curve fitting parameters *f* and *g* in equation (8.1.23) vary primarily with the relative density of the sand being tested. Thus, the uncertainty in the relative density of the sand, a state parameter reflected in the results of both CONPOINT and the ABAQUS pile base model, is a source of uncertainty for the *f* and *g* parameters as well as for G_0.

The plots in Figure 8.1.14 illustrate the uncertainty in parameters *f* and *g* for cases where the relative density is known. This uncertainty represents the transformation uncertainty from relative density to parameters *f* and *g*.

The uncertainty for variables *DL*, and *LL* have been identified previously (refer to Table 4.1.1). Variable A_b is specified by the designer. However, the actual base area depends on quality control measures in the field. Since quality control varies from site to site, a systematic assessment of A_b uncertainty is not possible. It is recommended that the designer take reasonable precautions concerning the value of A_b used in predicting base capacity.

Steps 5 and 6. Evaluate the composite uncertainties and select PDFs for reliability analysis

The composite effect of all of the uncertainties introduced by CONPOINT, measurement of e_{max} and e_{min}, transformations to *f* and *g*, and transformations (8.1.21) and (8.1.23) have been assessed for each step in Figure 8.1.13 by numerical integration of a modified form of Equation (3.2.9). For example, to compute the histogram representing the composite uncertainty of modulus *G*, $p_X(x)$ was defined as a normal distribution with

COV = 0.084, representing G_0, $p_Y(y)$ was defined as a normal distribution with *COV* = 0.15, representing *f*, and $p_Z(z)$ was defined as a normal distribution with *COV* = 0.01, representing *g*. Conditional PDF $p_{W|XYZ}(w|xyz)$ was not used since any inaccuracy in Equation (8.1.23) depends completely on fitting parameters *f* and g. The histogram representing the uncertainty of *G* was produced for a series of different vertical strain values and relative densities. Based on this survey of uncertainties for *G*, a *COV* of 0.12 was taken as representative. The results of this survey are summarized in Table 8.1.1. Thus, according to the relationship in Equation (8.1.20) the *COV* for q_b is 0.12. Lee and Salgado (1999) calculated values of $q_{b,10\%}$ using this model and then normalized the results to obtain $q_{b,10\%}/q_{bL}$. Values of q_{bL} were determined using CONPOINT and soil properties used for the model. Note that the uncertainty of CONPOINT was incorporated at the beginning of Figure 8.1.13. Thus, the uncertainty of $q_{b,10\%}/q_{bL}$ is the same as for model determined values of q_b.

The uncertainty of q_{bL} was examined in Section 8.1.1. The resulting PDF is a

Table 8.1.1 – summary statistics for the evaluation of the composite uncertainty of modulus *G* in the Lee and Salgado (1999) model for different values of relative density and vertical strain at a point in the soil model.

DR	vertical strain	mean (μ_G)	Std. dev. (σ_G)	COV_G
50	0.1%	21.63364	2.695234	0.124585
60	0.1%	22.95865	2.79628	0.121796
80	0.1%	25.47008	2.93825	0.115361
50	0.5%	9.182838	1.122245	0.122211
60	0.5%	9.687383	1.073985	0.110864
80	0.5%	10.62515	1.092017	0.102777
50	1.0%	6.039453	0.859287	0.142279
60	1.0%	6.361194	0.774608	0.121771
80	1.0%	6.94989	0.771959	0.111075

normal distribution with COV = 0.16 and bias factor = 1.06.

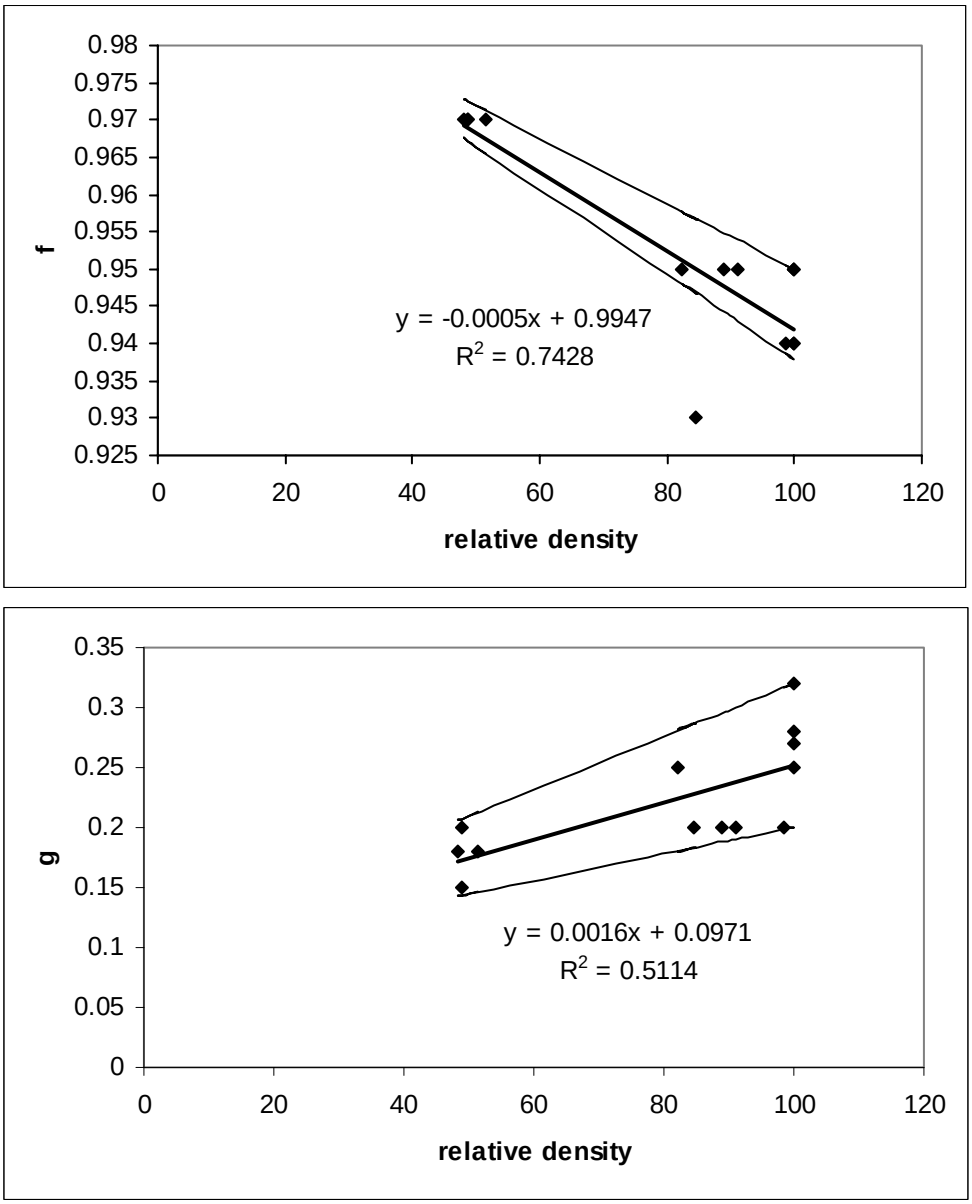

Figure 8.1.14 – Variation of curve fitting parameters *f* and *g* with D_R (Lee and Salgado 1999)

Direct Design of Shaft Capacity

We did not assess the uncertainty for direct design of shaft capacity because we had insufficient data to complete a satisfactory analysis.

Direct Design of Base Capacity

Step 1. Identify limit state equation

The limit state equation for base capacity is written

$$\left(\frac{q_{b,10\%}}{q_c}\right) q_c A_b - DL - LL = 0 \qquad \textbf{(8.1.24)}$$

where ($q_{b,10\%}/q_c$) is the ratio of s/B = 10% limit base pressure to CPT tip resistance q_c, A_b is the pile base area, DL is the dead load acting on the base of the pile, and LL is the live load acting on the base of the pile.

Step 2. Identify the component variables

Of the variables in Equation (8.1.24), A_b is selected by the designer; DL and LL are outputs of the design of the superstructure; q_c is measured directly; and ratio ($q_{b,10\%}/q_c$) is based on published results by Lee and Salgado (1999).

Step 3. Identify the geotechnical tests associated with each variable

Of the identified variables in equation (8.1.24), q_c can be measured in routine practice. The uncertainty of q_c has been examined in Section 4.1.

Step 4. Identify all component uncertainties for each variable, including transformations

The uncertainty of ($q_{b,10\%}/q_c$) has been examined for property-based design of drilled shafts. The resulting PDF is a normal distribution with COV = 0.12. The uncertainty of q_c was examined in Section 4.1. The resulting PDF is a normal distribution with COV = 0.07 and bias factor = 1.06.

Steps 5 and 6. Evaluate the composite uncertainties and select PDFs for reliability analysis

PDFs for ($q_{b,10\%}/q_c$) and q_c are selected in Step 4 and Section 4.1, respectively, and can be used directly with Equation (8.1.24) in reliability analysis.

8.2 Assessment of Resistance Factors

In this section, we will assess the resistance factors for the property-based and direct design methods for the different pile types we discussed in Section 8.1. To facilitate discussion, we summarize all design equations in Table 8.2.1. Table 8.2.1 also includes the resistance factors (RF) that would be used in design with ASCE-7 and AASHTO load factors. For reference purposes, we calculated an equivalent factor of safety (FS) that would be used in Working Stress Design (WSD). FS is taken as the ratio of a representative load factor over the resistance factor.

For design methods that are not mentioned in this Chapter, the designer has the option to assess the resistance factor for the total capacity from direct design methods. This procedure is discussed in detail in Section 9.2.1.

For every computation of RF, we check different ratios of LL/DL since live load is more uncertain than dead load and different ratios of LL/DL will yield different RFs. As seen in Chapter 5, depending on the relative uncertainty of resistance and load, lower LL/DL ratios will occasionally yield lower resistance factors. Therefore, both high and low ratios of LL/DL are checked.

As we noted in Chapter 5, resistance factors vary with design variable values. For this reason, we also examine the effect of different design variable values on the design equations for the different pile types we considered. In general, for the equations we selected, the specific value of design variables has little influence on the final resistance factor.

Table 8.2.1 – Summary table for the design of deep foundations in sand. Resistance Factors (*RF*) are given for use with ASCE-7 and AASHTO load factors. *FS* indicates an approximate value of WSD safety factor corresponding to the resistance factor given.

Property-Based Design of Driven, Closed-Ended Piles $(RF)_s R_s + (RF)_b R_b \geq \sum (LF)_i Q_i$	
Shaft Capacity: $R_s = \int_L f_s a_s dL$ $f_s = \frac{K_s}{K_0} K_0 \tan\left(\frac{\delta_c}{\phi_c}\phi_c\right)\sigma'_v$ $\frac{K_s}{K_0} = 7.2\left(0.0112 D_R(\%) - 0.0141\right),\ 20\% < D_R(\%) < 90\%$ $\frac{\delta_c}{\phi_c} = 0.85$	$(RF)_s$ = 0.37 (ASCE-7) $(RF)_s$ = 0.40 (AASHTO) *FS* = 3.9
Base Capacity: $R_b = q_{b,10\%} A_b$ $q_{b,10\%} = \left(\frac{q_{b,10\%}}{q_{bL}}\right) q_{bL}$ $\frac{q_{b,10\%}}{q_{bL}} = 1.02 - 0.0051 D_R(\%)$ $\frac{q_{bL}}{p_A} = C_1 \exp(C_2 D_R)\left(\frac{\sigma'_h}{p_A}\right)^{C_3}$	$(RF)_b$ = 0.50 (ASCE-7) $(RF)_b$ = 0.52 (AASHTO) *FS* = 3.0
Direct (CPT) Design of Driven, Closed-Ended Piles $(RF)_s R_s + (RF)_b R_b \geq \sum (LF)_i Q_i$	
Shaft Capacity: $R_s = \int_L f_s a_s dL$ $f_s = \left(\frac{f_s}{q_c}\right) q_c = 0.002 q_c$	$(RF)_s$ = 0.51 (ASCE-7) $(RF)_s$ = 0.53 (AASHTO) *FS* = 2.9
Base Capacity: $R_b = q_{b,10\%} A_b$ $q_{b,10\%} = \left(\frac{q_{b,10\%}}{q_c}\right) q_c$ $\frac{q_{b,10\%}}{q_c} = 1.02 - 0.0051 D_R(\%)$	$(RF)_b$ = 0.56 (ASCE-7) $(RF)_b$= 0.59 (AASHTO) *FS* = 2.6

Property-Based Design of Driven, Open-Ended Piles

$$(RF)_s R_s + (RF)_b R_b \geq \sum (LF)_i Q_i$$

Shaft Capacity:

$$R_s = \int_L f_s a_s dL$$

$$f_s = \frac{K_s}{K_0} K_0 \tan\left(\frac{\delta_c}{\phi_c}\phi_c\right)\sigma'_v$$

$$\frac{K}{K_0} = \beta(7.2 - 4.8\text{PLR})$$

$$\frac{\delta_c}{\phi_c} = 0.85$$

$$\beta = 0.0112 D_R(\%) - 0.0141, \;\; 20\% < D_R(\%) < 90\%$$

$(RF)_s$ = 0.37 (ASCE-7)
$(RF)_s$ = 0.40 (AASHTO)
FS = 3.9

Base Capacity:

$$R_b = q_{b,10\%} A_b$$

$$q_{b,10\%} = \left(\frac{q_{b,10\%}}{\sigma'_h}\right)\sigma'_h$$

$$\frac{q_{b,10\%}}{\sigma'_h} = \alpha\left(326 - 295\frac{\text{IFR}(\%)}{100}\right)$$

$$\alpha = 0.0112 D_R(\%) - 0.0141, \;\; 20\% < D_R(\%) < 90\%$$

$$A_b = \pi\left(\frac{d_o}{2}\right)^2$$

$(RF)_b$ = 0.58 (ASCE-7)
$(RF)_b$ = 0.60 (AASHTO)
FS = 2.6

Direct (CPT) Design of Driven, Open-Ended Piles

$$(RF)_s R_s + (RF)_b R_b \geq \sum (LF)_i Q_i$$

Shaft Capacity:

$$R_s = \int_L f_s a_s dL$$

$$f_s = \left(\frac{f_s}{q_c}\right) q_c = 0.002 q_c$$

$(RF)_s$ = 0.37 (ASCE-7)
$(RF)_s$ = 0.40 (AASHTO)
FS = 3.9

Base Capacity:

$$R_b = q_{b,10\%} A_b$$

$$q_{b,10\%} = \left(\frac{q_{b,10\%}}{q_c}\right) q_c$$

$$\frac{q_{b,10\%}}{q_c} = -0.00443 IFR(\%) + 0.557$$

$$A_b = \pi\left(\frac{d_o}{2}\right)^2$$

$(RF)_b$ = 0.66 (ASCE-7)
$(RF)_b$ = 0.69 (AASHTO)
FS = 2.3

Property-Based Design of Drilled Shafts

$$(RF)_s R_s + (RF)_b R_b \geq \sum (LF)_i Q_i$$

Base Capacity:

$$R_b = q_{b,10\%} A_b$$

$$q_{b,10\%} = \left(\frac{q_{b,10\%}}{q_{bL}} \right) q_{bL}$$

$$\left(\frac{q_{b,10\%}}{q_{bL}} \right) = 0.225 - 0.0011 D_R (\%)$$

$$\frac{q_{bL}}{p_A} = C_1 \exp(C_2 D_R) \left(\frac{\sigma'_h}{p_A} \right)^{C_3}$$

$(RF)_b = 0.56$ (ASCE-7)
$(RF)_s = 0.58$ (AASHTO)
$FS = 2.7$

Direct (CPT) Design of Drilled Shafts

$$(RF)_s R_s + (RF)_b R_b \geq \sum (LF)_i Q_i$$

Base Capacity:

$$R_b = q_{b,10\%} A_b$$

$$q_{b,10\%} = \left(\frac{q_{b,10\%}}{q_c} \right) q_c$$

$$\left(\frac{q_{b,10\%}}{q_c} \right) = 0.225 - 0.0011 D_R (\%)$$

$(RF)_b = 0.64$ (ASCE-7)
$(RF)_b = 0.67$ (AASHTO)
$FS = 2.3$

8.2.1 Closed-Ended Driven Piles in Sand

Property-Based Design of Shaft Capacity

Table 8.2.2 shows a summary of the relevant PDFs and their *COV*s for the property-based design method of shaft capacity that were determined in Section 8.1. Adjusted resistance factors *RF* were computed using a target reliability index β of 3.0. A summary of the results appears in Table 8.2.2. Note that values of *RF* do not depend on values of K_0 and ϕ_c. Note that the value of K_0 to be used in design was taken as deterministic, as explained in Section 8.1. However, had some uncertainty for K_0 been introduced, the *RF* would have been less. Also note that the PDFs and design equations assessed for the design of closed-ended piles is the same as for open-ended piles. Accordingly, the resistance factor found match that of the open-ended pile case. Since

Table 8.2.2 – Results of Resistance Factor Evaluation for Property-Based Shaft Capacity of Closed Ended Piles in Sand for ASCE-7 Load Factors

Principal Random Variables and Associated PDFs			
Variable		PDF	COV
K/K_0		normal, bias factor = 1.0	0.22
δ_c/ϕ_c		normal, μ = 0.9	0.10
ϕ_c		normal, bias factor = 1.0	0.01
Resistance Factor Results, β = 3.0			
K_0	ϕ_c	LL/DL	RF
0.4	33	1	0.37
0.4	33	4	0.41
1.0	33	1	0.38
1.0	33	4	0.41
1.0	30	1	0.38
1.0	30	4	0.41

the shaft resistance of driven open-ended piles is inherently more uncertain than driven closed-ended piles, due to the added complication of partial plugging, then the uncertainty in shaft resistance for open-ended piles is a reasonable upper bound to the uncertainty for closed-ended piles. Thus, these resistance factors are conservative.

From the results of the resistance factor computations presented in Table 8.2.2, a representative value of *RF* for use in design is 0.37.

Property-Based Design of Base Capacity

Table 8.2.3 shows a summary of the PDFs and their *COV*s for the property-based design method of base capacity that were determined in Section 8.1. Adjusted resistance factors *RF* were computed using a target reliability index β of 3.0. A summary of the results appears in Table 8.2.3. Note that values of *RF* do not depend on the value of D_R. A representative value of *RF* for use in design is 0.50.

Table 8.2.3 – Results of Resistance Factor Evaluation for Property-Based Base Capacity of Closed Ended Piles in Sand for ASCE-7 Load Factors

Principal Random Variables and Associated PDFs		
Variable	PDF	COV
$q_{b,10\%}/q_c$	normal, bias factor = 1.0	0.17
q_{bL}	normal, bias factor = 1.06	0.16
Resistance Factor Results, $\beta = 3.0$		
D_R(%)	LL/DL	RF
80	1	0.52
80	4	0.50
60	1	0.52
60	4	0.51

Direct Design of Shaft Capacity

Although there are several methods available to estimate the shaft capacity of closed-ended piles from the results of in-situ tests such as the CPT, insufficient data has been collected to accurately assess the uncertainty of the various techniques. However, some inferences about likely values of *RF* can be made based on a mechanical understanding of the problem. First, both closed- and open-ended piles displace a certain amount of sand when driven. In the case of open-ended piles, the amount of sand displaced is highly variable, depending on in-situ soil conditions and pile driving conditions that affect how much soil enters the pipe. In contrast, the amount of soil displaced by a closed-ended pile varies relatively little. Thus, it is expected that the variability of shaft capacity in closed-ended piles will be less than that for open-ended piles. This observation implies that *RF*s for closed-ended piles should be higher than for open-ended piles. Second, most direct design methods avoid the dilemma faced by property-based methods of inferring several properties from one or two kinds of

measurements. By correlating pile performance directly with an in-situ measurement, it can be expected that the uncertainty associated with the prediction of pile capacity can be reduced. This statement holds true when direct methods are applied to the same soils and conditions as were used to calibrate them. Thus, in many cases, *RF*s for one type of pile should be the same or higher for direct design than for property-based design methods for the same pile type.

These observations are helpful in inferring a reasonable value of RF to use for the direct design of shaft capacity for closed ended piles. From the first observation, note that the *RF* will likely be higher than 0.37, the *RF* value for open-ended piles, which are more uncertain. From the second observation, note that the *RF* could be higher than 0.51, the value found for property-based design of closed-ended pile shaft resistance. Assuming the *RF* for the property-based method to be a representative number, a conservative estimate of *RF* for the direct design of closed-ended pile shaft resistance is 0.51.

Direct Design of Base Capacity

Based on the high-quality pile load test data collected in Chapter 7, the correlation between CPT measurement and base capacity for s/B = 10% was used. Table 8.2.4 shows a summary of the relevant PDFs and their COVs for this data. Adjusted resistance factors (*RF*) were computed for $\beta = 3.0$ and for different values of D_R and LL/DL. A summary of the results appears in Table 8.2.4. Note that different values of relative density do not change the computed *RF*. Based on these results, an *RF* value of 0.56 is taken as representative for this design method.

Table 8.2.4 – Results of Resistance Factor Evaluation for Direct Base Capacity of Closed Ended Piles in Sand for ASCE-7 Load Factors

Principal Random Variables and Associated PDFs		
Variable	PDF	COV
$q_{b,10\%}/q_c$	normal, bias factor = 1.0	0.17
q_c	normal, bias factor = 1.06	0.07
Resistance Factor Results, $\beta = 3.0$		
D_R(%)	LL/DL	RF
80	1	0.59
80	4	0.57
60	1	0.59
60	4	0.56

8.2.2 Open-Ended Driven Piles in Sand

Property-Based Design of Shaft Capacity

Table 8.2.5 shows a summary of the PDFs and their COVs determined for the relevant design variables of the property-based design method of shaft capacity. Adjusted *RF* values were found using a target reliability index β of 3.0. A summary of the results appears in Table 8.2.5. Note that varying K_0 and ϕ_c practically does not affect the value of *RF* obtained. A representative value of *RF* for use in design is 0.37. Note that the value of K_0 to be used in design was taken as deterministic as explained in Section 8.1. However, had some uncertainty for K_0 been introduced, the *RF* would have been less.

Table 8.2.5 – Results of Resistance Factor Evaluation for Property-Based Shaft Capacity of Open Ended Piles in Sand for ASCE-7 Load Factors

Principal Random Variables and Associated PDFs			
Variable		PDF	COV
K/K_0		normal, bias factor = 1.0	0.22
δ_c/ϕ_c		normal, $\mu = 0.9$	0.10
ϕ_c		normal, bias factor = 1.0	0.01
Resistance Factor Results, $\beta = 3.0$			
K_0	ϕ_c	LL/DL	RF
0.4	33	1	0.37
0.4	33	4	0.41
1.0	33	1	0.38
1.0	33	4	0.41
1.0	30	1	0.38
1.0	30	4	0.41

Property-Based Design of Base Capacity

Table 8.2.6 shows a summary of the PDFs and their COVs for the variables of the property-based design method of base capacity. Adjusted *RF*s were computed using a target reliability index β of 3.0. A summary of the results appears in Table 8.2.6. Note that *RF* does not vary with relative density. A representative value of *RF* for use in design is 0.58.

Table 8.2.6 – Results of Resistance Factor Evaluation for Property-Based Base Capacity of Open Ended Piles in Sand for ASCE-7 Load Factors

Principal Random Variables and Associated PDFs		
Variable	PDF	COV
$q_{b,10\%}/\sigma'_h$	normal, bias factor = 1.0	0.15
Resistance Factor Results, $\beta = 3.0$		
D_R(%)	LL/DL	RF
90	1	0.61
90	4	0.58
60	1	0.61
60	4	0.58

Direct Design of Shaft Capacity

Table 8.2.7 shows a summary of the PDFs and their *COVs* for the direct design method of shaft capacity as determined in Section 8.1. Adjusted resistance factors *RF* were determined for a target reliability index (β) of 3.0. A summary of the results appears in Table 8.2.7. Based on this analysis, a reasonable RF for use in design is 0.37.

Table 8.2.7 – Results of Resistance Factor Evaluation for Direct Shaft Capacity of Open-Ended Pipe Piles in Sand for ASCE-7 Load Factors

Principal Random Variables and Associated PDFs		
Variable	PDF	COV
f_s/q_c	normal, $\mu = 0.002$	0.23
q_c	Normal, bias factor = 1.06	0.07
Resistance Factor Results, $\beta = 3.0$		
	LL/DL	RF
	1	0.37
	4	0.40

Note that the *RF* obtained for the property-based prediction of pile capacity does not differ from that found for direct design. Considering the source of the data, this is likely

caused by the fact that the primary source of uncertainty for open-ended piles is the degree of plugging during driving. Thus, the effect of additional uncertainties introduced by attempting to estimate soil properties is minimized.

Direct Design of Base Capacity

Table 8.2.8 shows a summary of the PDFs and their COVs selected to model the uncertainty of ($q_{b,10\%}/q_c$) and (q_c) discussed in Section 8.1. Adjusted resistance factors were computed using a target reliability index (β) of 3.0. A summary of the results also appears in Table 8.2.8. Note that although different input values of *IFR*(%) were used to compute *RF*, there is no effect on the resulting value. There is an effect of different values of *LL*/*DL* ratio which has been accounted for by trying two different values of live-to-dead load ratio. A reasonable value of *RF* for use in design is 0.66.

Table 8.2.8 – Results of Resistance Factor Evaluation for Direct Base Capacity of Open Ended Piles in Sand for ASCE-7 Load Factors

Principal Random Variables and Associated PDFs		
Variable	PDF	COV
$q_{b,10\%}/q_c$	normal, bias factor = 1.0	0.10
q_c	normal, bias factor = 1.06	0.07
Resistance Factor Results, β = 3.0		
IFR(%)	LL/DL	RF
60	1	0.66
60	4	0.69
20	1	0.66
20	4	0.69

8.2.3 Drilled Shafts in Sand

Property-Based Design of Shaft Capacity

We did not calculate resistance factors for property-based design of shaft capacity because we had insufficient data to complete a satisfactory analysis.

Property-Based Design of Base Capacity

Table 8.2.9 shows a summary of the PDFs and their *COV*s for the property-based design method of base capacity that were determined in Section 8.1. Adjusted resistance factors *RF* were computed using a target reliability index β of 3.0. A summary of the results appears in Table 8.2.9. Note that values of *RF* do not depend on the value of D_R. A representative value of *RF* for use in design is 0.56.

Table 8.2.9 – Results of Resistance Factor Evaluation for Property-Based Base Capacity of Drilled Shafts in Sand for ASCE-7 Load Factors

Principal Random Variables and Associated PDFs		
Variable	PDF	COV
$q_{b,10\%}/q_{bL}$	normal, bias factor = 1.0	0.12
q_{bL}	normal, bias factor = 1.06	0.16
Resistance Factor Results, $\beta = 3.0$		
D_R(%)	LL/DL	RF
60	1	0.59
60	4	0.56
80	1	0.59
80	4	0.56

Direct Design of Shaft Capacity

We did not calculate resistance factors for property-based design of shaft capacity because we had insufficient data to complete a satisfactory analysis.

Direct Design of Base Capacity

Table 8.2.10 shows a summary of the PDFs and their *COVs* selected in Section 8.1 for direct design of base capacity for drilled shafts. Adjusted resistance factors *RF* were computed using a target reliability index of 3.0. A summary of the results appears in Table 8.2.10. Note that values of *RF* do not depend on the value of D_R. From these results, a representative value of *RF* for use in design is 0.64. Note that in practice, the reliability of a drilled shaft base depends heavily on the quality control exercised during construction.

Table 8.2.10 – Results of Resistance Factor Evaluation for Direct Base Capacity of Drilled Shafts in Sand for ASCE-7 Load Factors

Principal Random Variables and Associated PDFs		
Variable	PDF	COV
$q_{b,10\%}/q_c$	normal, bias factor = 1.0	0.12
q_c	normal, bias factor = 1.06	0.07
Resistance Factor Results, $\beta = 3.0$		
D_R(%)	LL/DL	RF
60	1	0.67
60	4	0.64
80	1	0.67
80	4	0.64

CHAPTER 9. RESISTANCE FACTORS FOR DEEP FOUNDATIONS ON CLAY

9.1 Assessment of Variable Uncertainties for Deep Foundations on Clay

9.1.1 Design of Driven Piles in Clay

Property-Based Design of Shaft Capacity

Step 1. Identify limit state equation

For shaft resistance using the α method, the limit state equation is taken as

$$[\alpha s_u] a_s dL - DL - LL = 0 \qquad \textbf{(9.1.1)}$$

where a_s is the shaft area per unit pile length.

Step 2. Identify the component variables

Of the variables in equation (9.1.1), α is estimated from results by Randolph and Murphy (1985), s_u can be determined from either CPT correlations or from laboratory tests on samples extracted from the field, *dL* is a given unit length, and *DL* and *LL* are outputs of the design of the superstructure. According to Randolph and Murphy (1985) values of α are calculated based on an estimate of s_u/σ'_v as follows:

$$\alpha = \begin{cases} \left(\frac{s_u}{\sigma'_v}\right)_{NC}^{0.5} \left(\frac{s_u}{\sigma'_v}\right)^{-0.5}, \text{for} \frac{s_u}{\sigma'_v} \le 1 \\ \left(\frac{s_u}{\sigma'_v}\right)_{NC}^{0.5} \left(\frac{s_u}{\sigma'_v}\right)^{-0.25}, \text{for} \frac{s_u}{\sigma'_v} > 1 \end{cases} \qquad \textbf{(9.1.2)}$$

Undrained shear strength s_u can found using the CPT q_c, the vane shear test, other in-situ tests, or directly from laboratory tests.

Step 3. Identify the geotechnical tests associated with each variable

There are several possible tests that can be used to estimate s_u. For the purpose of this report, we assess the uncertainty of s_u from CPT measurements as determined using the following equation:

$$s_u = \frac{q_c - \sigma_v}{N_k} \qquad \textbf{(9.1.3)}$$

Values of s_u/σ'_v can also be deduced from these measurements.

Step 4. Identify all component uncertainties for each variable, including transformations

The uncertainty for variables *DL* and *LL* have been identified previously (refer to Table 4.1.1). Variable a_s is specified by the designer and has negligible uncertainty since driven pile sections are fabricated at relatively small tolerances. Variable *dL* is used only for design purposes and has no affect on the final design prediction.

The data in Figure 9.1.1 obtained from Flemming et al. (1992) can be detrended by subtracting the mean trend given by (9.1.2) as follows:

$$error_\alpha = \frac{(\alpha)_{data} - \alpha\left(\left(\frac{s_u}{\sigma'_v}\right)_{NC}, \left(\frac{s_u}{\sigma'_v}\right)\right)}{\alpha\left(\left(\frac{s_u}{\sigma'_v}\right)_{NC}, \left(\frac{s_u}{\sigma'_v}\right)\right)} \qquad \textbf{(9.1.4)}$$

Since we divide by the mean trend value in (9.1.4), the standard deviation of $error_\alpha$ is equal to the *COV* of α. Using Equation (3.2.1), we get a *COV* of 0.21 for α. This value is the uncertainty of Equation (9.1.2). Figure 9.1.2 is a histogram of the α datapoints

detrended by Equation (9.1.2). A PDF representing the uncertainty in α is a normal distribution with COV = 0.21 and mean determined by (9.1.2).

The undrained shear strength s_u of clay, determined using the CPT, was found in Chapter 4 to be normally distributed with COV = 0.09 and a bias factor of 1.05. This PDF represents both the testing and transformation uncertainty in the determination of s_u. The uncertainty for lab determined values of s_u will be higher due to varying disturbance effects.

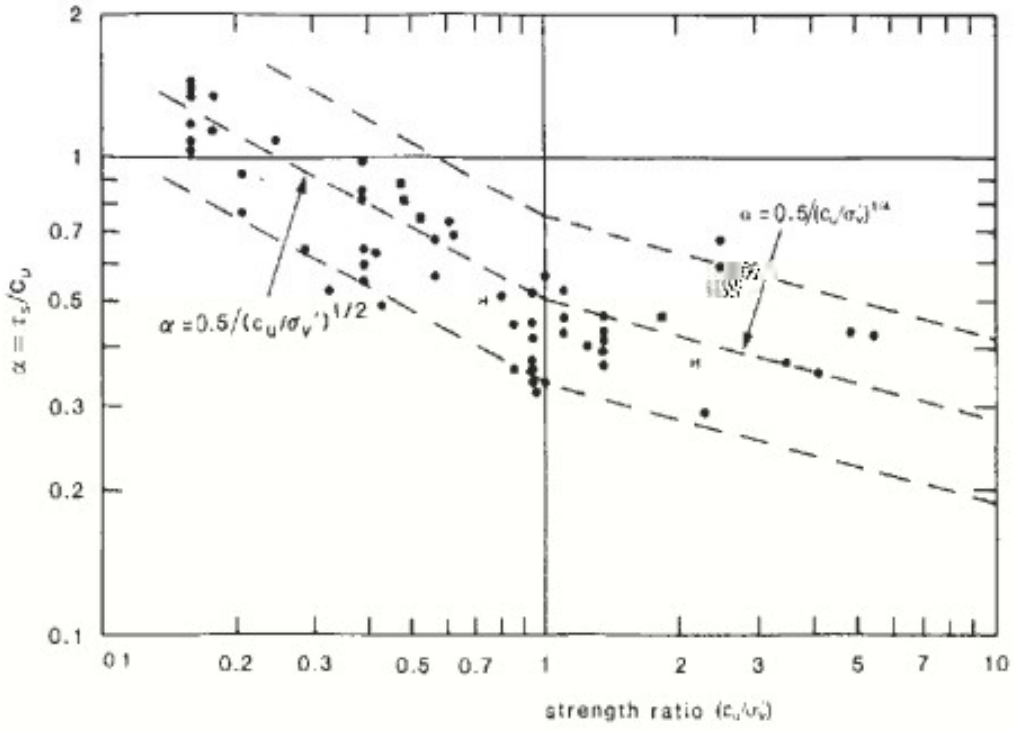

Figure 4.7 Variation of α with strength ratio

Figure 9.1.1 – Measured values of α compared to equations proposed by Randolph and Murphy (1985) (Flemming et al. 1992)

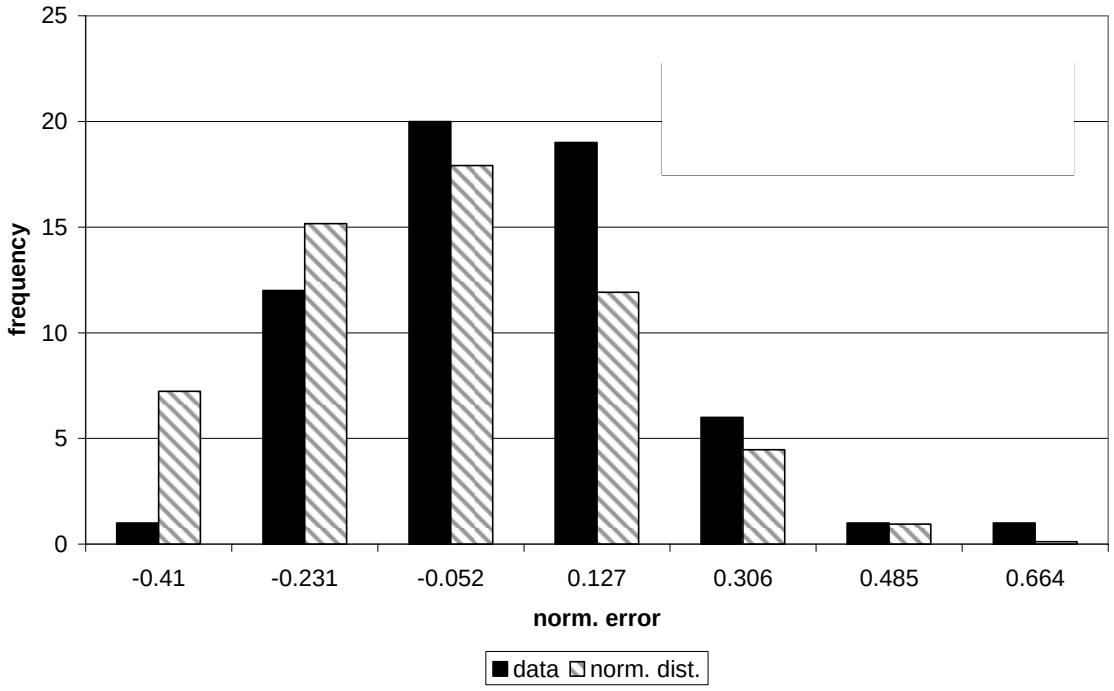

Figure 9.1.2 – Histogram of the α data points detrended by Equation (9.1.2).

Steps 5 and 6. Evaluate the composite uncertainties and select PDFs for reliability analysis

The PDFs of α and s_u are selected in Step 4 and can be used directly with Equation 9.1.1 in reliability analysis.

Property-Based Design of Base Capacity

Step 1. Identify limit state equation

The limit state equation for base resistance is taken as

$$\left[N_c s_u\right]A_b - DL - LL = 0 \qquad \textbf{(9.1.5)}$$

where N_c is a bearing capacity factor and A_b is the pile base area. An s/B = 10% criterion is desired for the base resistance of piles in clay. For soft to medium clays, piles reach a

plunging mode at relatively small settlements. Thus, values of N_c may be used directly for these soils. We do not comment on $q_{b,10\%}$ for stiff clays since there is not enough load testing results in the literature to compare q_{bL} to $q_{b,10\%}$.

Step 2. Identify the component variables

As stated earlier, there are different methods to estimate s_u. Values of N_c come from Salgado et al. (2004). *DL* and *LL* are outputs of the design of the superstructure.

Step 3. Identify the geotechnical tests associated with each variable

For the purpose of this report, we assume that s_u can be found using the CPT q_c and equation (9.1.3).

Step 4. Identify all component uncertainties for each variable, including transformations

Limit analysis of circular foundations in clay by Salgado et al. (2004) is used to analyze the expected value of N_c and its uncertainty. The value of N_c according to Salgado et al. (2004) is between 11.0 and 13.7. If no assumptions about the mean value of N_c are made, the least biased estimate of the PDF of N_c is a uniform distribution between 11.0 and 13.7.

The PDF for s_u was found in Chapter 4 to be a normal distribution with a COV of 0.09 and a bias factor of 1.05.

Steps 5 and 6. Evaluate the composite uncertainties and select PDFs for reliability analysis

The PDFs of N_c and s_u are selected in Step 4 and can be used directly with Equation 9.1.5 in reliability analysis.

Direct Design of Total Capacity

Unlike for sands, we do not have a satisfactory database to support separate resistance factors on shaft and base resistance for direct design methods in clay. Therefore, we propose using the total capacity form (7.1.2) of the LRFD equation so that total load pile test data can be used to estimate a reasonable resistance factor. Note that this decision will result in designs with less consistent reliabilities between different pile lengths. However, the method used to determine *RF* described in this section will allow practitioners to select *RF*s based on available load test data.

In the following development, we demonstrate how to obtain the *RF* for the Aoki and de Alencar Velloso (1975) design method since they present a useful load test database. Values of measured vs. predicted total pile capacity from Aokoi and de Alencar Velloso (1975) are presented in Figure 9.1.3.

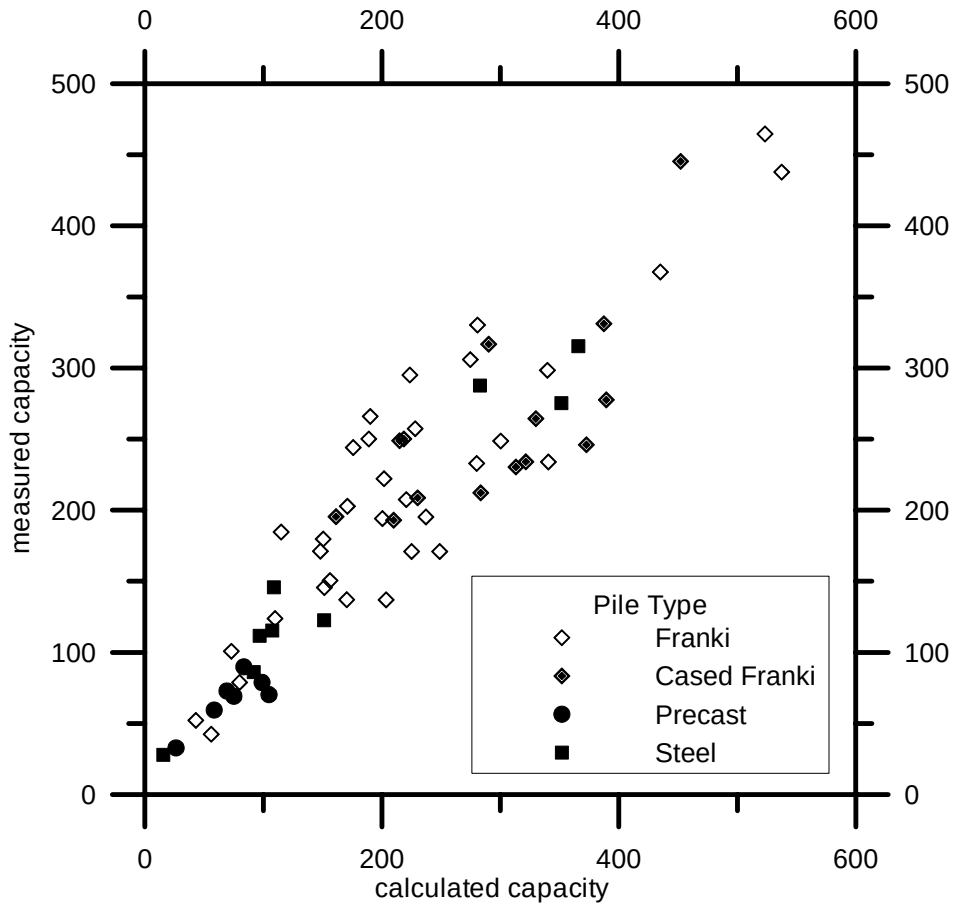

Figure 9.1.3 – Measured vs. calculated total pile resistance in study by Aoki and Velloso (1975) for Franki, Cased Franki, Precast, and Steel piles.

Step 1. Identify limit state equation

The limit state equation for total pile resistance is taken as

$$\left(R_s + R_b\right) - DL - LL = 0 \qquad \textbf{(9.1.6)}$$

where $\left(R_s + R_b\right)$ is the total resistance of the pile.

Step 2. Identify the component variables

There are no component variables for this limit state equation since the shaft and base resistances are lumped in the data available for reliability analysis.

Step 3. Identify the geotechnical tests associated with each variable

The uncertainty of the SPT contributes to the uncertainty of $\left(R_s + R_b\right)$ but cannot be extracted from the available data. This uncertainty is integral in the scatter of the datapoints in Figure 9.1.3

Step 4. Identify all component uncertainties for each variable, including transformations

Plots of measured vs. predicted capacity are one tool to assess the uncertainty of a direct design method. In the absence of instrumented pile load tests, these plots are the only available tool. Briaud and Tucker (1988) and Eslami and Fellenius (1997) are examples from the literature where this technique has been applied. It has the advantage of allowing a direct assessment of the likely deviation of pile capacity measurements from predictions, but has the disadvantage of limited applicability, as discussed earlier. For instance, if the designer has a particular method and a sufficient amount of calibration data where testing is done on the same type of pile and soil, a PDF can be

estimated to represent the uncertainty of total capacity. For the Aoki and de Alencar Velloso method, the first step is to detrend the data using the following equation:

$$error_{(R_s+R_b)} = \frac{\left(R_s + R_b\right)_{measured} - \left(R_s + R_b\right)_{predicted}}{\left(R_s + R_b\right)_{measured}} \qquad \textbf{(9.1.7)}$$

Note that the predicted value obtained from this design method is the mean trend since we need to assess the deviation of actual values from this predicted value. Since we divide by the mean trend value in (9.1.7), the standard deviation of $error_{(Rs+Rb)}$ is equal to the *COV* of $\left(R_s + R_b\right)$. Using Equation (3.2.1), we get a *COV* of 0.27 for $\left(R_s + R_b\right)$. This value is the uncertainty of predicted values of pile capacity using the Aoki and de Alencar Velloso (1975) design method. A histogram showing the detrended data is presented in Figure 9.1.4.

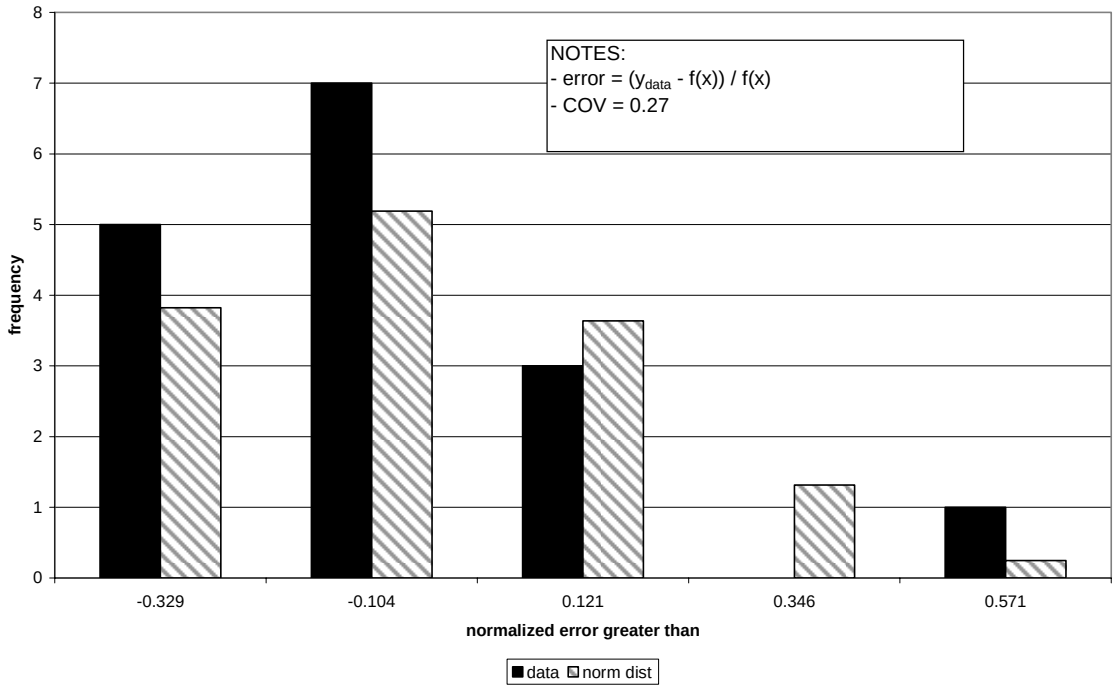

Figure 9.1.4 – Histogram of the $\left(R_s + R_b\right)$ measured data points detrended by the calculated datapoints from Figure 9.1.3.

Steps 5 and 6. Evaluate the composite uncertainties and select PDFs for reliability analysis

Based on recommendations of Briaud and Tucker (1988) and from the shape of the histogram in Figure 9.1.4, we selected a log-normal distribution to represent the uncertainty of $(R_s + R_b)$. The PDF selected is log-normal with mean equal to the design equation values presented in Chapter 7 for the Aoki and de Alencar Velloso (1975) method and COV equal to 0.27.

9.1.2 Design of Drilled Shafts in Clay

Property-Based Design of Shaft Capacity

We did not assess the uncertainty for property-based design of shaft capacity because we had insufficient data to complete a satisfactory analysis.

Property-Based Design of Base Capacity

As explained in Chapter 7, the ultimate limit state base load for soft and medium stiff clays is the plunging limit bearing capacity. As a result, plunging limit bearing capacity q_{bL} is applied to the design of both drilled shafts and driven piles. Thus the uncertainties are the same as determined in Section 9.1.1.

Direct Design of Total Capacity

Similar to the case of driven piles in clays, we do not have a satisfactory database to support separate resistance factors on shaft and base capacity for drilled shafts. Accordingly, the only available tool is to assess the uncertainty of total capacity based on

the same procedure presented in Section 9.1.1. We recommend that the designer take advantage of available pile load tests on drilled shafts to support the selection of resistance factor for design using the method outlined in the following Section.

9.2 Assessment of Resistance Factors

In this section, we will assess the resistance factors for the property-based and direct design methods for the different pile types we discussed in Section 9.1. To facilitate discussion, we summarize all design equations in Table 9.2.1 and we refer to it hereinafter. Table 9.2.1 also includes the resistance factors (RF) that would be used in design with ASCE-7 and AASHTO load factors. For reference purposes, we calculated an equivalent factor of safety (FS) that would be used in Working Stress Design (WSD). FS is taken as the ratio of a representative load factor over the resistance factor.

For every computation of RF we check different ratios of LL/DL since live load is more uncertain than dead load and different ratios of LL/DL will yield different RFs. As seen in Chapter 5, depending on the relative uncertainty of resistance and load, lower LL/DL ratios will occasionally yield lower resistance factors. Therefore, both high and low ratios of LL/DL are checked.

As we noted in Chapter 5, resistance factors vary with design variable values. For this reason, we also examine the effect of different design variable values on the design equations for the different pile types we considered. In general, for the equations we selected, the specific value of design variables has little influence on the final resistance factor.

Table 9.2.1 – Summary table for the design of deep foundations in clay. Resistance Factors (*RF*) are given for use with ASCE-7 and AASHTO load factors. *FS* indicates an approximate value of WSD safety factor corresponding to the resistance factor given.

Property-Based Design of Driven Piles in Clay $(RF)_s R_s + (RF)_b R_b \geq \sum (LF)_i Q_i$	
Shaft Capacity: $R_s = \int_L f_s a_s dL$ $f_s = \alpha s_u$ $\alpha = \begin{cases} \left(\frac{c_u}{\sigma'_v}\right)_{NC}^{0.5} \left(\frac{c_u}{\sigma'_v}\right)^{-0.5}, \text{for} \frac{c_u}{\sigma'_v} \leq 1 \\ \left(\frac{c_u}{\sigma'_v}\right)_{NC}^{0.5} \left(\frac{c_u}{\sigma'_v}\right)^{-0.25}, \text{for} \frac{c_u}{\sigma'_v} > 1 \end{cases}$	$(RF)_s$ = 0.44 (ASCE-7) $(RF)_s$ = 0.46 (AASHTO) *FS* = 2.9
Base Capacity: $R_b = q_{b,10\%} A_b$ $q_b = N_c s_u$ $N_c = 12$	$(RF)_b$ = 0.66 (ASCE-7) $(RF)_b$ = 0.69 (AASHTO) *FS* = 2.3
Direct (SPT) Design of Driven Piles in Clay – Aoki and Velloso (1975) $(RF)(R_s + R_b) \geq \sum (LF)_i Q_i$	(*RF*) = 0.50 (ASCE-7) (*RF*) = 0.52 (AASHTO) *FS* = 3.0
Shaft Capacity: $R_s = \int_L f_s a_s dL$ $f_s = n_{si} N_{SPT}$ $n_{si} = \frac{\alpha_1 K}{F_2}$ ← α_1, *K*, and F_2 from Chapter 7	
Base Capacity: $R_b = q_b A_b$ $q_b = n_b N_{SPT}$ $n_b = \frac{K}{F_1}$ ← *K* and F_1 from Chapter 7	
Property-Based Design of Drilled Shafts $(RF)_s R_s + (RF)_b R_b \geq \sum (LF)_i Q_i$	
Base Capacity: $R_b = q_{b,10\%} A_b$ $q_b = N_c s_u$ $N_c = 12$	$(RF)_b$ = 0.66 (ASCE-7) $(RF)_b$ = 0.69 (AASHTO) *FS* = 2.3

9.2.1 Designer Assessed Resistance Factors for Direct Methods

The main goal of this report was to present resistance factors for use with shallow and deep foundations. These resistance factors were specifically developed based on the uncertainty that we could quantify for the different design variables in each of the design equations we considered. However, this is insufficient to cover all the cases that could arise in practice knowing that there are many direct design methods that are developed for specific design situations. As such, the designer needs the capability to select resistance factors that reflect the uncertainty of the design method used. A suitable technique is to assess the uncertainty of total capacity from predicted vs. measured load test data. It is important to note that the load test database used with the specific methods the designer chooses should contain numerous cases of similar soil conditions and pile type. This is necessary to ensure the applicability the design method and its uncertainty.

We are considering the case when the designer has predicted vs. measured total load data for a given design method. The LRFD equation used in this case would be:

$$(RF)(R_s + R_b) \geq \sum (LF)_i Q_i \qquad \textbf{(9.2.1)}$$

where (R_s + R_b) is the total load capacity of the pile. Thus, we are finding a single *RF* value to be applied to the total pile capacity. To allow the designer to readily find a value of *RF* for a specific method, we computed different RF values for a range of *COV* values for (R_s + R_b) and different target reliability indices β. Figures 9.2.1 and 9.2.2 present the charts of *RF*s for use with ASCE-7 and AASHTO load factors, respectively. To use these figures, one must have an input value of *COV* and reliability index β.

As was explained in Chapter 3, the reliability index is an expression of the likelihood of failure. Higher values of β indicate a lower probability of failure for the

design. All of the recommended resistance factors presented in this report were for a reliability index of 3.0, the conventional value for structural design.

The *COV* must be determined from the load test database. The first step is to calculate the "error" for each load test as follows:

$$error_{(R_s+R_b)} = \frac{(R_s + R_b)_{measured} - (R_s + R_b)_{predicted}}{(R_s + R_b)_{measured}} \qquad \textbf{(9.2.2)}$$

The predicted capacity is calculated for each load test case using the chosen design method and the available in-situ test data. The measured capacity is the total capacity obtained from the result of each load test. Note that we consider the predicted capacity to be the mean of the data since we need to assess the deviation of actual values from this predicted value. To compute the *COV* of (R_s + R_b), we apply Equations (3.2.1) and (3.2.2) to the "error" values for the entire load database.

The final step to assess a *RF* for the chosen design method is to enter either Figure 9.2.1 or 9.2.2 with the calculated *COV* and β.

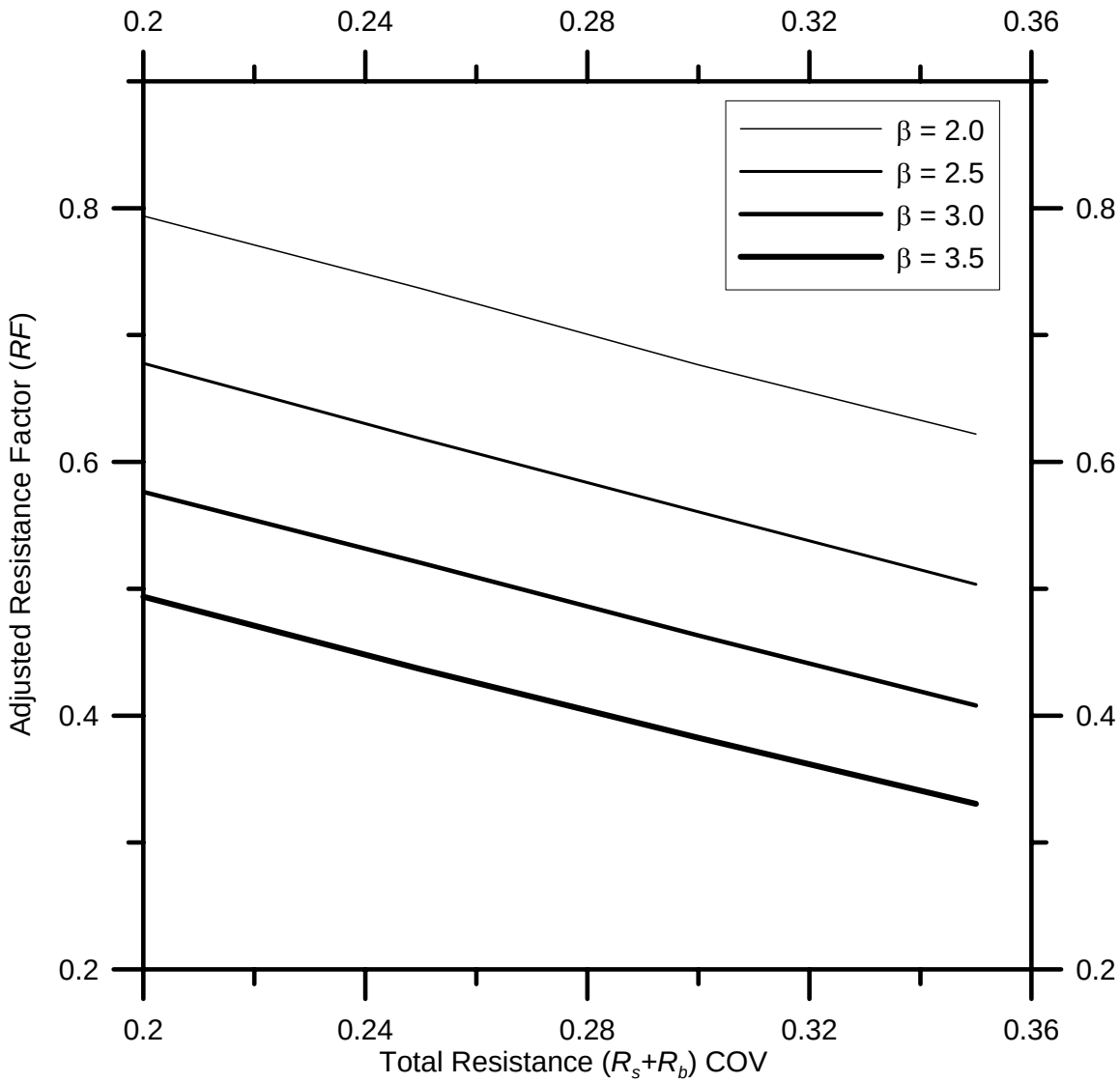

Figure 9.2.1 – Plot of Adjusted Resistance Factor *RF* varying with total resistance COV and target reliability index β, to be applied to total load capacity in the design of piles using ASCE-7 load factors. A bias factor of 1.06 for a lognormally distributed total resistance is assumed, implying that the resistance is assessed conservatively according to the CAM procedure.

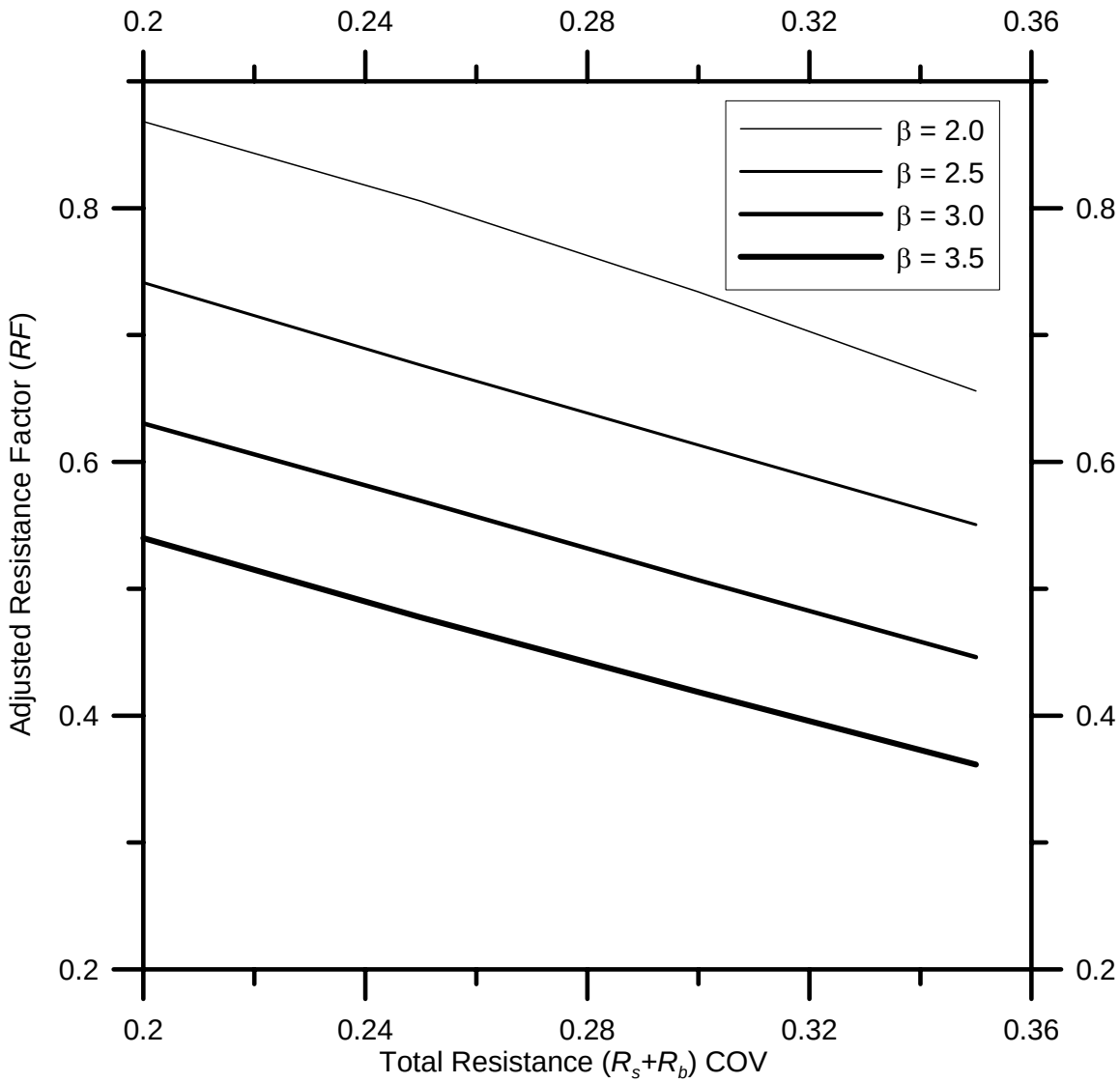

Figure 9.2.2 – Plot of Adjusted Resistance Factor *RF* varying with total resistance COV and target reliability index β, to be applied to total load capacity in the design of piles using AASHTO load factors. A bias factor of 1.06 for a lognormally distributed total resistance is assumed, implying that the resistance is assessed conservatively according to the CAM procedure.

9.2.2 Driven Piles in Clay

Property-Based Shaft Capacity

Table 9.2.2 shows a summary of the relevant PDFs and their *COV*s for the property-based design method of shaft capacity that were determined in Section 9.1. Adjusted resistance factors were computed using a target reliability index (β) of 3.0. A summary of the results also appears in Table 9.2.2. Note that, although different input values of (s_u/σ'_v) were used to compute *RF*, there is no effect on the resulting value. A reasonable value of *RF* for use in design is 0.44.

Table 9.2.2 – Results of Resistance Factor Evaluation for Property-Based Shaft Capacity of Driven Piles in Clay

Principal Random Variables and Associated PDFs		
Variable	PDF	COV
α	normal, bias factor = 1.0	0.21
s_u	normal, bias factor = 1.05	0.09
Resistance Factor Results		
(s_u/σ'_v)	LL/DL	RF
0.3	1	0.44
0.3	4	0.46
1.0	1	0.44
1.0	4	0.46
5.0	1	0.44
5.0	4	0.46

Property-Based Base Capacity

Table 9.2.3 shows a summary of the relevant PDFs and their *COV*s for the property-based design method of base capacity that were determined in Section 9.1. Adjusted resistance factors were computed using a target reliability index (β) of 3.0. A

summary of the results also appears in Table 9.2.3. A reasonable value of *RF* for use in design is 0.66.

Table 9.2.3 – Results of Resistance Factor Evaluation for Property-Based Base Capacity of Driven Piles in Clay

Principal Random Variables and Associated PDFs		
Variable	PDF	COV
N_c	uniform: [11.0, 13.7]	0.28
s_u	normal, bias factor = 1.05	0.09
Resistance Factor Results		
	LL/DL	RF
	1	0.68
	4	0.66

Direct Design of Total Capacity

Table 9.2.4 shows a summary of the relevant PDFs and their *COV*s for the direct design method of total capacity that were determined in Section 9.1. Adjusted resistance factors were computed using a target reliability index (β) of 3.0. A summary of the results also appears in Table 9.2.4. A reasonable value of *RF* for use in design is 0.50.

Table 9.2.4 – Results of Resistance Factor Evaluation for Aoki and de Velloso (1975) Direct SPT Design Method

Principal Random Variables and Associated PDFs		
Variable	PDF	COV
Q_{total}	lognormal, bias factor = 1.06	0.27
Resistance Factor Results		
	LL/DL	RF
	1	0.52
	4	0.50

9.2.3 Design of Drilled Shafts in Clay

Property-Based Design of Shaft Capacity

We did not calculate resistance factors for property-based design of shaft capacity because we had insufficient data to complete a satisfactory analysis.

Property-Based Design of Base Capacity

As explained in Chapter 7, the ultimate limit state base load for soft and medium stiff clays is the plunging limit bearing capacity. As a result, plunging limit bearing capacity q_{bL} is applied to the design of both drilled shafts and driven piles. Thus the uncertainties are the same as determined in Section 9.1.1. An appropriate resistance factor for use in property-based design of base capacity of drilled shafts is the same as that proposed for driven piles. A reasonable value of *RF* for use in design is 0.66.

Direct Design of Total Capacity

We did not calculate resistance factors for direct design of total capacity because we had insufficient data to complete a satisfactory analysis. However, in Section 9.2.1 we discussed a way for designers to select values of resistance factors for different design methods. We recommend the use of this technique for direct design of drilled shafts provided sufficient load test data is available.

CHAPTER 10. DESIGN EXAMPLES FOR DEEP FOUNDATIONS

Design Using LRFD

As in Chapter 6 for shallow foundations, this chapter explains how to use the resistance factors found in the previous chapters to design. Two design examples are considered. In the first example, we design a pile in a primarily medium dense sand soil profile. The second example demonstrates how to select a resistance factor (*RF*) for use with a direct design method not presented in this report.

In both examples the basic process of LRFD design is illustrated according to the flow chart in Figure 10.1.

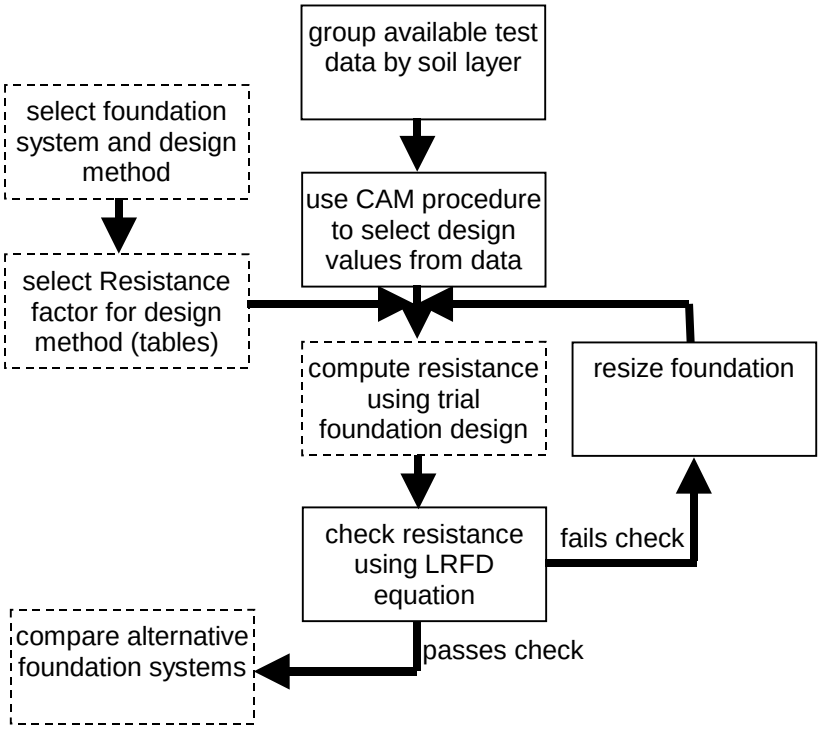

Figure 10.1. LRFD flow chart for ULS checks for foundation design. Dashed line boxes indicate steps specific to a particular design method, solid line boxes indicate steps common to all foundation types.

As shown in the figure, the first step in design for a particular foundation element is to group the relevant test data together by soil layer for consideration in the CAM method. Relevant test data is any data that tests the same soil that will be loaded by the foundation element. By grouping the same test measurements of the same soil together, we can take advantage of the improved knowledge of the soil made available by having several tests. The CAM procedure is then used to find the 80% exceedance values of the test data as is illustrated in the examples below as well as in Chapter 6. With these CAM values of the test measurements, the designer can proceed to compute resistances for a trial foundation design. At this point, it is necessary to select the correct value of resistance factor corresponding to the design method used to compute resistance. This

dependency is illustrated using the dashed line borders in Figure 10.1. After finding a resistance value for a particular design, its suitability can be checked using the basic LRFD equation. Factored design resistances that are greater than factored loads represent trial designs that have passed the check while factored design resistances that are less than the design load have failed the check. It is possible with several trial designs to compare design alternatives. In the following examples, the process of selecting a CAM value, selecting a resistance factor, and performing an LRFD check is illustrated.

Design of Open Ended Pipe Pile in Sand Using Direct Method

A number of CPT soundings were taken at the site and the measured tip resistance (q_c) profile is presented in Figure 10.2. A pile with 150 kN (34 kip) live load and 350 kN (79 kip) dead load will be designed against ultimate limit states. The pile cap base elevation is to be located at a depth of 2.0 m (6.6 ft). An open-ended pipe pile will be driven to 9 m (29.5 ft) at the sand site to take advantage of the relatively dense sand layer overlying the looser layer below 10m. Using live load and dead load factors of 1.6 and 1.2 (ASCE-7 factors), respectively, the design load is 660 kN (148 kip). The water table is at depth.

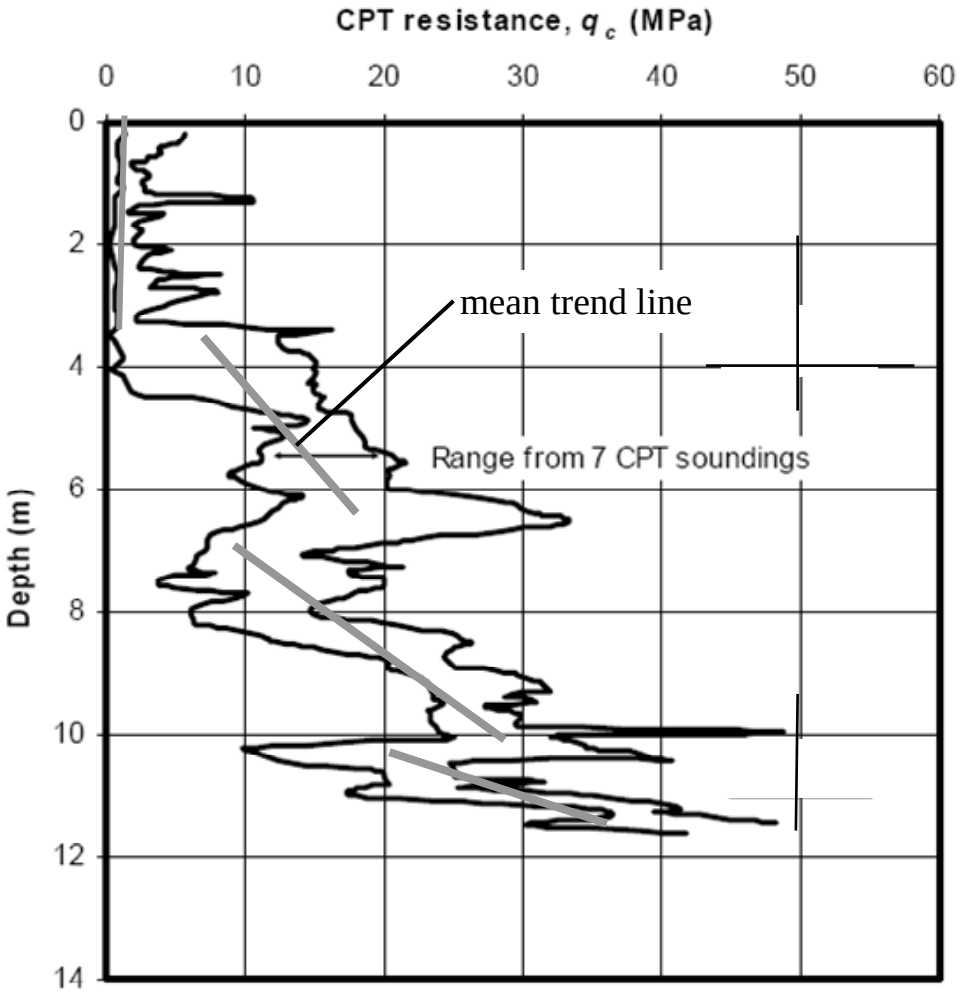

Figure 10.2. Results from 7 CPT logs in sand with mean trend ("best fit") lines and Range Lines (BCP Committee 1971)

The first step to design the foundation is to establish the CAM trend line for the combined CPT logs. A CAM method using an 80% exceedance criterion is illustrated using linear regression – a tool readily available to engineers in spreadsheet applications. These lines represent the mean function of a soil parameter with depth for the soils. Lines can also be drawn bounding the q_c data points, representing the entire range of q_c data for those depths. Both sets of lines are included in Figure 10.2. Table 10.1 presents

the statistics used to find the 80% exceedance criterion CAM line using the 6σ procedure for sand, effectively shifting the mean lines to the left on the plot. In the sand layers for this example, the CAM lines are given by the equation

$$q_{c,CAM} = \begin{cases} 0.7(MPa) & ,0 < z < 3.5m \\ 4(MPa/m)\cdot z - 8.9(MPa) & ,3.5m < z < 6.5m \\ 6(MPa/m)\cdot z - 35.1(MPa) & ,6.5m < z < 10m \\ 13(MPa/m)\cdot z - 115.5(MPa) & ,10m < z < 11.5m \end{cases} \quad \textbf{(10.1)}$$

where z is the depth.

Table 10.1. CPT q_c log statistics to find CAM line in sand layers in Figure 10.2

sand layer	0 < z < 3.5m	3.5m < z < 6.5m	6.5m < z < 10 m	10m < z < 11.5 m
Range (MPa) (R)	9	14	15	18
One Standard Deviation (MPa) ($\sigma = R / 6$)	1.5	2.3	2.5	3.0
Number of Standard Deviations for 80% Exceedance	0.84	0.84	0.84	0.84
Value to subtract from mean trend line to get CAM line (MPa)	1.3	1.9	2.1	2.5

For this example the design method derived from work by Paik and Salgado (2003) and Lee et al. (2003) is used. Shaft resistance will be designed first. A 305mm (12 in.) diameter pipe is selected as the trial pile section. This section has a unit shaft surface area a_s of 0.958m^2/m (3.14 ft^2/ft). According to this design method, shaft resistance R_s is given by

$$R_s = \int_L f_s a_s dL \quad \textbf{(10.2a)}$$

$$f_s = \left(\frac{f_s}{q_c}\right) q_c = 0.002 q_c \quad \textbf{(10.2b)}$$

For design purposes (10.2a), is written

$$R_s = \sum f_{s,i} a_{s,i} dL_i \qquad \textbf{(10.3)}$$

where subscript *i* denotes a section of some length along the pile. By summing the resistance contribution from all sections, we arrive at the total shaft capacity for the pile. In this example, a few sections will need to be considered for an accurate design in each sand layer. For example purposes, one section is considered in the first layer and 3 sections are considered in the second and third. Table 10.2 summarizes the analysis of shaft resistance.

Table 10.2 – summary of design trial for shaft resistance in sand

section no.#	starting depth (m)	ending depth (m)	mid depth (m)	dL (m)	$q_{c,CAM}$ (MPa)*	f_s (kPa)	$f_s a_s dL$ (kN)
1	2	3.5	2.75	1.5	0.7	1.4	2.0
2	3.5	4	3.75	0.5	6.1	12.2	5.8
3	4	5	4.5	1	9.1	18.2	17.4
4	5	6	5.5	1	13.1	26.2	25.1
5	6	7	6.5	1	3.9	7.8	7.5
6	7	8	7.5	1	9.9	19.8	19.0
7	8	9	8.5	1	15.9	31.8	30.5

*$q_{c,CAM}$ computed at mid depth using (10.1)

The total unfactored shaft capacity is computed by summing the "$f_s a_s dL$" column in Table 10.2, yielding a value of 107 kN (24 kip).

According to this design method, base resistance R_b is given by

$$R_b = q_{b,10\%} A_b \qquad \textbf{(10.4a)}$$

$$q_{b,10\%} = \left(\frac{q_{b,10\%}}{q_c} \right) q_c \qquad \textbf{(10.4b)}$$

$$\frac{q_b}{q_c} = -0.00443 IFR(\%) + 0.557 \qquad \textbf{(10.4c)}$$

To estimate $q_{b,10\%}$, an estimate of IFR(%) must be made first. Figure 10.3 is a plot from Lee et al. (2003) that can be used to estimate IFR before driving.

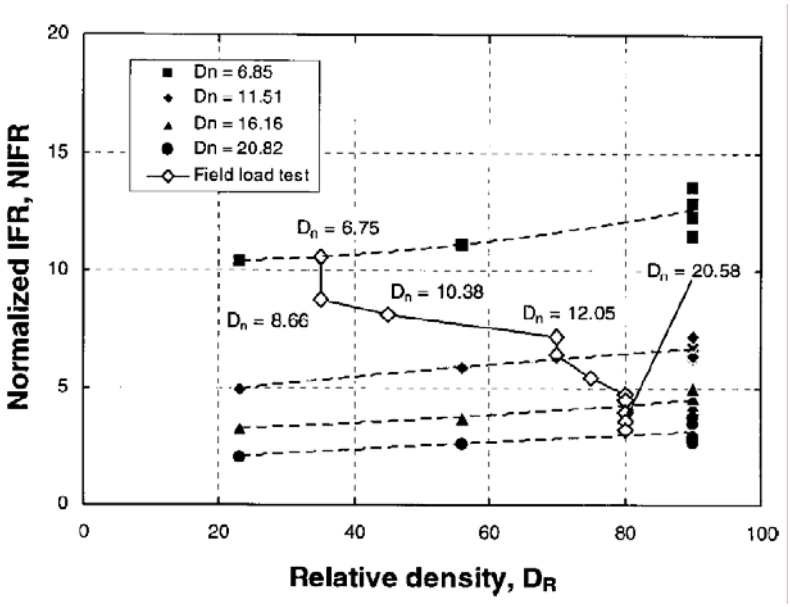

Figure 10.3 – Normalized IFR plot from Lee et al. (2003), used to estimate IFR.

Normalized IFR (NIFR) is

$$NIFR = \frac{IFR}{D_n} \qquad \textbf{(10.5)}$$

where D_n is

$$D_n = \frac{z_d}{d_i} \qquad \textbf{(10.6)}$$

where z_d is the driving depth and d_i is the inner pile diameter. For this case, with z_d = 9 m (29.5 ft) and $d_i \approx$ 0.305m (1 ft), equation (10.6) yields a D_n of 30. Figure 10.3 indicates a NIFR of about 2% if we assume a D_R of 65% for the medium dense sand. From equation (10.5), IFR(%) is computed as 59%. Thus, from equation (10.4c), ($q_{b,10\%}/q_c$) is estimated as 0.30. From CAM trendline (10.1), a conservative average q_c in the region of soil near the pile base is 18.9 MPa (395 ksf). Using (10.4b), we get a value of 5,580 kPa (117 ksf) for $q_{b,10\%}$.

The pile base area is computed

$$A_b = \pi\left(\frac{d_o}{2}\right)^2 = \pi\left(\frac{0.305m}{2}\right)^2 = 0.073m^2 \qquad \textbf{(10.7)}$$

Finally, from equation (10.4a) we obtain a value of 407 kN (91.5 kip) for the unfactored base resistance. From Table 8.2.1, the recommended RF_s and RF_b for use with ASCE-7 load factors is 0.37 and 0.66, respectively. Using the LRFD equation for piles,

$$(RF)_s R_s + (RF)_b R_b \geq \sum (LF)_i Q_i \qquad \textbf{(10.8)}$$

the total, factored resistance is 309 kN (69.5 kip), which is much less than the factored load of 660kN (148 kip). This is an unsafe design. An equivalent factor of safety of 1.0 is computed for this design using the unfactored loads and resistances.

For the next design iteration, assuming we decide to leave the pile base at the same elevation, a trial pile diameter of 457mm (18in.) is selected. The computations for shaft resistance remain nearly the same, except for the value of a_s. The computed value of unfactored shaft resistance is 161 kN (36.2 kip). For base resistance, note that since the pile diameter has changed, D_n and *IFR* will also change. From equation (10.5), we compute D_n as about 20. We get a new NIFR of 3% from Figure 10.3. Equation (10.5) gives an IFR(%) of 59%, yielding a $q_{b,10\%}$ and an unfactored base resistance of 5,580 kPa (117 ksf) and 917 kN (206 kip), respectively. The total, factored capacity, computed using (10.8), is 664 kN (149 kip), an acceptable design. An equivalent factor of safety for this design, computed using the unfactored loads and resistances, is 2.2. Note that this factor of safety only applies to this design method and load and resistance combination.

Finding an RF for use in Design of Piles Using Direct Method

In Chapter 9, we presented the Aoki and de Alencar Velloso (1975) method as a general direct design method. We will use this design example to demonstrate how other direct methods can be used to develop resistance factors based on available load test data. It is important to note that the load test database used for such design methods should contain numerous cases of similar soil conditions and pile type. This is necessary to ensure the applicability the design method and its uncertainty.

The Bustamante and Gianeselli (1982) method is selected for design since our hypothetical design firm (performing these example calculations) has pile load test data to support use of the method for similar soils and pile type. Table10.3 is the pile load test database for the hypothetical company.

The task in this example will be to determine what value of resistance factor to use in design. Note from the discussion in Chapters 7, 8, and 9, when load test data of this type is available (measured vs. predicted total capacity), the following LRFD equation must be used,

$$(RF)(R_s + R_b) \geq \sum (LF)_i Q_i \qquad \textbf{(10.9)}$$

where (R_s + R_b) is the total load capacity of the pile. Thus, we are finding a single *RF* value to be applied to the total pile capacity. Since we are using ASCE-7 load factors for the example, Figure 10.3 must be used to estimate *RF*. To use this figure, we must have an input value of *COV* and reliability index β. The reliability index for this example will be set at 3.0, the conventional value for structural design. The *COV* must be determined from the load test database in Table 10.3. The first step to find the *COV* is to calculate

the “error” for each load test. The predicted capacity is calculated using the Bustamante and Gianeselli (1982) method. Note that we assume the predicted capacity to be the mean of the data since we need to assess the deviation of actual values from this predicted value. To compute the *COV* of (R_s + R_b), we apply Equations (3.2.1) and (3.2.2) to column (4) in Table 10.3. The resulting *COV* is 0.23. The final step to assess a *RF* for this design is to enter Figure 10.4 with a *COV* of 0.23 and a β of 3.0. The resulting *RF* is 0.55.

Table 10.3 – Hypothetical load test database: column (1) is the load test number, column (2) is the predicted total pile load capacity (resistance) using the Bustamante and Gianeselli (1982) method for the pile tested, column (3) is the total pile load capacity measured from the pile load test, and column (4) is the normalized difference ("error") of the measured capacity from the predicted capacity. The data indicates a COV of 0.23 for total load capacity.

(1) load test	(2) predicted (KN)	(3) measured (KN)	(4) (measured - predicted) / predicted
1	1142	1025	-0.102
2	956	1174	0.228
3	1378	1543	0.119
4	917	931	0.015
5	957	981	0.024
6	1014	1501	0.480
7	988	767	-0.223
8	864	1123	0.299
9	1095	1013	-0.075
10	1020	895	-0.123
11	924	740	-0.199
12	1341	1301	-0.030
13	863	840	-0.026
14	1374	1254	-0.087
15	1340	2074	0.547
16	1126	965	-0.143
17	1112	778	-0.300
18	1144	1338	0.170
19	1110	788	-0.290
20	1065	828	-0.222
21	902	823	-0.088
22	851	1005	0.181
23	880	589	-0.330
24	900	1273	0.415
25	1103	1856	0.683
26	1267	1250	-0.013
27	976	907	-0.071
28	917	1278	0.393
29	903	945	0.047
30	1012	1212	0.198
31	950	986	0.038
32	1252	1188	-0.051
33	867	1087	0.254
34	821	897	0.093
35	1291	1429	0.106

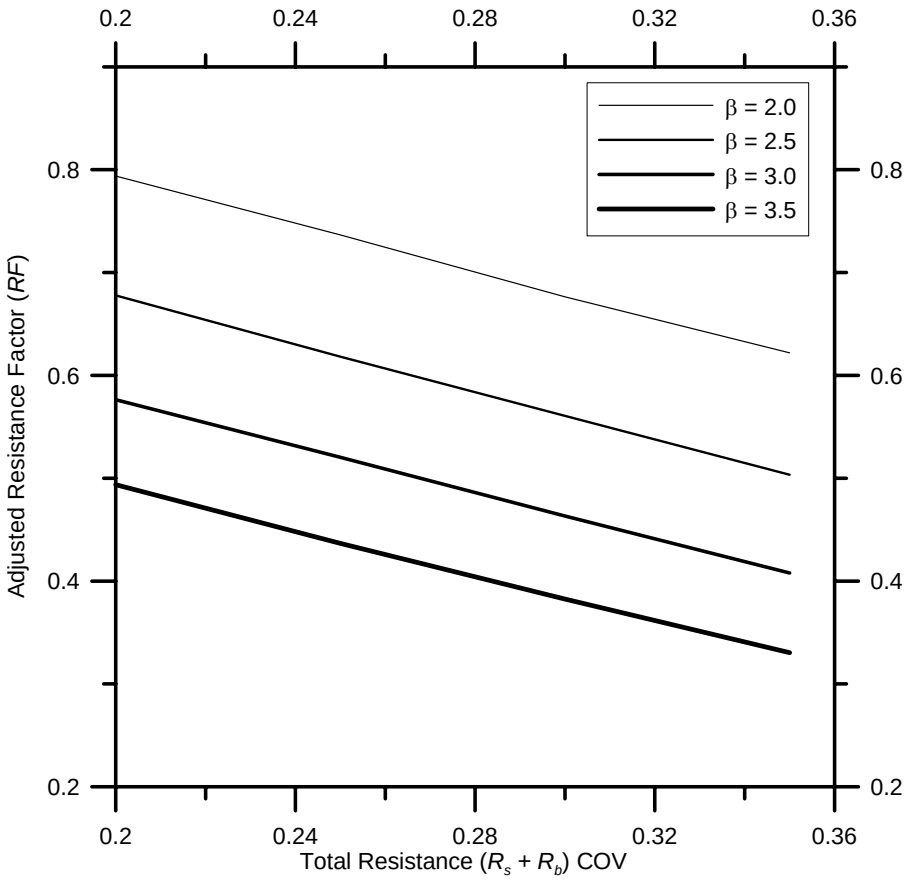

Figure 10.4 – Plot of Adjusted Resistance Factor *RF* varying with total resistance COV and target reliability index β, to be applied to total load capacity in the design of piles using ASCE-7 load factors. A bias factor of 1.06 for a lognormally distributed total resistance is assumed, implying that the resistance is assessed conservatively according to the CAM procedure.

The *RF* found in this example could then be applied with the Bustamante and Gianeselli (1982) method to perform design checks on pile designs using Equation (10.9). Bandini and Salgado (1998) have summaries of several direct pile design methods, including the Bustamante and Gianeselli (1982) method.

Example Conclusion

From the first design example, observe that pile design methods can be applied in nearly the same way as for WSD. Now, resistance factors are applied instead of safety factors and factored loads are used instead of unfactored loads. In the sand example, a design method for open ended piles was demonstrated that takes advantage of recent research results by Paik and Salgado (2003) and Lee and Salgado (2003). In the second example, a technique was demonstrated where practitioners can estimate resistance factors for use in design based on pile load test data in similar soils with the same type of pile. In this way, the uncertainty likely to be encountered for a particular design can be addressed specifically. From this technique, it should be possible to expand the use of LRFD to design methods other than those mentioned in this report.

CHAPTER 11. SUMMARY AND CONCLUSIONS

The first step in the present research was to assess the suitability of available load factors for use in geotechnical Load and Resistance Factor Design (LRFD). The load factors proposed by various current structural and foundation LRFD Codes were reviewed. Usually, a larger number of limit states, load types and load combinations are considered in the bridge and offshore foundation design codes, compared with building and onshore foundation design codes. In this study, the load factors for four major load types (i.e. dead, live, wind and earthquake loads) that control most design cases were examined and compared between the Codes.

A simple FOSM reliability analysis was implemented to find appropriate ranges of the load factor values for each load considered in this study. The analysis produced results consistent with all the Codes reviewed, although the values produced lie in rather wide ranges due to the relatively wide range of the input parameters. The analysis shows even better agreement with the Codes when considering only the US Codes (AASHTO, ACI, and AISC). The values presented in the US Codes lie in the middle of the acceptable range determined by the analysis, as summarized by Figure 2.6.1. Both the present ACI and AISC codes use the ASCE-7 recommended load factors. Therefore, the present load factors prescribed by ASCE-7 and AASHTO are acceptable for use in geotechnical LRFD.

Once we established that the code load factors can be used with confidence, the next step was to investigate a method to evaluate resistance factors in the most theoretically sound manner possible. We proposed a framework for the objective

development of resistance factors. Several steps comprise this framework. First, identify the design equation. Second, identify all component quantities. Define probabilistic models for the uncertain quantities using available data. Next, use reliability analysis to determine the limit state values corresponding to a set of nominal design values at a specified reliability index. Resistance factors can be determined algebraically from the corresponding nominal and limit state values.

Using probabilistic models, optimum load and resistance factors are developed. To make the results of this work compatible with established code load factors, an adjustment must be made to the resistance factors. We presented a method in Section 3.3 that will satisfactorily accomplish this task.

Table 5.1.1 presents recommended resistance factors for use with ASCE-7 (1996) or AASHTO (1998) live- and dead-load factors for shallow foundations. These tables contain simplified guidelines based on the more thorough results of Figures 5.1.1, 5.1.2 and 5.1.4 for ASCE-7 load factors.

Serviceability and ultimate limit states should be treated separately. Results of the present analysis suggest traditional WSD factors of safety may be overly conservative for shallow foundations in clay. However, addressing safety factors alone will not offer any improvement to present practice. The design process of interpreting data and using transformation models to develop design resistance values must be examined. Without the availability of consistent criteria for defining design resistance values, the safety margin of a design is unknown and cannot be compared to other designs. The development of statistically consistent methods to select design values, such as the CAM

method in Section 5.2, is quite feasible and will pave the way for the benefits of reliability-based design to be fully realized.

LRFD of foundations will yield designs with consistent reliabilities if a statistically consistent approach is used. The method proposed for establishing a conservative mean for use in design is readily reproducible in practice. Resistance factors have been determined that are compatible with this procedure. Three advantages are offered by this method. First, since the method uses statistical tools to determine values, the need for arbitrary judgment calls within a given soil layer is reduced. Second, as a statistically consistent tool for evaluating design inputs, the method can be expected to yield designs with much more consistent reliabilities than is possible otherwise. Finally, the method has been shown to be a useful tool for maintaining consistent reliability with respect to soil profiles with variabilities that differ from those used to determine the resistance factors. This result is highly significant to the practical implementation of LRFD methods in geotechnical engineering, since soil deposits vary significantly from site to site.

In order to develop a complete set of LRFD factors for use in the ultimate limit state design of shallow footings, uncertainties associated with different test methods, load inclination factors, footing base inclination factors, and ground inclination must be incorporated into future reliability analyses.

For the design of deep foundations, two major classes of design methods are available: direct methods, which use in-situ tests to directly determine a resistance; and property-based methods, which use soil properties determined from a variety of tests to compute resistance. A major difference between property-based methods and direct

methods is that property-based methods tend to have higher uncertainty (lower *RF*), but apply to general cases, while direct methods tend to have lower uncertainty (higher *RF*) and only apply to specific cases resembling the specific piles and soils they were developed for. One implication of this difference is that it may be riskier to apply a direct method to a design situation that is different from the pile load test database supporting the method, even though the method may show excellent agreement with measured values in the database.

In the course of the literature review, it was often discovered that the experimental and theoretical support for many design methods is incomplete. Thus, many design methods can be expected to produce unpredictable deviations between measured and predicted load capacities. This means that we are unable to rationally assess the uncertainty for some design methods within the framework established in Chapter 3. The available data to support existing design methods for drilled shafts and piles in clay, in particular, were found to be limited.

Tables 8.2.1 and 9.2.1 present recommended resistance factors for use with ASCE-7 (1996) or AASHTO (1998) live- and dead-load factors for deep foundations on sand and clay, respectively. These tables also contain summaries of the design equations to be used with each resistance factor.

In the course of this study, we attempted to investigate the most promising design methods for deep foundations. However, any effort will be insufficient to cover all the cases that could arise in practice knowing that there are many direct design methods that are developed for specific design situations. As such, the designer needs the capability to select resistance factors that reflect the uncertainty of the design method used. A suitable

technique is to assess the uncertainty of total capacity from predicted vs. measured load test data. A methodology to apply this technique was presented in Section 9.2.1 and demonstrated in Chapter 10.

Recommendations Reached in the Study

In this section, we summarize the various conclusions reached in the study concerning how to implement LRFD properly for geotechnical design. These recommendations are grouped according to their area of application.

- Selecting Load factors for use in Geotechnical LRFD
    - Designers should use load factors in geotechnical LRFD that are consistent with structural LRFD.
- Selecting Resistance Factors for use in Geotechnical LRFD
    - Reliability analysis is the most rational technique available to assess resistance factors.
    - The process of specifying resistance factors in the code that yield the same design proportions as previously used factors of safety is known as factor calibration. Factor calibration is useful as a first step to implementing LRFD and is the most common method currently in use.
    - For shallow foundations, the single, “lumped” resistance factor approach should be used.
    - Better control over the uncertainty of a pile design is offered by the multiple factor approach. However, some designs will not have enough data to support this approach and the lumped factor must be used.

- There is a significant difference between designs supported by a pile load test verification program and those without. Reliability analysis was performed to support recommended values of *RFs* for cases without load verification. *RFs* for verified pile designs are necessarily higher.
- For direct pile design methods not covered in the report, designers can determine their own resistance factor using the figures provided. This is possible when they have access to load test data supporting a design method that is sufficiently similar to the design circumstances considered. Thus, the results of this report can be extended beyond the cases considered.

- Developing Resistance Factors Using Reliability Analysis
  - Reliability analysis is the most rational technique available to assess resistance factors.
  - It is important to use a systematic approach to evaluate the uncertainty of design variables.
  - The proposed framework in Section 3.1 should be used to develop resistance factors since it is a rational, systematic, and credible approach.
  - For thorough investigations of design variable uncertainty, numerical integration of the fundamental PDF equations is recommended to handle the transformation to dependent PDFs in favor of Monte Carlo simulation or first-order approximations.

- It is useful to develop target reliability indices based on current acceptable practice, to allow the cautious, gradual adjustment of safety levels (reliability indices and the resulting design proportions) over time.
- To assess currently acceptable reliability indices, reliability indices can be back calculated from existing factors of safety.
- *RF*s have been produced in this report for a target reliability index of 3.0. Existing practice or acceptable risk may vary and alternative target reliability indices may be used. For piles, tools have been provided to do this on a limited basis. More complete reliability analyses are required for more thorough adjustments.
- The process of specifying resistance factors in the code that yield the same design proportions as previously used factors of safety is known as factor calibration. Factor calibration is useful as a first step to implementing LRFD and is the most common method currently in use.

- Selecting Characteristic Values of Strength for Design
  - It is critical to realizing the full potential of reliability-based design methods to determine characteristic resistance in a reproducible way.
  - Use of the Conservatively Assessed Mean (CAM) procedure outlined in Chapter 5 is necessary to achieve more uniform inputs to design and take advantage of the benefits offered by using LRFD. The CAM procedure is also demonstrated in Chapters 6 and 10.
  - In-situ test soundings and other soil tests should be grouped together for analysis when they are known to be measurements of the same soil or soil

layer. Tests of different materials or in-situ soundings revealing different features at a site are necessarily kept separate.

- Spatial variability in the vertical direction can be readily taken into account using some in-situ tests. However, spatial variability in the horizontal direction is impossible to determine routinely and the best treatment of the problem is to use the "worst" applicable sounding, or group of soundings.

- Engineering Education about LRFD
  - Engineers will have to be educated about the rationale behind matching proper and consistent values of *RF*s, *LF*s and characteristic resistance within LRFD.
  - Engineers will have to become familiar with the number of different factors to adjust to and accept LRFD.
- General Recommendations Concerning the Design of Deep Foundations
  - A number of deep foundation design methods were selected for this study on the basis of the completeness of their supporting data. These should be used in design since the methods have such good support.
  - Several aspects of pile design require further investigation as data is incomplete.
  - For property-based design of piles, the value of K_0 selected for use in shaft design is very important – it is a highly relevant parameter and should be selected with care.

LIST OF REFERENCES

Aas, G., Lacasse, S., Lunne, T. and Hoeg, K. (1986) "Use of In Situ Tests for Foundation Design on Clay." *In Situ '86: Use of In Situ Tests in Geotechnical Engineering.* Samuel Clemence, ed. ASCE. 1-30.

AASHTO (1994). *LRFD Bridge Design Specifications, 1st ed*. American Association of State Highway and Transportation Officials, Washington D.C.

AASHTO (1998). *LRFD Bridge Design Specifications, 2nd ed.* American Association of State Highway and Transportation Officials, Washington D.C.

ACI (1990). *Standard Specifications for Tolerances for Concrete Construction and Materials (117-90).* American Concrete Institute, Detroit.

ACI (1999). *Building Code Requirements for Structural Concrete (318-99) and Commentary (318R-99).* American Concrete Institute, Detroit.

ACI (2002). *Building Code Requirements for Structural Concrete (318-02) and Commentary (318R-02).* American Concrete Institute, Detroit.

AISC (1994). *Load and Resistance Factor Design Specification for Structural Steel Buildings, 2nd ed.* American Institute of Steel Construction, Inc., Chicago, Illinois.

AISC (2001). *Manual of Steel Construction: Load and Resistance Factor Design.* 3rd ed. American Institute of Steel Construction, Chicago.

Allen, D. E. (1975). "Limit states design-probabilistic study." *Can. J. Civ. Engrg*., 2, 36-49.

Altaee et al. (1992). "Axial load transfer for piles in sand: I. Tests on an instrumented precast pile." *Canadian Geotechnical Journal.* 29. 11-20.

Altaee et al. (1993). "Load transfer for piles in sand and the critical depth." *Canadian Geotechnical Journal*. 30. 455-463.

American Petroleum Institute (API) (1993). *Recommended practice for planning, designing and constructing fixed offshore platforms-load and resistance factor design*. American Petroleum Institute, Washington D.C.

American Society of Civil Engineers (ASCE). (1996). ''Minimum design loads for buildings and other structures.'' ASCE 7-95, ASCE, Reston,Va.

Ang, A. H-S., and W-H. Tang (1975). *Probability Concepts in Engineering Planning and Design, Volume I: Basic Principles.* Wiley.

Aoki, N. and D. de Alencar (1975). "An Approximate Method to Estimate the Bearing Capacity of Piles." *Proc. 5th Pan-American Conference of Soil Mechanics and Foundation Engineering*, Buenos Aires. 1. 367-376.

Baligh, M. M., V. Vivatrat, and C. C. Ladd (1980). "Cone Penetration in Soil Profiling." Journal of the Geotechnical Engineering Division, ASCE. 106:4. 447-461.

Bandini, P. (2003) PhD Thesis. Purdue University.

Bandini, P. and R. Salgado (1998). "Methods of Pile Design Based on CPT and SPT Results." *Geotechnical Site Characterization*. Robertson and Mayne, eds. 967-976.

Barker, R. M., Duncan, J. M., Rojiani, K. B., Ooi, P. S. K., Tan, C. K., and Kim, S. G. (1991). *Manuals for the design of bridge foundations*. Transportation Research Board, NCHRP report 343.

BCP Committee (1971). "Field tests on piles in sand." *Soils and Foundations*. 11:2. 29-49.

Becker, D. E. (1996). “Eighteenth Canadian Geotechnical Colloquium: Limit States Design for Foundations. Part II. Development for the National Building Code of Canada.” *Can. Geotech. J.*, 33, 984-1007.

Becker, D. E. (1996). “Eighteenth Canadian Geotechnical Colloquium: Limit States Design for Foundations. Part I. An overview of the foundation design process.” *Canadian Geotechnical Journal*. 33:6. 956-983.

Beringen F.L., Windle D. & Van Hooydonk W.R. (1979). “Results of loading tests on driven piles in sand.” *Proc. Conference on Recent Developments in the Design and Construction of Piles*. ICE, London. 213-225.

Bolton, M. D. (1986). “The Strength and Dilatancy of Sands.” *Geotechnique*. 36. 65-78.

Briaud, J.-L. and L. M. Tucker (1988). “Measured and Predicted Axial Load Response of 98 Piles.” *Journal of Geotechnical Engineering*, ASCE. 114:9. 984-1001.

Briaud, J.-L., L. M. Tucker, and E. Ng. (1989). “Axially Loaded 5 Pile Group and a Single Pile in Sand.” *Proc. 12th Int. Conf. Soil Mechanics and Foundation Engineering*, Rio de Janeiro. 2. 1121-1124.

Brinch Hansen, J. (1970). “A Revised and Extended Formula for Bearing Capacity.” The Danish Geotechnical Institute, Bulletin No. 28.

Brinch Hansen, J. (1970). “A Revised and Extended Formula for Bearing Capacity.” The Danish Geotechnical Institute, Bulletin No. 28.

Bustamante, M. and L. Gianeselli (1982). “Pile Bearing Capacity Prediction by Means of Static Penetrometer CPT.” *Proc. 2nd European Symposium on Penetration Testing*, Amsterdam. 2. 493-500.

Chow, F.C. (1997). *Investigations into the Behaviour of Displacement Piles for Offshore Foundations*. PhD dissertation, University of London (Imperial College).

Cornell, C. A. (1969). "A Probability-Based Structural Code." *ACI Journal*. 974-985.

Cornell, C. A. (1969). "Structural safety specifications based on second-moment reliability." *Symp. Int. Assn. Brid. and Struct. Engrg*., London.

Darrag, A. A. (1987). *Capacity of Driven Piles in Cohesionless Soils Including Residual Stresses*. PhD Thesis, Purdue University.

DeBeer, E. E. (1970) "Experimental Determination of the Shape Factors and the Bearing Capacity Factors of Sand." *Geotechnique*, 20, 387-411.

DGI (1985). *Code of practice for foundation engineering*. Danish Geotechnical Institute, Copenhagen, Denmark.

ECS (1994). *Eurocode 7:Geotechnical Design-Part I: General Rules*. European Committee for Standardization, Central Secretariat, Brussels.

ECS (1995). *Eurocode 1:Basis of Design and Actions on Structures-Part I: Basis of Design*. European Committee for Standardization, Central Secretariat, Brussels.

Ellingwood, B. R. (1999). "Wind Load Statistics for Probability-Based Structural Design." *Journal of Structural Engineering*, ASCE. 125:4. 453-463.

Ellingwood, B., Galambos, T. V., MacGregor, J. G., and Cornell C. A. (1980). *Development of a probability based load criterion for American National Standard A58 - Building Code Requirements for Minimum Design Loads in Buildings and other Structures*. National Bureau of Standards, Washington, D.C.

Ellingwood, Bruce, James G. MacGregor, Theodore V. Galambos, and C. Allin Cornell. (1982). "Probability Based Load Criteria: Load Factors and Load Combinations." *Journal of the Structural Division*, ASCE. 108:5. 978-997.

Eslami, A. and B. H. Fellenius (1997). "Pile Capacity by Direct CPT and CPTu Methods Applied to 102 Case Histories." *Canadian Geotechnical Journal*. 34. 886-904.

Fellenius, B. H. and A. A. Altaee (1995). "Critical Depth: How it Came into Being and Ehy it Does not Exist." *Proceedings, ICE, Geotehcnical Engineering*. 113. 107-111.

Fisher, John W., Theodore V. Galambos, Geoffrey L. Kulak, Mayasandra K. Ravindra (1978). "Load and Resistance Factor Design Criteria for Connectors." *Journal of the Structural Division, ASCE*. 104:9. New York: ASCE. pp. 1427-1441.

Fleming, W. G. K., A. J. Weltman, M. F. Randolph, and W. K. Elson (1992). *Piling Engineering*. Halsted Press, New York.

Foye, K. C., R. Salgado and B. Scott (2004). "Assessment of Variable Uncertainties for Reliability-Based Design of Foundations." *Journal of Geotechnical and Geoenvironmental Engineering.* ASCE. In press.

Foye, K. C., R. Salgado and B. Scott (2004). "Resistance Factors for Use in Shallow Foundation LRFD." *Journal of Geotechnical and Geoenvironmental Engineering*. ASCE. In press.

Franke, E. (1993). "EUROCODE Safety Approach as Applied to Single Piles." *4th International DFI Conference*. 13-18.

Galambos, Theodore V., Bruce Ellingwood, James G. MacGregor, and C. Allin Cornell. (1982). "Probability Based Load Criteria: Assessment of Current Design Practice." *Journal of the Structural Division*, ASCE. 108:5. 959-977.

Goble, G. (1999). *Geotechnical Related Development and Implementation of Load and Resistance Factor Design (LRFD) Methods*. Transportation Research Board, NCHRP synthesis 276.

Gregersen O.S., G. Aas, and E. Dibiagio (1973). "Load tests on friction piles in loose sand." *Proc. 8th Int. Conf. Soil Mechanics & Foundation Engineering*, Moscow. 2. 109-117.

Haldar, A. and Mahadevan, S. (2000). *Probability, Reliability, and Statistical Methods in Engineering Design.* John Wiley and Sons, Inc. New York.

Hammitt, G. M. (1966). "Statistical Analysis of Data from a Comparative Laboratory Test Program Sponsored by ACIL." Miscellaneous Paper 4-785. U. S. Army Engineering Waterways Experiment Station, Corps of Engineers.

Hanna, T.H. and R.H.S. Tan (1973). "The Behavior of Long Piles under Compressive Loads in Sand." *Canadian Geotechnical Journal*. 10:2. 311-340.

Hardin, B. O., and Black, W. L. (1966). ''Sand Stiffness Under Various Triaxial Stresses.'' *J. Soil Mech. and Found. Div.*, ASCE. 92:2. 27–42.

Harr, M. E. (1987). *Reliability Based Design in Civil Engineering*. Dover, Mineola, NY.

Hasofer, A. M. and N. C. Lind (1974). "Exact and Invariant Second-Moment Code Format." *Journal of the Engineering Mechanics Division*. ASCE. 100:1. 111-121.

Hettler, A. (1982). "Approximation Formula for Piles Under Tension." *Proc., IUTAM, Conf. on Deformation and Failure of Granular Materials*. 603–608.

Ismael, N. F. and Jeragh, A. M. (1986) "Static Cone Tests and Settlement of Calcareous Desert Sands." *Can. Geotech. J.*, 23, 297-303.

Jacobs, P. A., and J. S. Coutts (1992). "A Comparison of Electric Piezocone Tips at the Bothkennar Test Site." *Géotechnique*. 42:2. 369-375.

Jardine, R., Chow, F.C., (1998). *Research into the Behaviour of Displacement Piles for Offshore Foundations*. OTO 98 833. Health and Safety Executive.

Jaynes, E. T. (1957). "Information Theory and Statistical Mechanics, II," *Phys. Rev.*, 108.

Journal of Geotechnical Engineering, ASCE. 102:3. 197-228.

Kerisel, J. (1964). "Deep Foundations, Basic Experimental Facts." *Proc. North American Conf. Deep Foundations*, Mexican Society of Soil Mechanics. 1. 5-44.

Kishida, H., and M. Uesugi (1987). "Tests of the interface between sand and

Kraft, L. M. (1990). "Computing Axial Capacity in Sands for Offshore Conditions." *Marine Geotechnology*. 9. 61-92.

Kraft, L.M. (1991) "Performance of Axially Loaded Pipe Piles in Sand." *Journal of Geotechnical Engineering*, ASCE. 117:2. 272-296.

Kulhawy, F. H, and K. K. Phoon (2002). "Observations on Geotechnical Reliability-Based Design Development in North America." *Proceedings*. International Workshop on Foundation Design Codes and Soil Investigation in view of International Harmonization and Performance Based Design, Hayama, Japan. 31-48.

Kulhawy, F. H., and C. H. Trautmann (1996). "Estimation of In-Situ Test Uncertainty." *Uncertainty in the Geologic Environment: From Theory to Practice*. C. D. Shackelford, P. P. Nelson, M. J. S. Roth, eds. ASCE. 269-286.

Kulhawy, F.H. (1984) "Limiting Tip and Side Resistance: Fact or Fallacy?" *Proceed. of the symposium on the Analysis and Design of pile Foundations. American Society of Civil Engineers, San Francisco, Calif.* 80-98.

Lee, J. and R. Salgado (1999). "Determination of Pile Base Resistance in Sands." *Journal of Geotechnical and Geoenvironmental Engineering*, ASCE. 125:8. 673-683.

Lee, J., R. Salgado, and K. Paik (2003). "Estimation of Load Capacity of Pipe Piles in Sand Based on Cone Penetration Test Results." *Journal of Geotechnical and Geoenvironmental Engineering*, ASCE. 129:6. 391-403.

Lehane, B.M., and Randolph, M. F. (2002). "Evaluation of a minimum base resistance for driven pipe piles in siliceous sand." *Journal of Geotechnical and Geoenvironmental Engineering*, ASCE, 128(3), 198-205.

Lehane, B.M., Jardine, R.J., Bond, A.J., and Frank, R. (1993). "Mechanisms of Shaft Friction in Sand from Instrumented Pile Tests." *Journal of Geotechnical Engineering*, ASCE. 119:1. 19-35.

Liao, S. C. and R. V. Whitman (1986). "Overburden Correction Factors for SPT in Sand." *Journal of Geotechnical Engineering*, ASCE. 112:3. 373-377.

Lind, N. C. (1971). "Consistent partial safety factors." *J. Struct. Engrg. Div*., ASCE, 97(ST6), 1651-1670.

Low, B. K., and W. H. Tang. (1997). "Efficient Reliability Evaluation Using Spreadsheet." *Journal of Geotechnical and Geoenvironmental Engineering*. 123:7. 749-752.

Lunne, T. and Eide, O. (1976). "Correlations between cone resistance and vane shear strength in some Scandinavian soft to medium stiff clays." *Can. Geotech. J.*, 13, 430-441.

MacGregor, J. G. (1976). "Safety and limit states design for reinforced concrete." *Can. J. Civ. Engrg*., 3, 484-513.

MacGregor, J. G. (1997). *Reinforced Concrete Mechanics and Design, 3rd ed*. Prentice Hall.

Meyerhof, G. G. (1951). "The Ultimate Bearing Capacity of Foundations." *Geotechnique*. 2:4. 301-332.

Meyerhof, G.G. (1976). "Bearing Capacity and Settlement of Pile Foundations."

Milford, R. V. (1987). "Load Factors for Limit Sates Codes." *Journal of Structural Engineering*, ASCE. 113:9. 2053-2057.

MOT (1992). *Ontario highway bridge design code*. Ministry of Transportation Ontario, Downsview.

Nowak, A. S. (1994). "Load model for bridge design code." *Can. J. Civ. Engrg*., 21, 36-49.

Nowak, A. S. and Grouni, H. N. (1994). "Calibration of the Ontario highway bridge design code 1991 edition." *Can. J. Civ. Engrg*., 21, 25-35.

Nowak, A.S. (1994). "Load Model for Bridge Design Code." *Canadian Journal of Civil Engineering*. 21. 36-49.

NRC (1995). *National building code of Canada*. National Research Council of Canada, Ottawa.

Outokumpu Stainless (2004). "Definition of Surface Roughness." http://www.outokumpu.com/template/Page____5852.asp

Paik, K. and R. Salgado (2003). "Determination of Bearing Capacity of Open-Ended Piles in Sand." *Journal of Geotechnical and Geoenvironmental Engineering*, ASCE. 129:1. 46-57.

Paik, K., R. Salgado, J. Lee, and B. Kim (2003). "Behavior of Open- and Closed-Ended Piles Driven Into Sands." *Journal of Geotechnical and Geoenvironmental Engineering*, ASCE. 129:4. 296-306.

Paikowsky, Samuel G. 2004. *Load and Resistance Factor Design for Deep Foundations*. NCHRP Report 507. Washington, D.C.: Transportation Research Board.

Phoon, K. K., and F. H. Kulhawy (1999). "Characterization of Geotechnical Variability." *Canadian Geotechnical Journal*. 36. 612-624.

Prandtl, L. (1920). "Über die Härte Plasticher Körper." Nachr. Ges. Wiss. Gött., Math-Phys. Kl., 12, 74-85.

Randolph, M. F. and B. J. Murphy (1985). "Shaft Capacity of Driven Piles in Clay." *Proc. 17th Offshore Technology Conf.*, Houston. 1. 371-378.

Randolph, M.F., Dolwin, J., and Beck, R. (1994). "Design of Driven Piles in Sand". *Géotechnique*. 44:3. 427-448.

Rao, K. S., M. M. Allam, and R. G. Robinson (1998). "Interfacial Friction Between Sands and Solid Surfaces." *Proc. ICE, Geotechnical Engineering.* 131. 75-82.

Reissner, H. (1924). "Zum Erddruckproblem." *Proceedings of the First International Congress forf Applied Mechanics.* C. B. Biezeno and J. M. Burgers, eds. Delft. 295-311.

Robertson, P. K., Campanella, R. G., and Wightman, A. (1983). "SPT-CPT Correlations." *Journal of Geotechnical and Geoenvironmental Engineering*, ASCE, 109, 1449-1459.

Rosenblueth, E. (1975). "Point Estimates for Probability Moments." *Proceedings of the National Academy of Sciences of the United States of America.* 72:10. 3812-3814.

Salgado, R. (2003). *CONPOINT User Manual*.

Salgado, R. (2004). *The Engineering of Foundations.* McGraw-Hill, app. 1500 pages w/figures (in preparation).

Salgado, R. and J. K. Mitchell (2003). "Computation of Penetration Resistance in Sands." Geotechnical Report Number 2003-2. School of Civil Engineering, 550 Stadium Mall Drive, Purdue University. West Lafayette, Indiana.

Salgado, R. and J. K. Mitchell (2003). "Computation of Penetration Resistance in Sands." Geotechnical Report Number 2003-2. School of Civil Engineering, 550 Stadium Mall Drive, Purdue University. West Lafayette, Indiana.

Salgado, R., A. V. Lyamin, S. W. Sloan, and H. S. Yu (2004). "Two- and Three-Dimensional Bearing Capacity of Foundations in Clay." *Géotechnique*. accepted for publication.

Salgado, R., J. K. Mitchell, and M. Jamiolkowski (1997). "Cavity Expansion and Penetration Resistance in Sand." *Journal of Geotechnical and Geoenvironmental Engineering*, ASCE, 123:4, 344-354.

Scott, B. (2002) "Development of Load and Resistance Factor Design Method for Shallow Foundations." PhD thesis, Purdue University, West Lafayette, Indiana.

Scott, B., B. J. Kim and R. Salgado (2003). "Assessment of Current Load Factors for Use in Geotechnical LRFD." *Journal of Geotechnical and Geoenvironmental Engineering*, ASCE. 129:4. 287-295.

Shooman, M. L. (1968). *Probabilistic Reliability: An Engineering Approach*. McGraw-Hill. New York.

Skempton, A. W. (1986). "Standard Penetration Test Procedures and the Effects in Sand of Overburden Pressure, Relative Density, Particle Size, Ageing and Overconsolidation." *Geotechnique*. 36:3. 425-337.

Sloan, S. W. and Yu, H. S. (1996). "Rigorous Plasticity Solutions for the Bearing Capacity Factor N_γ." Proceedings of the 7th Australia-New Zealand Conference on Geomechanics, Adelaide. 544-550.

Stark, T. D. and J. E. Juhrend (1989). "Undrained Shear Strength from Cone Penetration Tests." *Proc. 12th Int. Conf. Soil Mechanics and Foundation Engineering*. 327-330.

steel in the simple shear apparatus," *Géotechnique.* 37:1. 45-52.

Tabsh, Sami W. (1997). "Safety of Reinforced Concrete Members Designed Following ACI 318 Building Code." *Engineering Structures*. 19:10. 843-850.

Tippett, L. H. C. (1925). "On the Extreme Individuals and the Range of Samples Taken from a Normal Population." *Biometrika*. 17:3/4. New York : Macmillan. 364-387.

Toolan, F. E., M. L. Lings, and U. A. Mirza (1990). "An Appraisal of API RP2A Recommendations for Determining Skin Friction of Piles in Sand." *Proc. 22nd Offshore Technology Conf.*, Houston. OTC 6422. 4. 33-42.

Vesic, A. S. (1964). "Model Testing of Deep Foundations in Sand and Scaling Laws." *Proc. Conf. Deep Foundations*, Mexican Society of Soil Mechanics and Geotechnical Engineering. Mexico City. 2. 525-533.

Vesic, A. S. (1967). "A Study of Bearing Capacity of Deep Foundations." *Final rep., Project B-189*, Georgia Institute of Technology. Atlanta, GA.

Vesic, A. S. (1970). "Tests on Instrumented Piles, Ogeechee River Site." *J. Soil Mech. Found. Div.*, ASCE. 96:2. 561–504.

Vesic, A. S. (1973). "Analysis of Ultimate Loads of Shallow Foundations." *Journal of the Soil Mechanics and Foundations Division*, ASCE. 99:1. 45-73.

White, D. J. (2003). "Field Measurements of CPT and Pile Base Resistance in Sand." CUED/D-SOILS/TR327. University of Cambridge.

Withiam, J. L., Voytko, E. P., Barker, R. M., Duncan, J. M., Kelly, B. C., Musser, S. C., and Elias, V. (1997). *Load and resistance design (LRFD) for highway bridge substructures*. Federal Highway Administration, Washington, D.C.

Yu, H. S., L. R. Herrmann, and R. W. Boulanger (2000). "Analysis of Steady Cone Penetration Resistance in Clay." *Journal of Geotechnical and Geoenvironmental Engineering*, ASCE. 126:7. 594-605.